TÉCNICO LISBOA

Plasmonics in two-dimensional materials:
a wave-kinetic description

José Luís Sampaio de Figueiredo

Thesis to obtain the Master of Science Degree in

Engineering Physics

Supervisor(s): Prof. Hugo Fernandes Santos Terças
Prof. João Pedro Saraiva Bizarro

Examination Committee

Chairperson: Prof. Horácio João Matos Fernandes
Supervisor: Prof. Hugo Fernandes Santos Terças
Member of the Committee: Prof. Vasco António Dinis Leitão Guerra
Prof. Vítor João Rocha Vieira

January 2021

Dedicated to my parents and brother.

Acknowledgments

To start with, I would like to direct a spatial thanks to my supervisors, Prof. Hugo Terças and Prof. João Pedro Bizarro, for the all the indispensable support, guidance and patience throughout this entire process. I make them no favour when I stress their intelligence and assertiveness, which made this work possible, specially during such a complicated year for everyone. It was indeed a great pleasure to have been given the opportunity to work with such distinct physicists.

In addition, I would also like to thank my family and friends. Although indirectly and without really knowing, their constant presence and encourage was crucial in finishing this work. A special thanks to my dear friend Catarina Murta, who helped me with all the necessary illustrations.

Resumo

A plasmónica de grafeno é um tema excitante de investigação hoje em dia, não apenas devido ao seu potencial para produzir avanços tecnológicos, mas também por servir de teste a nova física. Assim, de modo a considerar a natureza quântica dos portadores de carga, contruímos um modelo baseado no formalismo cinético, partindo de uma equação de Schrödinger para o campo médio de eletrões e buracos. A equação de movimento para os componentes da matriz de Wigner é derivada de primeiros princípios, levando-nos a um conjunto fechado de equações conhecido como modelo de Wigner-Poisson. Para grandes comprimentos de onda, recuperamos a relação de dispersão esperada para os plasmões em grafeno. Depois, as equações da hidrodinâmica são também obtidas, tomando os momentos da equação cinética, e cujos resultados convergem, no limite clássico, para o esperado para um fluido de Dirac. As equações obtidas são comparadas com o caso parabólico, com o termo cinético usual $\xi(\boldsymbol{p}) = \boldsymbol{p}^2/2m$, e as principais diferenças são sublinhadas. Além disso, damos expressões analíticas para a massa efetiva dos campos hidrodinâmicos, resultante da comparação entre velocidade e momento de fluido. Por fim, voltamos à equação cinética para descrever uma instabilidade num sistema de duas placas de grafeno separadas. Encontramos soluções instáveis, com taxas de crescimento até 20THz para condições experimentais realistas.

Palavras-chave: Plasmónica em grafeno; Quasi-partículas; Teoria cinética; Formalismo de Wigner; Hidrodinâmica.

Abstract

Plasmonics in graphene is a hot topic of research nowadays, not just because of its potential applicability in future optoelectronic devices, but also because it serves as a playground to test new physics. In order to take into account the quantum nature of carriers, a quantum kinetic model is proposed, starting from the Schrödinger equation for the collective mean field wave functions for electrons and holes. The equation of motion for the components of the Wigner matrix in phase space is established, where the Coulomb interactions are introduced in the Hartree approximation. Using the Wigner-Poisson model, the long wavelength limit for the plasmon dispersion relation is obtained. The corresponding hydrodynamical equations are also derived, by taking the moments of Wigner's equation, and those are shown to converge, in the classical limit, to the expected result, if one starts with the Vlasov-Poisson model instead. The obtained equations are compared with the usual parabolic case, for which the kinetic term takes the form $\xi(\boldsymbol{p}) = \boldsymbol{p}^2/2m$. Moreover, we give analytical expressions for the effective mass, for the case of linear dispersion relation, which comes after relating the fluid momentum and velocity fields. The Wigner-Poisson model is further used to describe an instability under a specific configuration, for which we found unstable plasmon solutions with growth rates as high as $20\mathrm{THz}$ for realistic experimental conditions.

Keywords: Graphene plasmonics; Quasi-particles; Kinetic theory; Wigner formalism; Hydrodynamics.

Contents

List of Figures

Nomenclature

Greek symbols

α_s	Graphene's structure constant.
β	Inverse temperature.
$\boldsymbol{\nabla}$	Divergence operator with respect to the real-space variable $\boldsymbol{r}$.
$\boldsymbol{\nabla}_{\boldsymbol{y}}$	Divergence operator with respect to a generic variable $\boldsymbol{y}$.
χ	Quantum degeneracy factor.
δx	Fluctuation of x.
$\delta(x)$	Dirac-delta function.
ϵ	Dielectric function.
γ	Quasi-relativistic Lorentz factor.
Γ_C	Classical coupling constant.
Γ_Q	Quantum coupling constant.
$\hat{\rho}$	Density operator.
λ_F	Fermi wavelength.
ω	Frequency.
ω_i	Imaginary part of the frequency.
ω_p	Plasma frequency.
ω_r	Real part of the frequency.
ϕ	Electrostatic potential.
Π	Polarizability function.
ρ_{ij}	Mass density tensor.
τ_0	Mean-time between collisions.

$\Theta(x)$ Heaviside's step function.

ε Absolute permittivity.

ε_0 Vacuum's permittivity.

ε_r Relative permittivity.

$\xi(\boldsymbol{q})$ Single-particle dispersion relation.

ξ_K Average kinetic energy.

ξ_P Average potential energy.

Roman symbols

h Planck's constant.

$\boldsymbol{A}$ Vector potential.

$\boldsymbol{a}_i$ Lattice vectors.

$\boldsymbol{b}_i$ Reciprocal lattice vectors.

$\boldsymbol{F}$ Force field.

$\boldsymbol{G}_{ij}$ Reciprocal lattice points.

$\boldsymbol{J}$ Current density.

$\boldsymbol{p}$ Momentum.

$\boldsymbol{q}, \boldsymbol{k}$ Wave-vector variable.

$\boldsymbol{r}, \boldsymbol{s}$ Position variable.

$\boldsymbol{R}_{ij}$ Lattice points.

$\boldsymbol{u}$ Fluid velocity.

$\boldsymbol{v}$ Velocity.

$\boldsymbol{v}_g$ Group velocity.

$\boldsymbol{v}_p$ Phase velocity.

$\boldsymbol{\mathcal{B}}$ Magnetic field.

$\boldsymbol{\mathcal{E}}$ Electric field.

$\boldsymbol{V}_\alpha$ Kinetic velocity.

$\hat{a}$ Sublattice A annihilation operator.

$\hat{a}^\dagger$ Sublattice A creation operator.

$\hat{b}$ Sublattice B annihilation operator.

$\hat{b}^\dagger$ Sublattice B creation operator.

$\hat{c}$ Conduction electron annihilation operator.

$\hat{c}^\dagger$ Conduction electron creation operator.

$\hat{H}$ Hamiltonian operator.

$\hat{h}$ Hole annihilation operator.

$\hat{h}^\dagger$ Hole creation operator.

$\hat{v}$ Valence electron annihilation operator.

$\hat{v}^\dagger$ Valence electron creation operator.

$\hbar$ Reduced Planck's constant.

$|\mathfrak{n}\rangle$ Fock state.

$\mathcal{K}\{...\}$ Kinetic operator.

$\mathcal{M}$ Drude's mass.

$\mathcal{Q}$ Electric charge.

$\mathcal{T}\{...\}$ Weyl transform.

$\overline{\boldsymbol{p}}^\alpha$ Fluid momentum for band α

$\overline{\boldsymbol{i}}^\alpha$ Fluid electrical current for band α.

$\overline{\boldsymbol{j}}^\alpha$ Fluid current for band α.

$\overline{\boldsymbol{v}}^\alpha$ Fluid velocity for band α.

BZ First Brillouin zone.

$\mathrm{sign}(x)$ Sign function.

$\mathrm{Tr}\{...\}$ Trace.

$\tilde{\boldsymbol{V}}_\alpha$ Osmotic velocity.

a Graphene's lattice parameter.

c Speed of light.

$D(E)$ Density of states.

d_c Carbon-carbon distance.

e Elementary charge.

f	Classical distribution function.
f_0	Equilibrium distribution function.
f_{FD}	Fermi-Dirac distribution function.
g_s	Spin degeneracy factor.
g_v	Pseudo-spin (or valley) degeneracy factor.
i	Imaginary unit.
$J_n(x)$	Bessel function of the n-kind.
k_B	Boltzmann constant.
k_F	Fermi wave-number.
$K_n(x)$	Complete elliptical function of the n-kind.
L_ϕ	Thouless length.
m	Mass.
m^*	Effective mass.
m_{ij}	Mass tensor.
n	Density.
n^1	Electron density.
n^2	Hole density.
n_0	Average density.
P_{ij}^{α}	Pressure tensor for band α.
P_{ij}	Pressure tensor.
P_{ij}^{K}	Kinetic pressure tensor.
P_{ij}^{O}	Osmotic pressure tensor.
Q	Quality factor.
$S\{...\}$	Collision integral.
T	Temperature.
t	Time variable; hopping integral.
U	Voltage.
v_F	Fermi velocity.

W Wigner function.

$W^{\alpha\gamma}$ Wigner matrix.

W_0 Equilibrium Wigner function.

Subscripts

i, j, l Spatial componets.

Superscripts

$'$ Dimensionless variable.

α, λ Band superscript.

$*$ Complex conjugation

T Transpose.

$\dagger$ Hermitian conjugate.

Chapter 1

Introduction

Over the last decades, two-dimensional (2D) materials have brought exceptional research interest. The experimental discovery of gated graphene, back in 2004 by Geim and Novoselov [1], marks the beginning of a new era in the field of theoretical and experimental physics, and material engineering, due to its unique optical, electronic and mechanical properties [2]. In fact, this experimental realisation has paved the way to the understanding of more complex structures [3].

A true characterization of the dimensionality of such systems relies on a microscopic definition. For example, if we can describe it with a wave-function $\psi_{\boldsymbol{k}}(\boldsymbol{r},t)$ carrying a quantized 2D wave-vector $\boldsymbol{k} = (k_x, k_y)$, then $\psi_{\boldsymbol{k}}(\boldsymbol{r},t) = e^{-z/L_\phi}\psi_{\boldsymbol{k}}(x,y,t)$, where L_ϕ is the Thouless length [4]. Therefore, the system is considered 2D-localized if its dimensions are smaller than L_ϕ. At sufficient low temperatures, $T \ll T_F$, where T_F is the Fermi temperature, L_ϕ is relatively large. As a result, the dynamics of thin films and wires can be treated quantum mechanically as low dimensional systems (2D and 1D, respectively). For a thin planar film at low temperatures, this condition reduces to $w/\lambda_F \ll 1$, where λ_F is the Fermi wavelength and w is the width in the perpendicular z direction. In particular, for a graphene layer with density n, $\lambda_F \sim 1/\sqrt{n}$ and even for rampant density values, $w \ll \lambda_F$ still holds, when w is of the order of the monolayer thickness. Hence, a full quantum model to describe graphene electronics is desired.

Experimentally, a way to define a 2D system is to show that the orbital dynamics is only sensitive to perpendicular magnetic fields ($\boldsymbol{\mathcal{B}}_\perp = \mathcal{B}_z \boldsymbol{e}_z$), which indicates that electronic motion is effectively confined to the 2D plane. Moreover, another evidence of dimensionality is the observation of quantum Hall effect, a 2D-phenomenon, namely, by measuring a quantized Hall plateau. Both cases are true for graphene [5, 6], ensuring its 2D nature, even at room temperature.

Graphene is a single layer of sp^2-bonded carbon atoms, which are densely packed, forming a benzene ring structure. Furthermore, 2D graphene rolled upon in the plane is a carbon nanotube, and multilayer graphene with weak interlayer tunneling is graphite. In addition to its strict 2D nature, one of the most irreverent properties of graphene is that, in the long wavelength limit $q \to 0$, the electron density excitations are described by a Dirac-like equation [7]. This feature is responsible for the famous linear energy-momentum dispersion relation, with the conduction and valence bands both intersecting at $q = 0$. This is only the case for single-layer graphene, whereas for higher number of layers we re-

cover the usual parabolic expression for the long wavelength limit $\xi(\boldsymbol{q}) = m^* v_F^2 (q/q_0)^2/2 \sim q^2$ [8], where m^* is the effective mass in this regime, v_F is the Fermi velocity, $q_0 = t_\perp/(\sqrt{2}\hbar v_F)$ is the characteristic wave-vector [9], and $t_\perp$ is the hopping integral in the perpendicular direction. For single layer graphene, the effective mass m^* is not possible to obtain with simple band-theory arguments, due to the cone-like discontinuity of $m_{ij} \sim [\partial^2 \xi(\boldsymbol{q})/(\partial q_i \partial q_j)]^{-1}$ near $q_i = 0$.

Moreover, graphene possesses exceptionally high quantum efficiency for light-matter interactions [10]. While metal plasmonics exhibit large Ohmic losses, which restraints their electronic application, doped graphene appears as an alternative. Its large conductivities, that arise from the zero mass carriers, enclose a wide range of potential appliance, such as high-frequency nanoelectronics, nanomechanics, transparent electrodes, and composite materials [11]. For this reason, the possibility of electric gating has been extensively studied in graphene, allowing for the manipulation of the Fermi level [12]. Recently, gating with a solid electrolyte allowed carrier concentrations to reach 10^{14} cm^{-2}, which results in $E_F \approx 1$ eV, such that a modulation of optical transmission in the visible light spectrum is possible [13, 14]. All these unique characteristics make the screening properties in graphene to exhibit significantly different behaviour from the conventional 2D systems, therefore providing an excellent playground for testing new physics, besides technological improvements [15].

In the present thesis, we will be interested in understanding these electronic properties, resorting to a kinetic formalism, which will allow for a collective description of its behaviour. We will focus on plasmonic excitations and quantum transport of graphene electrons and holes, specially in the pure electron case, for which a quantum hydrodynamical model will be put forward.

1.1 Graphene plasmonics

Plasmonics is a theoretical and experimental field of condensed matter physics and material engineering that has gathered a great amount of interest among the scientific community, due to its large potential of triggering technological advances. Although the number of publications has risen exponentially since the experimental realization of graphene [1], the first developments in the field of plasmonics can be traced back to the beginning of last century, starting with Wood's observations of dark and bright patterns in the light reflected by the surface of a metal [16]. These anomalies, which would later be called Wood's anomalies, were only explained by Lord Rayleigh a few years after [17], in terms of singularities of the scattered fields. Subsequent works of Sommerfeld and Zenneck [18, 19] reported a special solution to the Maxwell equations describing electromagnetic fields propagating at the surface of a conductor. These results paved the way to the conclusion that Wood's anomalies where actually a consequence of the propagation of surface plasmons, made by Fano [20] and Ritchie [21].

Plasmons are the elementary excitations of electronic environments, which correspond to coherent collective oscillations of the electronic density. These oscillations produce electromagnetic fields that interact again with the electronic density. To a good plasmonic material corresponds a high quality factor, $Q = \omega\tau$. This parameter measures how many optical oscillations does the free propagation of the plasmon undergoes before it decays, and is related to its frequency, ω, and lifetime, τ [22]. Additionally,

these excitations produce a collective electric field, $\boldsymbol{\mathcal{E}}$, from the charge displacement, which can be used to locally enhance an external field, $\boldsymbol{\mathcal{E}}_0$, up to $\mathcal{E}^2/\mathcal{E}_0^2 \simeq Q^2$. [23]. Moreover, the field confinement [24] is also an important feature to allow for plasmonic applications, such as optoelectronic devices or photodetectors [25].

Nowadays, modern plasmonics is a fast developing field, due to large improvements in nanoscale fabrication processes and experimental resources, as well as theoretical tools. The emerging of advanced condensed matter, quantum optics, photonics and solid-state physics techniques have allowed for novel discoveries, specially when the quantum nature of the materials plays a major role. This is often the case when dealing with the atomic scale, and quantum dynamics of atomic and electronic systems is necessary to a clear description of these phenomena.

Going further, a great advantage of 2D semi-conductors is the longer lifetime of the plasmonic modes and the tunability of both plasmon dispersion and damping by changing the doping, intercalating chemical species or applying electric fields [26]. This facilitates their interaction with light, leading to localization and guiding of light into electrical signals, which can be technologically used for devising plasmonic devices for diverse applications [27]. Furthermore, the graphene relativistic nature of electrons and holes, resulting from the cone-like dispersion relation near the Dirac points, makes it useful for high-performance optoelectronic devices.

The states near the edge of the conduction and valence bands are filled, at zero doping, because fermions cannot occupy the same quantum state, making light absorption to be saturated. Compared with traditional semiconductors, like silicon and GaAs, this unique saturable character of graphene under strong light excitation makes it promising in the high speed communication field, as ultrathin saturable optical fiber absorbers. All these unique features might lead to a new generation of highly integrated low-noise optical communication systems with very low cost.

1.2 The THz problem

Terahertz (THz) radiation is located between the microwave and infrared limits of the electromagnetic spectrum, and is known to be particularly useful in a number of applications, ranging from imaging and sensing to spectroscopy [28].

In particular, THz radiation is sensitive to intermolecular and intramolecular vibrations, which can be used in drug identification, as most pharmaceutic compounds display terahertz spectra. Other important medical applications include dermatology, oncology and oral healthcare [29]. Moreover, THz radiation is an alternative to more invasive medical imaging techniques, with X-rays being the most paradigmatic one. This is because the photon frequencies in the THz range are significantly less damaging for tissues and DNA, being non-ionising and thus biologically secure.

Another important application is related to imaging in the context of security. Given that THz radiation can penetrate inorganic fabrics, such as plastic, without penetrating the skin, it could provide a more efficient way to detect undesired objects, where other sources of radiation have proved to be inefficient.

Despite its utility, it is true that current technology is still incapable of easily producing and detecting

in the THz range. At the moment, converting electrical energy into coherent electromagnetic radiation is achievable in both the low frequency regime (microwaves and below), using oscillating circuits based on high-speed transistors, and in the high frequency (visible light) using semiconductor lasers. The low frequencies are currently limited to 30 GHz, whereas semiconductor lasers can be brought to about 30 THz, leaving an opening hiatus in between $0.03 - 30$ THz [30]. This range of frequencies is known in the literature as the *terahertz gap* [29], due to the aforementioned reasons.

Some advances have been achieved in the past decade, concerning the THz production. The most prominent technologies comprise gas lasers, free electron lasers (FEL) and quantum cascade lasers (QCL) [29]. While gas lasers present low efficiency, FEL are bulky and inappropriate for low-power applications. On the other hand, QCL's efficiency has a strong temperature dependence, becoming inadequate for $T > 180$ K, thus not providing a solution for room temperature conditions. At the same time, the recent developments in graphene plasmonics have gathered a great amount of interest in the field of THz-production, mainly due the graphene field-effect transistor (GFET), capable of emitting and detecting THz-radiation. As such, shining a light on graphene dynamics might set the stage towards a future solution to the current technological problem.

1.3 Thesis motivation

Recently, graphene has been pointed out as a way to circumvent the *terahertz gap*, mainly resorting to some unstable regimes that have been studied theoretically in the past [31–33]. It was found that the the small-wavelength plasmon frequencies lie precisely on the THz part of the spectrum. Additionally, the possibility of exciting unstable plasmons within this frequency range puts graphene in the podium for future table-top solutions for the production of THz-radiation. Notwithstanding, some questions remain unanswered, specially in what concerns the mathematical models that have been put forward, which rely on a classical picture of charge transport [34–36]. The linear dispersion relation of electrons and holes in graphene has no classical counterpart, meaning that there is no chance of obtaining such relation, starting from classical laws. However, having set the relevant approximation for the dispersion relation, it is of common approach to simply include that dispersion, "by hand", into a classical Boltzmann-like equation. Such procedure will obviously fail under some conditions, that depend primarily on the temperature and density of the system. Furthermore, the purely quantum nature of the Dirac dispersion relation leads us to think that a good approach would encompass an *ab-initio* quantum formalism, capable of including the dynamics of massless particles into a field equation, where all quantum effects would be recast. To the best of our knowledge, that has not been done successfully so far, and this thesis will concentrate on achieving such a description.

1.4 Thesis objectives and outline

The main goal of the present work is the construction of an *ab initio* formulation, capable of incorporating the quantum nature of charge carriers in graphene. We shall focus on the case of doped graphene,

where the relevant kinetic processes take place on the conduction band, and the role of holes is of less importance. In the ultra-cold limit, the equilibrium of the carriers is dictated by the Fermi-Dirac distribution. Hence, we shall put forward a quantum kinetic equation, based on the Wigner representation of quantum mechanics. Such a formalism will further allow for a hydrodynamical description, based on the microscopic Hamiltonian that models the kinetic dispersion of charge carriers. Furthermore, the interactions will be casted in the mean-field approximation, which provides a closure relation between the Wigner function and the macroscopic density.

To fulfil those objectives, this thesis is organised as follows: in chapter 2, we start by revising the most important concepts of the classical and quantum kinetic theories; the first relies on the definition of a classical distribution function, whose meaning breaks down at the quantum scale; to extend the concept to a quantum regime, we will introduce the Wigner function. In the quantum case, we show how a hydrodynamical model can be constructed starting from a quantum distribution function. We focus on particles with parabolic dispersion relation (thus a well defined mass), which, as we shall see, greatly simplifies our calculations. Moreover, in chapter 3, we repeat the same discussion but for the case of graphene, which comprises a Dirac-like term that introduces further complications. By changing the basis to that of electrons and holes, it will be possible to derive a quantum kinetic equation for electrons and holes. Still on chapter 3, we show how the present formalism is equivalent to the random phase approximation (RPA), by deriving the plasmon dispersion relation. In chapter 4, we rely on the previous kinetic description to build a closed set of hydrodynamical equations. In that scope, we examine the relation between velocity and momentum variables, and determine the validity of the constant mass approximation. Chapter 5 is dedicated to a special configuration of two parallel graphene layers, for which an unstable regime is unveiled. Finally, we draw our main conclusions in chapter 6.

Chapter 2

Kinetic theory and the hydrodynamical limit

2.1 Classical kinetic theory

In plasma physics, the most usual approach to study a classical system is to work with a kinetic description, that relies on the possibility of defining a distribution function $f(\boldsymbol{r}, \boldsymbol{p}, t)$, denoting the average number of particles in a given infinitesimal phase space volume $d\boldsymbol{r}\ d\boldsymbol{p}$, centred in $(\boldsymbol{r}, \boldsymbol{p})$. The density may be expressed in terms of the distribution function as

$$n(\boldsymbol{r}, t) = \int d\boldsymbol{p}\ f(\boldsymbol{r}, \boldsymbol{p}, t), \tag{2.1}$$

which verifies the normalisation condition $\int d\boldsymbol{r} d\boldsymbol{p}\ f(\boldsymbol{r}, \boldsymbol{p}, t) = N$, where N is the total number of particles. In the absence of collisions (or equivalently, for weakly coupled systems) the evolution of the distribution function is governed by theVlasov equation [37]

$$\frac{d}{dt}\ f(\boldsymbol{r}, \boldsymbol{p}, t) = \left(\frac{\partial}{\partial t} + \frac{\boldsymbol{p}}{m} \cdot \boldsymbol{\nabla} + \boldsymbol{F}(\boldsymbol{r}, \boldsymbol{p}, t) \cdot \boldsymbol{\nabla}_{\boldsymbol{p}} \right) f(\boldsymbol{r}, \boldsymbol{p}, t) = 0, \tag{2.2}$$

where $\boldsymbol{\nabla} \equiv \boldsymbol{\nabla}_{\boldsymbol{r}}$ and $\boldsymbol{\nabla}_{\boldsymbol{p}}$ denote the gradient with respect to $\boldsymbol{r}$ and $\boldsymbol{p}$, and $\boldsymbol{F}(\boldsymbol{r}, \boldsymbol{p}, t)$ is the force acting on the particles. In one hand, for a conservative system, the force is usually momentum-independent, and it is convenient to rewrite it in terms of a potential field V, using $\boldsymbol{F}(\boldsymbol{r}, t) = -\boldsymbol{\nabla} V(\boldsymbol{r}, t)$. On the other hand, when the Coulomb interaction plays a major role (which is typically the case of a plasma), we must use the Lorentz force, $\boldsymbol{F}(\boldsymbol{r}, \boldsymbol{p}, t) = \mathcal{Q}[\boldsymbol{\mathcal{E}}(\boldsymbol{r}, t) + \frac{\boldsymbol{p}}{m} \times \boldsymbol{\mathcal{B}}(\boldsymbol{r}, t)]$. $\boldsymbol{\mathcal{E}}(\boldsymbol{r}, t)$ and $\boldsymbol{\mathcal{B}}(\boldsymbol{r}, t)$ denote the macroscopic electric and magnetic fields, while $\mathcal{Q}$ and m are the particle's charge and mass, respectively. Those macroscopic fields must include any external applied fields, as well as the collective fields created by the charges in the system, which verify the Maxwell equations. These can be expressed in terms of the

scalar and vector potential, $\phi(\boldsymbol{r},t)$ and $\boldsymbol{A}(\boldsymbol{r},t)$, related to the macroscopic fields by

$$\boldsymbol{\mathcal{E}} = -\boldsymbol{\nabla}\phi - \frac{\partial \boldsymbol{A}}{\partial t}, \tag{2.3}$$

$$\boldsymbol{\mathcal{B}} = \boldsymbol{\nabla} \times \boldsymbol{A}. \tag{2.4}$$

In the Coulomb gauge[1], we are led to the Poisson scalar and vectorial equations

$$\boldsymbol{\nabla}^2\phi = -\frac{\mathcal{Q}n}{\varepsilon}, \tag{2.5}$$

$$\boldsymbol{\nabla}^2\boldsymbol{A} = -\mu\boldsymbol{J}, \tag{2.6}$$

with ε and μ denoting the medium permittivity and permeability, respectively. In addition, $\boldsymbol{J}(\boldsymbol{r},t)$ is the macroscopic current density (total current per unit area), that can be written as $\boldsymbol{J}(\boldsymbol{r},t) = \mathcal{Q}n(\boldsymbol{r},t)\boldsymbol{u}(\boldsymbol{r},t)$, where $\boldsymbol{u}$ is the averaged velocity. The latter can be found through the distribution function, *viz.*

$$\boldsymbol{u}(\boldsymbol{r},t) = \frac{1}{nm}\int d\boldsymbol{p}\; \boldsymbol{p}\; f(\boldsymbol{r},\boldsymbol{p},t). \tag{2.7}$$

Hence, a solution to (2.5) and (2.6) is readly found[2]

$$\phi(\boldsymbol{r},t) = \frac{\mathcal{Q}}{4\pi\varepsilon}\int d\boldsymbol{r}'d\boldsymbol{p}\; \frac{f(\boldsymbol{r}',\boldsymbol{p},t)}{|\boldsymbol{r}-\boldsymbol{r}'|}, \tag{2.8}$$

$$\boldsymbol{A}(\boldsymbol{r},t) = \frac{\mu\mathcal{Q}}{4\pi m}\int d\boldsymbol{r}'d\boldsymbol{p}\; \boldsymbol{p}\; \frac{f(\boldsymbol{r}',\boldsymbol{p},t)}{|\boldsymbol{r}-\boldsymbol{r}'|}. \tag{2.9}$$

Therefore, the macroscopic fields $\boldsymbol{\mathcal{E}}$ and $\boldsymbol{\mathcal{B}}$ are completely determined by the distribution function, provided the closure relations of (2.8) and (2.9), such that a complete set of equations is established. Moreover, the inclusion of collisions is achieved by adding a collision integral to the r.h.s. (right-hand side) of (2.2), $\mathcal{S}\{f\}$, which is a functional of f and corresponds to the variation in particle's phase space density, due to non conservative effects,

$$\mathcal{S}\{f\} = \left.\frac{\partial f}{\partial t}\right|_{\text{coll}}. \tag{2.10}$$

In a variety of situations, the long-range interactions dominate over short-range two-body interactions (collisions). This situation verifies whenever the average potential energy, ξ_P, for two electrons separated by the mean inter-particle distance, $\overline{r} = n^{-1/3}$, is much smaller than the average kinetic energy, ξ_K. Those can be estimated as $\xi_P = \mathcal{Q}^2 n_0^{1/3}/4\pi\epsilon_0$ and $\varepsilon_K = k_B T$, where T is the temperature, k_B is the Boltzmann constant, and n_0 is the equilibrium density. Therefore, a classical coupling parameter, $\Gamma_C = \xi_P/\xi_K$, can be settled to distinguish between the collisional and non-collisional regimes,

$$\Gamma_C = \frac{\mathcal{Q}^2 n^{1/3}}{4\pi\varepsilon_0 k_B T}. \tag{2.11}$$

[1] $\boldsymbol{\nabla}\cdot\boldsymbol{A} = 0$.

[2] This can be checked resorting to the relation $\boldsymbol{\nabla}^2\frac{1}{|\boldsymbol{r}-\boldsymbol{r}'|} = -4\pi\delta(\boldsymbol{r}-\boldsymbol{r}')$.

The collisionless limit is valid whenever $\Gamma_C \ll 1$. For those cases, the collision integral $\mathcal{S}$ can be neglected. As the value of Γ_C increases, the short-range interactions start to play an important role and the plasma is said to be collisional, or strongly coupled. Eventually, an appropriate form for $\mathcal{S}$ must be included. A recurrent one is that given by the relaxation time approximation (RTA) [37]

$$\mathcal{S}\{f\} \simeq -\frac{f - f_0}{\tau}, \tag{2.12}$$

where f_0 is the equilibrium distribution function, and τ is the characteristic time scale between collisions. The meaning of this term can be understood as follows: the effect of collisions is simply to restore, locally, the equilibrium, so that f reaches f_0 exponentially, within a time-scale of the order of τ. The value of τ should be obtained consistently, *viz.*

$$\tau^{-1}(\boldsymbol{r}, \boldsymbol{p}, t) = \frac{N}{m} \int d\boldsymbol{p}_1 d\Omega \; |\boldsymbol{p}_1 - \boldsymbol{p}| \sigma(|\boldsymbol{p}_1 - \boldsymbol{p}|, \Omega) \; f(\boldsymbol{r}, \boldsymbol{p}, t), \tag{2.13}$$

where $|\boldsymbol{p}_1 - \boldsymbol{p}|\sigma(|\boldsymbol{p}_1 - \boldsymbol{p}|, \Omega)$ is the scattering cross-section, denoting the probability of a particle with momentum $\boldsymbol{p}$ being scattered to a state $\boldsymbol{p}_1$, with relative solid angle Ω. RTA is valid whenever the energy change of the carrier energy per collision is small compared to $k_B T$. The appropriate form of σ should be found regarding the scattering potential between the particles, which in turn requires knowledge of the particular two-body interaction. A famous example is the so-called Rutherford cross-section, defining the scattering of a beam of electrons colliding with a nucleus of charge Ze. In that case, σ reads

$$\sigma(|\boldsymbol{p}_1 - \boldsymbol{p}|, \Omega) = \left(\frac{Ze^2}{8\pi\varepsilon_0 m_e v_0^2} \right)^2 \frac{1}{\sin^4 \frac{\theta}{2}}, \tag{2.14}$$

where θ is the angle between $\boldsymbol{p}$ and $\boldsymbol{p}_1$, m_e is the electron mass and v_0 is the initial velocity of the beam.

2.2 The Wigner formalism

Up to now, we have just been concerned with the classical limit, for which particles are regarded as point-like. Such a condition is verified whenever the De Broglie wavelength, $\Lambda_{\mathrm{DB}} = h/p$, is much smaller than the mean inter-particle distance; equivalently, the quantum degeneracy parameter

$$\chi = \Lambda_{\mathrm{DB}}^3 n, \tag{2.15}$$

must be much smaller than one. Nevertheless, in the case of $\chi \geq 1$, particles may be able to come very close, and quantum effects should not be discarded. If $\chi \gg 1$, a full quantum treatment is mandatory. Moreover, it is convenient to define

$$\Gamma_Q = \frac{\hbar^2 \omega_p^2}{E_F^2}, \tag{2.16}$$

which plays the role of the classical parameter Γ_C for the case of quantum systems, with ω_p denoting the plasma frequency and E_F the Fermi energy [38]. For systems working at the quantum level, the uncer-

tainty principle makes the concept of phase space problematic, because both position and momentum can't be measured simultaneously, and a true phase-space distribution function is not possible to obtain. In other words, due to the commutation relation between $\boldsymbol{r}$ and $\boldsymbol{p}$,

$$[r_i, p_j] = i\hbar\delta_{ij}, \tag{2.17}$$

one cannot localise particles in a specific phase-space point, and a proper distribution function is not possible to construct. Fortunately, in 1932, Wigner first proposed a way of overcoming this difficulty, by defining a *quasi-distribution* function called the Wigner function, denoted by $W(\boldsymbol{r}, \boldsymbol{p}, t)$, with the specific purpose of calculating quantum corrections to thermodynamic equilibrium. What Wigner cleverly realised was that the uncertainty principle does not prevent us from writing a function of both a position and a momentum coordinate, and indeed the statistical information of the system can be transferred to complex-valued functions. Although $\boldsymbol{r}$ and $\boldsymbol{p}$ are not each other's conjugated coordinates, they both give information about the spatial and momentum distributions of the system, which is, in the most generic case, described by a superposition $|\psi(t)\rangle = \sum_\alpha c_\alpha |\psi_\alpha(t)\rangle$. Note that we work in the Schrödinger representation, such that state vectors display a time dependence of the form $|\psi_\alpha(t)\rangle = e^{-i\hat{H}t/\hbar}|\psi_\alpha(0)\rangle$, where $\hat{H}$ is the Hamiltonian operator. The set of coefficients $\{c_\alpha\}$ are related with the probability P_α of finding the system in each $|\psi_\alpha\rangle$ by $P_\alpha = |c_\alpha|^2$, thus verifying $\sum_\alpha |c_\alpha|^2 = 1$. The original definition of the Wigner function reads [39]

$$W(\boldsymbol{r}, \boldsymbol{p}, t) = \sum_\alpha c_\alpha \int \frac{d\boldsymbol{s}}{(2\pi)^d} e^{i\boldsymbol{s}\cdot\boldsymbol{p}/\hbar} \psi_\alpha^*(\boldsymbol{r} + \boldsymbol{s}/2, t)\, \psi_\alpha(\boldsymbol{r} - \boldsymbol{s}/2, t), \tag{2.18}$$

where $\psi_\alpha(\boldsymbol{r}, t) = \langle \boldsymbol{r}|\psi_\alpha(t)\rangle$ is the projection of the wave function onto some orthonormal position basis $|\boldsymbol{r}\rangle$ of a $d-$dimensional space, and the integration runs from $-\infty$ to $+\infty$ (this will always be the case, unless otherwise indicated). Its more general applicability was better recognised in the works of Groenewold [40] and Moyal [41], where it was proposed that this function was nothing but the corresponding function associated with the Weyl transform [42] for the density operator $\hat{\rho}$. The quantum signature is present in the fact that this *quasi-distribution* function may take negative values, and so it cannot be interpreted as a particle density. However, we can easily check in (2.18) that $W^*(\boldsymbol{r}, \boldsymbol{p}, t) = W(\boldsymbol{r}, \boldsymbol{p}, t)$ holds. As we will see, the Wigner representation is very handy to treat the electronic properties in graphene, and its usage might allow for a deeper understanding of quantum effects (for instance, by linking its negative values to interference and scattering phenomena [43]).

The Weyl transform provides a mapping between an operator defined in a n-dimensional Hilbert space and a classical function,

$$\mathcal{T}\{\hat{A}\}(\boldsymbol{r}, \boldsymbol{p}, t) = \int \frac{d\boldsymbol{s}}{(2\pi)^d} e^{i\boldsymbol{s}\cdot\boldsymbol{p}/\hbar} \langle \boldsymbol{r} - \boldsymbol{s}/2|\hat{A}|\boldsymbol{r} + \boldsymbol{s}/2\rangle\,. \tag{2.19}$$

Here, $\mathcal{T}\{...\}$ denotes the Weyl transform, and $\hat{A}$ is the operator subjected to the transformation. It is

simple to verify that (2.19) allows to write

$$\mathrm{Tr}\{\hat{\mathrm{A}}\hat{\mathrm{B}}\} = \int\int \mathrm{d}\boldsymbol{r}\ \mathrm{d}\boldsymbol{p}\ \mathcal{T}\{\hat{\mathrm{A}}\}\ \mathcal{T}\{\hat{\mathrm{B}}\}. \tag{2.20}$$

where $\mathrm{Tr}\{...\}$ is the trace. By defining the density operator as

$$\hat{\rho} = \sum_{\alpha} c_\alpha \left|\psi_\alpha\right\rangle \left\langle\psi_\alpha\right|, \tag{2.21}$$

we can use (2.20) to show that the average value of $\hat{A}$ is given by

$$Tr\{\hat{\rho}\hat{A}\} = \int\int d\boldsymbol{r}\ d\boldsymbol{p}\ W(\boldsymbol{r},\boldsymbol{p},t)\ \mathcal{T}\{\hat{A}\}. \tag{2.22}$$

As such, we further define the (spatial and time dependent) expectation value of an operator as

$$\overline{A}(\boldsymbol{r},t) = \frac{1}{n(\boldsymbol{r},t)} \int d\boldsymbol{p}\ W(\boldsymbol{r},\boldsymbol{p},t)\ \mathcal{T}\{\hat{A}\}, \tag{2.23}$$

where $n(\boldsymbol{r},t)$ is the density. Furthermore, we can immediately see that the marginal probabilities are given as

$$n(\boldsymbol{r},t) = \sum_{\alpha} c_\alpha\ |\psi_\alpha(\boldsymbol{r},t)|^2 = \int d\boldsymbol{p}\ W(\boldsymbol{r},\boldsymbol{p},t), \tag{2.24}$$

$$n(\boldsymbol{p},t) = \sum_{\alpha} c_\alpha\ |\psi_\alpha(\boldsymbol{p},t)|^2 = \int \frac{d\boldsymbol{r}}{(2\pi\hbar)^d}\ W(\boldsymbol{r},\boldsymbol{p},t), \tag{2.25}$$

where $\psi_\alpha(\boldsymbol{p},t)$ is the Fourier transform of $\psi_\alpha(\boldsymbol{r},t)$ (and the same applies to the density). Now, starting from the Schrödinger equation

$$i\hbar\frac{\partial}{\partial t}\psi_\alpha(\boldsymbol{r},t) = \left(-\frac{\hbar^2}{2m}\boldsymbol{\nabla}^2 + V(\boldsymbol{r},t)\right)\psi_\alpha(\boldsymbol{r},t), \tag{2.26}$$

it is convenient to derive an equivalent equation for the time evolution of the Wigner function. Following the general procedure described in [44], we obtain

$$\left(\frac{\partial}{\partial t} + \frac{\hbar\boldsymbol{k}}{m}\cdot\boldsymbol{\nabla}\right)W = \frac{2}{\hbar}\ W\sin\left(\frac{1}{2}\ \overleftarrow{\boldsymbol{\nabla}_{\boldsymbol{k}}}\ \cdot\ \overrightarrow{\boldsymbol{\nabla}}\right)V, \tag{2.27}$$

where we used the relation $\boldsymbol{p} = \hbar\boldsymbol{k}$, and the arrows in the gradient operators refer to its action (either acting on the left or on the right). Note that a function of an operator must be understood using its Taylor expansion. In particular, for the sine-function, we have

$$\sin\left(\hat{A}\right) = \sum_{n=0}^{+\infty} \frac{(-1)^n}{(2n+1)!}\ \hat{A}^{2n+1}. \tag{2.28}$$

The potential in (2.27) should contain the electrostatic term, $V(\boldsymbol{r},t) = \mathcal{Q}\phi(\boldsymbol{r},\boldsymbol{t})$, plus other external EM fields, depending on the specific conditions. The electrostatic potential can be calculated with (2.8), by replacing f directly by W, *i.e.*, using the "quantum" density in the Poisson equation. If we neglect

all other potentials, this models is commonly known as the Wigner-Poisson model[3]. Introducing the definition (2.28) into (2.27), it allows to derive a more handy version for the Wigner transport equation,

$$i\hbar\left(\frac{\partial}{\partial t}+\frac{\hbar\boldsymbol{k}}{m}\cdot\boldsymbol{\nabla}\right)W=\int d\boldsymbol{q}\;e^{i\boldsymbol{q}\cdot\boldsymbol{r}}\;(W_{-}-W_{+})\;V(\boldsymbol{q},t), \tag{2.29}$$

where $V(\boldsymbol{q},t)$ is the Fourier transform of $V(\boldsymbol{r},t)$, and $W_{\pm}=W(\boldsymbol{r},\boldsymbol{k}\pm\boldsymbol{q}/2,t)$. By taking the limit $\hbar\to 0$, we can approximate

$$W_{\pm}\simeq W\pm\frac{\hbar\boldsymbol{q}}{2}\cdot\boldsymbol{\nabla}_{\boldsymbol{p}}W. \tag{2.30}$$

Replacing (2.30) into (2.29), followed by straightforward algebra, yields the ray-tracing (or classical) version of (2.29)

$$\left(\frac{\partial}{\partial t}+\frac{\boldsymbol{p}}{m}\cdot\boldsymbol{\nabla}-\boldsymbol{\nabla}V\cdot\boldsymbol{\nabla}_{\boldsymbol{p}}\right)W(\boldsymbol{r},\boldsymbol{p},t)=0, \tag{2.31}$$

which is nothing more than the Vlasov equation. If, instead, we keep some orders of $\hbar$, we obtain the corresponding semi-classical limits.

To illustrate the power of the Wigner representation, let us derive the dispersion relation of the electron density fluctuations, for a parabolic[4] electron-ion quantum plasma (with mass m_e and m_i, and charge $-e$ and $+eZ$, respectively), in two distinct cases. Given that $m_e/m_i\ll 1$, we can fairly neglect the ion motion, which corresponds to the limit of infinite inertia $m_i\to+\infty$, also known as the jellium model. Hence, the ions merely provide a neutralising positive background for the electronic motion. The potential, in the Hartree approximation, is given by

$$V(\boldsymbol{r},t)=\frac{e^2}{4\pi\varepsilon_0\varepsilon_r}\int d\boldsymbol{r'}\;\frac{n(\boldsymbol{r'},t)}{|\boldsymbol{r}-\boldsymbol{r'}|}\;-\frac{Ze^2n_i}{\varepsilon_0\varepsilon_r}, \tag{2.32}$$

where n is the electron density, n_i is the static background ion density, ε_0 is the vacuum permittivity and ε_r is the relative permittivity of the surrounding medium. It is straightforward to obtain the potential in Fourier space, which is done in D.1 for several cases of interest. In 3-D space, it yields

$$V(\boldsymbol{q},t)=\frac{e^2}{\varepsilon_0\varepsilon_r}\Big[\frac{n(\boldsymbol{q},t)}{q^2}-Zn_i\delta(\boldsymbol{q})\Big], \tag{2.33}$$

where $q\doteq|\boldsymbol{q}|$. In what follows, we consider small perturbations around an equilibrium configuration, keeping the lowest order contributions to the Wigner function. As such, we can write $W(\boldsymbol{r},\boldsymbol{k},t)=W_0(\boldsymbol{k})+\tilde{W}(\boldsymbol{r},\boldsymbol{k},t)$, where W_0 represents the equilibrium configuration, and $\tilde{W}$ allows for a small deviation from equilibrium. Therefore, as suggested by (2.24), we should also write the density as $n=n_0+\tilde{n}$, such that $n=\int d\boldsymbol{k}\;W_0$ and $\tilde{n}=\int d\boldsymbol{k}\;\tilde{W}$. Introducing these two expansions into (2.29) and neglecting second order quantities, we get

$$\tilde{W}(\boldsymbol{q},\boldsymbol{k},\omega)=\frac{e^2}{\varepsilon_0 q^2}\frac{W_0(\boldsymbol{k}-\boldsymbol{q}/2)-W_0(\boldsymbol{k}+\boldsymbol{q}/2)}{\hbar(\omega-\hbar\boldsymbol{k}\cdot\boldsymbol{q}/m_e)}\;\tilde{n}(\boldsymbol{q},\omega). \tag{2.34}$$

[3]This model is also called the Hartree model, because it is equivalent, at the single particle level, to the Hartree approximation for the one-particle Green's function.

[4]Parabolic refers to the kinetic term for electrons in the Schrödinger equation, $\hbar^2\boldsymbol{\nabla}^2/2m_e$, which reduces to the term $\hbar\boldsymbol{k}\cdot\boldsymbol{\nabla}/m_e$ in the Wigner equation. We will see shortly that this is not always the case.

Integrating over the $\boldsymbol{k}$-coordinate, the latter yields

$$1 = \frac{e^2}{\varepsilon_0 \varepsilon_r m_e q^2} \int d\boldsymbol{k} \, \frac{W_0(\boldsymbol{k} - \boldsymbol{q}/2) - W_0(\boldsymbol{k} + \boldsymbol{q}/2)}{\hbar(\omega - \hbar \boldsymbol{k} \cdot \boldsymbol{q}/m_e)}. \tag{2.35}$$

Two distinct cases will be considered: first, let us solve (2.35) for $W_0(\boldsymbol{k}) = n_0 \delta(\boldsymbol{k} - \boldsymbol{k}_0)$, where $n_0 = N/V$, which is valid in the case of a mono-energetic beam of electrons moving across the system with fluid velocity[5] $\boldsymbol{v}_0 = \hbar \boldsymbol{k}_0 / m_e$, in the limit of low temperature. The dispersion relation gives

$$\left[\omega(\boldsymbol{q}) - \boldsymbol{v}_0 \cdot \boldsymbol{q}\right]^2 = \omega_p^2 + \frac{\hbar^2 q^4}{4 m_e^2}, \tag{2.36}$$

where $\omega_p^2 = n_0 e^2 / \varepsilon_0 \varepsilon_r m_e$ is the usual plasma frequency for electrons, and the second term is the first non-zero quantum contribution, for plasma oscillations, in the case of a 3D electron plasma [45]. The second term on the l.h.s. (left-hand side) represents a Doppler shift [46]. This relation introduces dispersion, even at zero temperature, which is not predicted by the classical theory of electron-ion plasmas.

Secondly, we consider the case of small wave-numbers and high frequency. A more convoluted calculation, given in Appendix B.1, leads to the Bohm-Pines dispersion relation [46],

$$\omega(\boldsymbol{q})^2 = \omega_p^2 + 3 q^2 u_\parallel^2 + \frac{\hbar^2 q^4}{4 m_e^2}, \tag{2.37}$$

where $u_\parallel^2$ is the equilibrium value for the parallel velocity, with respect to the direction of propagation. Equation (2.37) serves as the quantum counterpart of the Bohm–Gross dispersion relation of high frequency electron plasma waves [47], and is valid no matter the form of W_0 (as far as small wave numbers and high frequencies are concerned). The term $\sim q^4$ is again the first quantum contribution, setting the distinction between classical and quantum longitudinal electronic oscillations.

This approach is general and powerful, as we may replace the Schrödinger equation by some other equation, governing the time evolution of the wave-function. Although being equivalent to the Hartree approximation, the present procedure turns out to be more practical in treating systems far from equilibrium, such as the case of plasma instabilities, with the configuration being solely defined by W_0. In Ref. [48], the same approach was followed for the case of an electron-positron quantum pair plasmas, where (2.27) is slightly modified due to an extra non-linear term added to the Shrödinger-Poisson system, accounting for the electron-positron density. Similar examples, for the case of the Gross–Pitaevskii equation modelling dynamics of a Bose-Einstein condensate, can be found in [49, 50].

2.3 Quantum hydrodynamical model

The kinetic theory using the Wigner description, although not always providing the most convenient set of equations, is a good starting point for more practical models. By computing the moments of the Wigner equation, under some assumptions that will be discussed shortly, we are capable of obtaining a new set of equations that govern the evolution of averaged quantities. These so called hydrodynamical models

[5] This situation is often referred to in the literature as one-stream plasma.

are valid for both the classical limit and quantum limits, depending on whether we use the classical distribution function or the Wigner function. The first quantum hydrodynamical model was introduced by Manfredi et al. [51]. Subsequently, several variants of these models have been used in many-body charged quantum systems, to study a variety of effects, such as attractive ion forces in warm-dense plasmas [52]; electronic instabilities in piezoelectric semiconductors [53]; ultrafast electronic dynamics in metallic thin films [54]; breather modes in semiconductor quantum wells [55]; magnetosonic waves in degenerate dusty plasmas [56][6]; or even more fundamental scenarios, such as a particles in a thermal bath, to investigate quantum dissipation and diffusion [57]. In the majority of these cases, a closure condition is needed, relating the effective potential with the density, which can be achieved, in the Hartree approximation, via the Poisson equation. When the interaction with photons plays a role, it is convenient to couple with other Maxwell equations.

In order to go from a kinetic theory to a fluid set of equations it is common to start with the macroscopic variables n and $\overline{\boldsymbol{p}}$, which respectively denote the density and the fluid (or averaged) momentum, written with respect to the Wigner function as

$$n(\boldsymbol{r},t) = \int d\boldsymbol{k}\; W(\boldsymbol{r},\boldsymbol{k},t), \tag{2.38}$$

$$\overline{\boldsymbol{p}}(\boldsymbol{r},t) = \frac{1}{n(\boldsymbol{r},t)} \int d\boldsymbol{k}\; \hbar\boldsymbol{k}\; W(\boldsymbol{r},\boldsymbol{k},t). \tag{2.39}$$

Usually, the set of macroscopic variables contains the averaged velocity $\overline{\boldsymbol{v}}$ instead of the averaged momentum $\overline{\boldsymbol{p}}$, when these are related by a momentum-independent mass, $\overline{\boldsymbol{v}} = \overline{\boldsymbol{p}}/m$. As long the latter holds, it is a matter of choice to use one or the other. However, as we shall see in the next chapters, for a linear kinetic term, the velocity field is not well defined, and the formulation in terms of the averaged momentum (or averaged wave-vector) is mandatory. Since phase-space variables do not depend on time (only their averages do), applying a partial derivative with respect to time to both sides of (2.38) and (2.39), it yields

$$\frac{\partial n}{\partial t} = \int d\boldsymbol{k}\; \Big[-\frac{\hbar}{m}\boldsymbol{k}\cdot\boldsymbol{\nabla}W + \frac{i}{\hbar}\int d\boldsymbol{q}\; e^{i\boldsymbol{r}\cdot\boldsymbol{r}}\big(W_+ - W_-\big)V(\boldsymbol{q},t)\Big], \tag{2.40}$$

$$\frac{\partial(n\overline{\boldsymbol{p}})}{\partial t} = \int d\boldsymbol{k}\; \hbar\boldsymbol{k}\; \Big[-\frac{\hbar}{m}\boldsymbol{k}\cdot\boldsymbol{\nabla}W + \frac{i}{\hbar}\int d\boldsymbol{q}\; e^{i\boldsymbol{r}\cdot\boldsymbol{r}}\big(W_+ - W_-\big)V(\boldsymbol{q},t)\Big], \tag{2.41}$$

where $W \equiv W(\boldsymbol{r},\boldsymbol{k},t)$ and $W_\pm = W(\boldsymbol{r},\boldsymbol{k}\pm\boldsymbol{q}/2,t)$. These integrals are calculated in Appendix B.2, and we simply present the results here. Equation (2.40) yields the continuity equation

$$\frac{\partial n}{\partial t} + \frac{1}{m}\boldsymbol{\nabla}\cdot\big(n\overline{\boldsymbol{p}}\big) = 0, \tag{2.42}$$

whereas (2.41) yields the force (or the momentum conservation) equation

$$\Big(\frac{\partial}{\partial t} + \frac{\overline{\boldsymbol{p}}}{m}\cdot\boldsymbol{\nabla}\Big)\overline{\boldsymbol{p}} = -\frac{1}{n}\boldsymbol{\nabla}P - \boldsymbol{\nabla}V, \tag{2.43}$$

[6] In Ref. [56], spin effects and exchange correlations are included in the results. The corresponding dispersion relations are calculated, in several configurations for the electric and magnetic fields.

where P is the pressure-tensor

$$P_{ij}(\boldsymbol{r},t) = \frac{n}{m}\Big(\overline{p_i p_j} - \overline{p_i}\,\overline{p_j}\Big). \tag{2.44}$$

We stress the fact that (2.42) is equal to its classical version, despite the averaged values being calculated with the Wigner function instead. On the contrary, (2.43) contains quantum contributions, present in the pressure-term. However, they only become evident after some manipulation, which will be done shortly. In terms of the averaged velocity,

$$\boldsymbol{u} = \overline{\boldsymbol{v}} = \frac{\overline{\boldsymbol{p}}}{m}, \tag{2.45}$$

the set of equations read[7]

$$\frac{\partial n}{\partial t} + \frac{\partial\big(nu_j\big)}{\partial r_j} = 0, \tag{2.46}$$

$$\frac{\partial u_i}{\partial t} + u_j\frac{\partial u_i}{\partial r_j} = -\frac{1}{nm}\frac{\partial P_{ij}}{\partial r_j} - \frac{1}{m}\frac{\partial V}{\partial r_i}, \tag{2.47}$$

$$P_{ij} = nm\big(\overline{v_i v_j} - u_i u_j\big), \tag{2.48}$$

More equations could be included by applying the same procedure to higher moments. The third natural equation would be the conservation equation for the quantity $n\overline{\boldsymbol{pp}}/2m$, which would give us the evolution of the averaged energy density. Repeating the process for higher and higher orders would lead to an hierarchy of equations, but our present model gives us enough information for the moment. The system of equations (2.46) and (2.47) takes into account diffraction, but neglects other quantum phenomena, like spin effects or exchange, as well as relativistic corrections. These, however, play a minimal role in a variety of quantum plasma systems [58].

Recalling the definition of (2.18), we may write (see Appendix B.3 for details)

$$n(\boldsymbol{r},t) = \sum_\alpha c_\alpha |\psi_\alpha(\boldsymbol{r},t)|^2, \tag{2.49}$$

$$n(\boldsymbol{r},t)\boldsymbol{u}(\boldsymbol{r},t) = \frac{i\hbar}{2m}\sum_\alpha c_\alpha\Big(\psi_\alpha\boldsymbol{\nabla}\psi_\alpha^* - \psi_\alpha^*\boldsymbol{\nabla}\psi_\alpha\Big), \tag{2.50}$$

as well as the intricate expression for the pressure

$$\begin{aligned} P_{ij}(\boldsymbol{r},t) = {}& \frac{\hbar^2}{4m}\sum_\alpha c_\alpha\left(\left|\frac{\partial\psi_\alpha^*}{\partial r_i}\frac{\partial\psi_\alpha}{\partial r_j}\right|^2 - \psi_\alpha\frac{\partial^2\psi_\alpha^*}{\partial r_i\partial r_j} - \psi_\alpha^*\frac{\partial^2\psi_\alpha}{\partial r_i\partial r_j}\right) \\ & + \frac{\hbar^2}{4mn}\sum_{\alpha,\beta} c_\alpha c_\beta\left(\psi_\alpha\frac{\partial\psi_\alpha^*}{\partial r_i} - \psi_\alpha^*\frac{\partial\psi_\alpha}{\partial r_i}\right)\left(\psi_\beta\frac{\partial\psi_\beta^*}{\partial r_j} - \psi_\beta^*\frac{\partial\psi_\beta}{\partial r_j}\right). \end{aligned} \tag{2.51}$$

We can readly recognise (2.50) as the usual quantum mechanical probability current of a superposition of states. Furthermore, by introducing the Madelung representation[8] [59] for each state ψ_α,

$$\psi_\alpha(\boldsymbol{r},t) = A_\alpha(\boldsymbol{r},t)e^{iS_\alpha(\boldsymbol{r},t)/\hbar}, \tag{2.52}$$

[7] We use Einstein's convention for repeated indices, and it will be used henceforth, used unless otherwise stated.

[8] Note that the Madelung representation is simply the most generic way of representing a complex number $\psi = Ae^{iS/\hbar}$, parameterised by real amplitude and phase fields A and $S/\hbar$. Because ψ depends on position and time, we should allow, in principle, for a space and time dependence on both the amplitude and the phase.

into (2.49)−(2.51), we get

$$n(\boldsymbol{r},t) = \sum_{\alpha} c_\alpha A_\alpha^2, \tag{2.53}$$

$$\boldsymbol{u}(\boldsymbol{r},t) = \frac{1}{nm}\sum_{\alpha} c_\alpha A_\alpha^2 \boldsymbol{\nabla} S_\alpha, \tag{2.54}$$

and

$$\begin{aligned} P_{ij}(\boldsymbol{r},t) = \frac{\hbar^2}{2m}\sum_{\alpha} c_\alpha \Big(\frac{\partial A_\alpha}{\partial r_i}\frac{\partial A_\alpha}{\partial r_j} - A_\alpha \frac{\partial^2 A_\alpha}{\partial r_i \partial r_j}\Big) - \frac{1}{2m}\sum_{\alpha} c_\alpha A_\alpha^2 \Big(\frac{\partial S_\alpha}{\partial r_i} - \frac{\partial S_\alpha}{\partial r_j}\Big)^2 \\ + \frac{1}{2mn}\sum_{\alpha\beta} c_\alpha c_\beta A_\alpha^2 A_\beta^2 \Big(\frac{\partial S_\alpha}{\partial r_i} - \frac{\partial S_\beta}{\partial r_j}\Big)^2. \end{aligned} \tag{2.55}$$

The first term in the pressure-tensor has now an explicit $\hbar-$dependence, which exposes its quantum nature. Besides that, there is also an implicit $\hbar-$dependence on the amplitudes and phases of the Madelung representation, as each of them is a solution to the Schrödinger equation of (2.26), which, in its turn, contains $\hbar$. Strictly speaking, equations (2.53)−(2.55) are purely quantum. However, we will identify a "classical" term on the pressure by comparing it with the expected expression for the classical limit. This becomes clear after the identification of the amplitudes A_α and phases S_α with two "classical" velocity fields $\boldsymbol{V}_\alpha$ (kinetic velocity) and $\tilde{\boldsymbol{V}}_\alpha$ (osmotic velocity)[9]

$$V_{\alpha i} = \frac{1}{m}\frac{\partial S_\alpha}{\partial r_i}, \tag{2.56}$$

$$\tilde{V}_{\alpha i} = \frac{\hbar}{m}\frac{\partial \ln A_\alpha}{\partial r_i}, \tag{2.57}$$

where the index i denotes each component, *i.e.*, $\boldsymbol{V}_\alpha = (V_{\alpha x}, V_{\alpha y}, V_{\alpha z})$ and $\tilde{\boldsymbol{V}}_\alpha = (\tilde{V}_{\alpha x}, \tilde{V}_{\alpha y}, \tilde{V}_{\alpha z})$. Both $\boldsymbol{V}_\alpha$ and $\tilde{\boldsymbol{V}}_\alpha$ have dimension of velocity, as they are the natural velocities that can be made up from A_α and S_α. The kinetic velocity is related to the phase velocity of each state α, whereas the osmotic velocity follows the density gradient. $\boldsymbol{V}_\alpha$ and $\tilde{\boldsymbol{V}}_\alpha$ are purely quantum, as a result of their dependence on A_α and S_α, which, in turn, depend on $\hbar$ implicitly. Contrarily, $\boldsymbol{u}$ has a classical counterpart, coming from the classical limit of (2.54)[10], as the Wigner function is replaced by the classical distribution function. The pressure-tensor can be written in terms of the new velocity fields as

$$P_{ij}(\boldsymbol{r},t) = P_{ij}^K(\boldsymbol{r},t) + P_{ij}^O(\boldsymbol{r},t) + P_{ij}^Q(\boldsymbol{r},t) \tag{2.58}$$

where

$$P_{ij}^K(\boldsymbol{r},t) = \frac{nm}{2}\sum_{\alpha\beta} c'_\alpha c'_\beta (V_{\alpha i} - V_{\beta j})^2 - \frac{nm}{2}\sum_{\alpha} c'_\alpha (V_{\alpha i} - V_{\alpha j})^2, \tag{2.59}$$

$$P_{ij}^O(\boldsymbol{r},t) = \frac{nm}{2}\sum_{\alpha\beta} c'_\alpha c'_\beta (\tilde{V}_{\alpha i} - \tilde{V}_{\beta j})^2 - \frac{nm}{2}\sum_{\alpha} c'_\alpha (\tilde{V}_{\alpha i} - \tilde{V}_{\alpha j})^2, \tag{2.60}$$

[9] Do not confuse $\tilde{\boldsymbol{V}}_\alpha$ with a first order quantity, following a previous definition which uses the same symbol ($\sim$). $\tilde{\boldsymbol{V}}_\alpha$ contains all orders, and represents a velocity field.

[10] Note that this is also a function of n, which in turn is given by (2.53).

$$P_{ij}^{Q}(\boldsymbol{r},t) = -\frac{\hbar^2 n}{4m}\frac{\partial^2 \ln n}{\partial r_i \partial r_j}. \tag{2.61}$$

We also defined the new set of coefficients $\{c'_\alpha(\boldsymbol{r},t)\}$ as

$$c'_\alpha(\boldsymbol{r},t) = \frac{c_\alpha A_\alpha^2(\boldsymbol{r},t)}{n}, \tag{2.62}$$

which verify $\sum_\alpha c'_\alpha = 1$. This property permits to establish a new average value for functions defined in the Hilbert space spanned by $\{\psi_\alpha\}$ as follows:

$$\langle g \rangle = \sum_\alpha c'_\alpha g_\alpha. \tag{2.63}$$

With this definition, we obtain

$$P_{ij}^{K}(\boldsymbol{r},t) = nm\Big(\langle V_i V_j\rangle - \langle V_i\rangle\langle V_i\rangle\Big), \tag{2.64}$$

$$P_{ij}^{O}(\boldsymbol{r},t) = nm\Big(\langle \tilde{V}_i \tilde{V}_j\rangle - \langle \tilde{V}_i\rangle\langle \tilde{V}_j\rangle\Big), \tag{2.65}$$

It is important to make a side note here: the exact calculation of P_{ij}^K and P_{ij}^O would require knowledge of a complete set of wave-functions, which in turn would come as a solution to the Schrödinger equations. However, such a procedure would offer no advantage over the direct computation of the Wigner function, which solves the problem exactly. Indeed, one of the strong points of this hydrodynamical formulation comes from the fact that the exact knowledge of the Wigner function is not necessary. Instead, we are led to a simpler model involving hydrodynamical variables. Following this reasoning, and knowing that the kinetic and osmotic pressures are related with velocity dispersion, it is a rather standard approach to set $P_{ij}^K + P_{ij}^O \simeq P_{ij}^C$, where P_{ij}^C is generically called the classical pressure. Then, one uses an equation of state to close the system, *i.e*, one finds a relation between the classical pressure and the density,

$$P_{ij}^{C} \equiv P_{ij}^{C}(n). \tag{2.66}$$

Hence, the total pressure P_{ij} now comprises a classical and a quantum contribution

$$P_{ij} = P_{ij}^{C}(n) - \frac{\hbar^2 n}{4m}\frac{\partial^2 \ln n}{\partial r_i \partial r_j}. \tag{2.67}$$

A convenient equation of state for P_{ij}^C, in the case of a strongly degenerate ($d-$dimensional) fermionic system at low temperatures is [60]

$$P_{ij}^{C} = \delta_{ij}\frac{n_0 m v_F^2}{d+2}\Big(\frac{n}{n_0}\Big)^{\frac{d+2}{d}}, \tag{2.68}$$

where v_F is the Fermi velocity, related to the Fermi wave-vector k_F by $v_F = \hbar k_F/m$. The term $(n(\boldsymbol{r},t)/n_0)^{(d+2)/d}$ extends the equilibrium result to an inhomogeneous configuration, via a local ap-

proximation. Finally, our complete models reads

$$\frac{\partial n}{\partial t} + \frac{\partial\big(nu_j\big)}{\partial r_j} = 0, \tag{2.69}$$

$$\frac{\partial u_i}{\partial t} + u_j\frac{\partial u_i}{\partial r_j} = -\frac{1}{nm}\frac{\partial P_{ij}^C}{\partial r_j} - \frac{1}{m}\frac{\partial V}{\partial r_i} + \frac{\hbar^2}{2m^2}\frac{\partial}{\partial r_i}\Big(\frac{\boldsymbol{\nabla}^2\sqrt{n}}{\sqrt{n}}\Big), \tag{2.70}$$

$$V(\boldsymbol{r},t) = \frac{\mathcal{Q}^2}{4\pi\varepsilon}\int d\boldsymbol{r}'\,\frac{n(\boldsymbol{r}',t)}{|\boldsymbol{r}-\boldsymbol{r}'|}, \tag{2.71}$$

$$P_{ij}^C = P_{ij}^C(n), \tag{2.72}$$

where we used the relation (see Appendix B.4)

$$\frac{1}{nm}\frac{\partial P_{ij}^Q}{\partial r_j} = -\frac{\hbar^2}{2m^2}\frac{\partial}{\partial r_i}\Big(\frac{\boldsymbol{\nabla}^2\sqrt{n}}{\sqrt{n}}\Big), \tag{2.73}$$

which allows us to write the quantum pressure term in the form of a quantum potential [61]. The latter is mathematically related with the quantum pressure but, physically, plays the role of an effective potential, which contributes to a quantum (Bohm) force, responsible for phenomena like wave-packet spreading or tunneling [62, 63].

To conclude, let us briefly mention some strengths and drawbacks of this (real space) formulation. We started by integrating the Wigner transport equation (2.29) multiplied by powers of momentum, which provided us a complete model for the evolution of averaged quantities. The main advantage of this model is that it is solvable without the need of calculating the Wigner function. As we showed, the aforementioned hydrodynamical model presents a much simpler solution, by describing the system using a smaller set of variables, upon which all other quantities, like the pressure or the interacting potential, depend on. In principle, there are no restrictions over these two variables, except that of being smooth functions. Moreover, the system of equations (2.69)$-$(2.72) is closed, by assuming an equation of state for the classical pressure, as suggested by (2.72). The choice of P^C may be able to retain some spin properties, like the fermionic or bosonic statistics. Nonetheless, higher order spin effects or magnetic field interactions where ignored, since only the electrostatic limit is treated. Taking into account magnetic-field interactions is straightforward, which can be done via the minimal coupling procedure, $\boldsymbol{p} \to \boldsymbol{p} - \mathcal{Q}\boldsymbol{A}$. Spin transport can also be included by adding another macroscopic variable, denoting the spin polarization density, and applying the same procedure [64, 65]. Higher order contributions of the Coulomb interaction have also been considered, in the scope of hydrodynamic theory [66, 67]. In the case of low temperatures and sufficiently high densities, it has been demonstrated that those play an important role [68–70]. Furthermore, on the grounds of the hydrodynamical approximation, the validity of the model is limited to the long wavelength limit, $q \ll \omega_p/v_F$. Shorter length scales cannot be resolved, as well as relativistic phase velocities, such that the condition $\omega/q < c$ must be verified. We also note that some effects, as Landau damping or instabilities, can only be accomplished with the complete information contained in the Wigner equation (2.27), since these are purely kinetic phenomena that rely on wave-particle interaction, and are not captured hydrodynamically [71].

Chapter 3

Wigner description of graphene

In this chapter, we introduce the main subject of this thesis. Our goal is to construct the Wigner function for quasi-electrons and quasi-holes in graphene, following the prescription given in the last chapter. As we will see, the effective Hamiltonian that describes this system is unusual, mostly because the kinetic term is linear (and not quadratic) in the momentum coordinate. Hence, we start by revising the graphene band structure, which is then incorporated into the Schödinger equation. Then, the Schrödinger-Poisson model is settled, which will lead to a peculiar modification in the Wigner transport equation.

3.1 Graphene band structure

Graphene refers to a monolayer of carbon atoms, arranged in an hexagonal structure. To cast the graphene geometry, we choose the coordinate system depicted in the left panel of Fig. 3.1, together with the lattice vectors $\boldsymbol{a_i}$. Each unit cell contains two carbon atoms that belong to different sublattices, A and B. The unit cells form a hexagonal Bravais lattice $\{\boldsymbol{R}\}_{\boldsymbol{l}}$, with positions

$$\boldsymbol{R_l} = n_i \boldsymbol{a_1} + n_j \boldsymbol{a_2}, \tag{3.1}$$

where $\boldsymbol{l} = (i, j)$ and $n_i, n_j \in \mathbb{Z}$. The lattice vectors are

$$\boldsymbol{a_1} = a\left(\frac{1}{2}, \frac{\sqrt{3}}{2}\right) \ , \quad \boldsymbol{a_2} = a\left(-\frac{1}{2}, \frac{\sqrt{3}}{2}\right) \ , \tag{3.2}$$

where $a \approx 2.6\,\text{Å}$ is the lattice parameter [72], which is related to the carbon-carbon distance d_c by $d_c = a/\sqrt{3}$. We also construct the reciprocal lattice $\{G\}_{\boldsymbol{l}}$

$$\boldsymbol{G_l} = m_i \boldsymbol{b_1} + m_j \boldsymbol{b_2}, \tag{3.3}$$

by imposing $\boldsymbol{a}_i \cdot \boldsymbol{b}_j = 2\pi\delta_{ij}$. This leads to

$$\boldsymbol{b_1} = \frac{4\pi}{3\sqrt{3}a}\left(\frac{\sqrt{3}}{2}, \frac{1}{2}\right), \quad \boldsymbol{b_2} = \frac{4\pi}{3\sqrt{3}a}\left(-\frac{\sqrt{3}}{2}, \frac{1}{2}\right). \tag{3.4}$$

By comparing the vectors $\boldsymbol{a}_i$ with $\boldsymbol{b}_i$ we conclude that the reciprocal lattice will also be hexagonal, yielding the structure depicted in the right panel of Fig. 3.1.

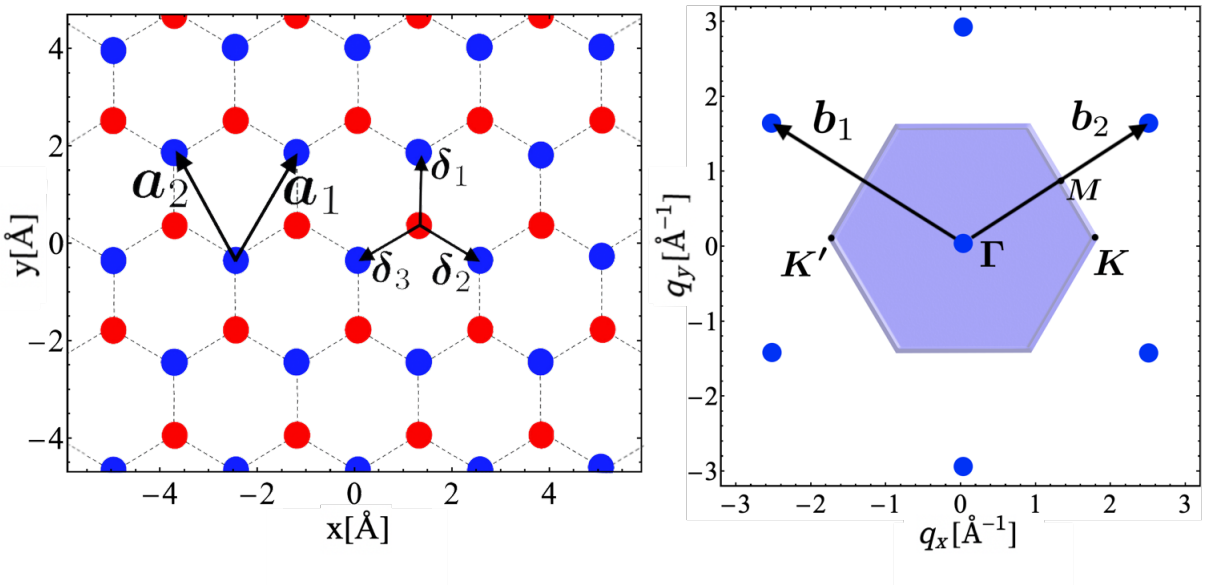

Figure 3.1: Left panel : Real lattice. The honeycomb structure can be seen as two inter-penetrating triagonal sublattices of carbon atoms, A (red) and B (blue). Right panel : Reciprocal lattice. The solid filling highlights the first Brillouin zone, with its two inequivalent corners $\boldsymbol{K}$ and $\boldsymbol{K'}$.

An isolated carbon atom has electronic configuration $1s^2\ 2s^2\ 2p^2$; whereas in graphene, among the four outer electrons, three of them are arranged in an sp_2 an hybridization and form an in-plane covalent σ-bounds. The remaining p_z electron is delocalized, and is responsible for most of the graphene electronic properties. In order to effectively describe the electron dynamics, we use a simple tight-binding model. In general, within the second quantization procedure, the Hamiltonian for the free motion of the system may be generically written as

$$\begin{aligned}\hat{H} = \sum_{ll'} \Big(&\hat{a}_l^\dagger \langle A, \boldsymbol{R_l}|\hat{H}|A, \boldsymbol{R_{l'}}\rangle \hat{a}_{l'} \ + \ \hat{a}_l^\dagger \langle A, \boldsymbol{R_l}|\hat{H}|B, \boldsymbol{R_{l'}}\rangle \hat{b}_{l'} \\ &+ \hat{b}_l^\dagger \langle B, \boldsymbol{R_l}|\hat{H}|A, \boldsymbol{R_{l'}}\rangle \hat{a}_{l'} \ + \ \hat{b}_l^\dagger \langle B, \boldsymbol{R_l}|\hat{H}|B, \boldsymbol{R_{l'}}\rangle \hat{b}_{l'} \Big) ,\end{aligned} \tag{3.5}$$

where $\hat{a}_l^\dagger/\hat{a}_{l'}$ ($\hat{b}_l^\dagger/\hat{b}_l$) creates/annihilates an electron of lattice A (B) in site $\boldsymbol{R_l}$. In the tight-binding approximation, we only allow hopping between nearest neighbour sites, therefore setting the matrix elements

to

$$\langle S_i, \boldsymbol{R_l}|\hat{H}|S_j, \boldsymbol{R_{l'}}\rangle = \begin{cases} \xi_{p_z} & \text{if } i = j \text{ and } \boldsymbol{R_l} = \boldsymbol{R_{l'}}, \\ -t & \text{if } i \neq j \text{ and } \boldsymbol{R_l} = \boldsymbol{R_{l'}} + \boldsymbol{\delta}, \\ 0 & \text{otherwise}, \end{cases} \tag{3.6}$$

where $S_i \in \{A, B\}$. Moreover, ξ_{p_z} is the kinetic energy of the p_z orbital, $t \approx 2.97$ eV is the hopping integral [8] and

$$\boldsymbol{\delta} \in \left\{ \; d_c(0,1) \; , \; d_c(\tfrac{\sqrt{3}}{2}, -\tfrac{1}{2}) \; , \; d_c(-\tfrac{\sqrt{3}}{2}, -\tfrac{1}{2}) \quad \right\}, \tag{3.7}$$

are the vectors depicted in left panel of Fig. 3.1. Furthermore, we are also free to set the energy ξ_{p_z} to zero, keeping in mind that any energy value will be measured relatively to ξ_{p_z}. Thus, we obtain

$$\hat{H} = -t \sum_{\boldsymbol{l\delta}} \left(\hat{a}^\dagger_{\boldsymbol{l}} \hat{b}_{\boldsymbol{l}+\boldsymbol{\delta}} + \hat{b}^\dagger_{\boldsymbol{l}+\boldsymbol{\delta}} \hat{a}_{\boldsymbol{l}} \right), \tag{3.8}$$

Expanding the operators in the momentum basis, it gives

$$\hat{a}^\dagger_{\boldsymbol{l}} = \frac{1}{\sqrt{N/2}} \sum_{\boldsymbol{q}} a^\dagger_{\boldsymbol{q}} \; e^{i\boldsymbol{q}\cdot\boldsymbol{R_l}}, \tag{3.9}$$

$$\hat{b}^\dagger_{\boldsymbol{l}} = \frac{1}{\sqrt{N/2}} \sum_{\boldsymbol{q}} b^\dagger_{\boldsymbol{q}} \; e^{i\boldsymbol{q}\cdot\boldsymbol{R_l}}, \tag{3.10}$$

where $N/2$ is the total number of carbon atoms in each sublattice and $\boldsymbol{q} = (q_x, q_y)$ is the 2-D wave-vector. Using these expression into (3.8), it yields

$$\hat{H} = -t \sum_{\boldsymbol{\delta},\boldsymbol{q}} \left(e^{-i\boldsymbol{q}\cdot\boldsymbol{\delta}} \hat{a}^\dagger_{\boldsymbol{q}} \hat{b}_{\boldsymbol{q}} + e^{i\boldsymbol{q}\cdot\boldsymbol{\delta}} \hat{b}^\dagger_{\boldsymbol{q}} \hat{a}_{\boldsymbol{q}} \right). \tag{3.11}$$

Electrons must obey anti-commutation relations, so we also impose

$$\{\hat{a}_{\boldsymbol{q}}, \hat{a}^\dagger_{\boldsymbol{q'}}\} = \delta_{\boldsymbol{qq'}}, \tag{3.12}$$

$$\{\hat{b}_{\boldsymbol{q}}, \hat{b}^\dagger_{\boldsymbol{q'}}\} = \delta_{\boldsymbol{qq'}}, \tag{3.13}$$

whereas anti-commutators between any two other operators are set to zero. By defining $\Phi^T_{\boldsymbol{q}} = \left(\hat{a}_{\boldsymbol{q}} \;\; \hat{b}_{\boldsymbol{q}} \right)$, (3.11) can be rewritten as

$$\hat{H} = \sum_{\boldsymbol{q}} \; \Phi^\dagger_{\boldsymbol{q}} \; \mathcal{H}(\boldsymbol{q}) \; \Phi_{\boldsymbol{q}}, \tag{3.14}$$

where

$$\mathcal{H}(\boldsymbol{q}) = \begin{pmatrix} 0 & -t\Delta \\ -t\Delta^* & 0 \end{pmatrix}, \tag{3.15}$$

and

$$\Delta(\boldsymbol{q}) = \sum_{\delta} e^{-i\boldsymbol{q}\cdot\boldsymbol{\delta}}. \tag{3.16}$$

The energy bands are easily obtained by calculating the eigen-values as

$$\mathcal{H}(\boldsymbol{q})\Phi_{\boldsymbol{q}} = \xi(\boldsymbol{q})\Phi_{\boldsymbol{q}}. \tag{3.17}$$

We find the eigen-frequencies

$$\omega(\boldsymbol{q}) = \pm\frac{t}{\hbar}\left[4\cos\left(\frac{\sqrt{3}d_c}{2}q_x\right)\cos\left(\frac{3d_c}{2}q_y\right) + 2\cos\left(\sqrt{3}d_c q_x\right) + 3\right]^{1/2}, \tag{3.18}$$

which are related to the energies by $\xi(\boldsymbol{q}) = \hbar\omega(\boldsymbol{q})$. These two branches are depicted in Fig. 3.2. As one can see, the graphene band structure is that of a zero-gap semi-conductor, with both band intersecting at $\xi(\boldsymbol{q}) = 0$, for $\boldsymbol{q} \in \{\boldsymbol{K}, \boldsymbol{K'}\}$. These two point belong to the vertices of the first Brillouin zone, and are given by $(\pm 4\pi/(3\sqrt{3}d_c), 0)$. In neutral graphene, each carbon atom has one orbital available and contributes with one electron. Due to spin degeneracy, each orbital gets filled with two electrons, which gives, at zero doping, a half-filled configuration, *i.e.*, the valence band gets completely filled, and the conduction band is unoccupied. Therefore, the Fermi surface is located at these two edges of the Brillouin zone, and the low energy excitations will happen around them. As we will see right after, the dynamics encompassing these two points is given, for sufficiently low deviations, by a Dirac-like Hamiltonian. For that reason, $\boldsymbol{K}$ and $\boldsymbol{K'}$ are called Dirac points.

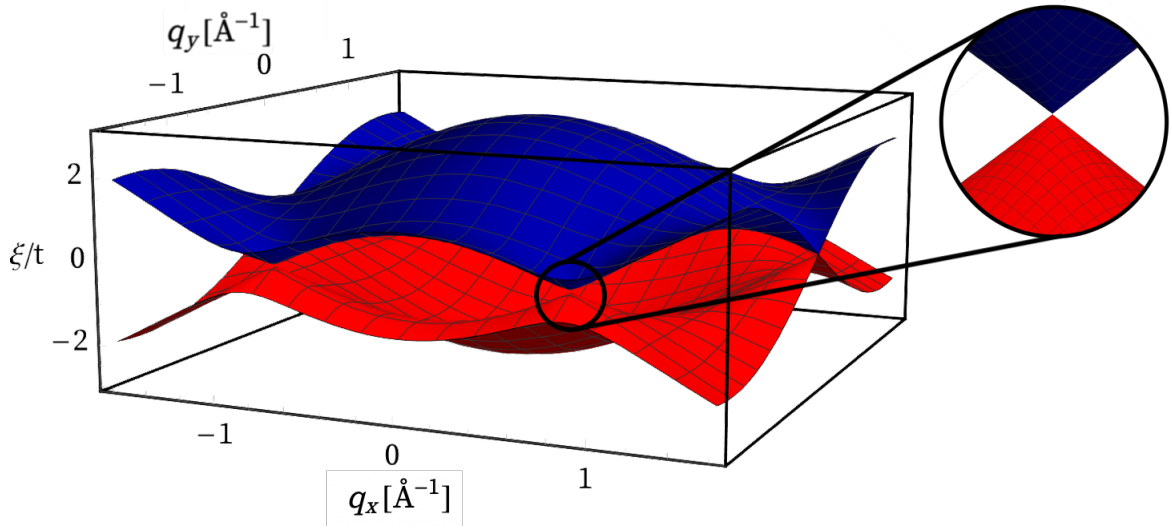

Figure 3.2: Energy of the conduction (blue) and valence (red) bands, normalised to the hopping integral. The points $\boldsymbol{K} = (4\pi/(3\sqrt{3}d_c), 0)$ and $\boldsymbol{K'} = (-4\pi/(3\sqrt{3}d_c), 0)$ are two local minima of energy, called Dirac points. They are both defined in the first Brillouin zone, so they are inequivalent. The close-up on the right is around $\boldsymbol{q} = \boldsymbol{K}$, highlighting the two bands touching, thus yielding a zero-gap, and displaying a conic symmetry for sufficiently small $\boldsymbol{q'} = \boldsymbol{q} - \boldsymbol{K}$.

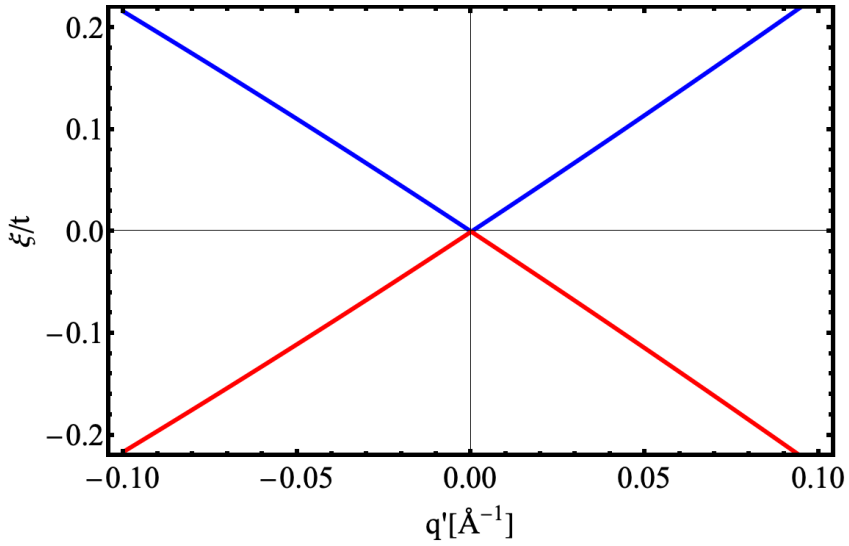

Figure 3.3: Close-up of the energy around the $\boldsymbol{K}$ direction, *i.e.*, $\boldsymbol{q'} = \boldsymbol{q} - \boldsymbol{K}$, for conducting (blue) and valence (red) electrons. For $aq' \ll 1$, we have $\xi \simeq \hbar v_F \pm q'$, where $q' \doteq |\boldsymbol{q}'|$ and a the lattice parameter. The spectrum resembles that of a zero mass particle, with a constant velocity, independent of momentum.

3.2 Wigner matrix in the lattice basis

For energies that verify $\xi \ll t$, we can expand (3.16) around the Dirac point $\boldsymbol{K}$ to obtain

$$\Delta(\boldsymbol{q}) \simeq -\frac{3\sqrt{3}d_c}{2}(q_x - iq_y), \tag{3.19}$$

Applying the canonical transformation to real space $\boldsymbol{q} \to -i\boldsymbol{\nabla}$, the Hamiltonian becomes

$$H^{\alpha\beta}(\boldsymbol{q}) \simeq -i\hbar v_F \boldsymbol{\sigma}^{\alpha\beta} \cdot \boldsymbol{\nabla}, \tag{3.20}$$

where $\boldsymbol{\sigma}$ is the vector of Pauli matrices in 2D, $\boldsymbol{\sigma} = (\sigma_x, \sigma_y)$. This describes a massless Dirac fermion, with a Fermi velocity

$$v_F = \frac{3\sqrt{3}td_c}{2h} \approx 10^6 \text{ms}^{-1}. \tag{3.21}$$

The Dirac structure becomes evident if one calculates the energy eigen-values for this Hamiltonian. We find

$$\xi(\boldsymbol{q}) = \pm\hbar v_F |\boldsymbol{q}|, \tag{3.22}$$

with corresponding eigen-vectors

$$|\boldsymbol{q}\rangle = \frac{1}{\sqrt{2}}\, e^{i\boldsymbol{q}\cdot\boldsymbol{r}} \begin{pmatrix} \mp i e^{-i\theta_{\boldsymbol{q}}/2} \\ e^{i\theta_{\boldsymbol{q}}/2} \end{pmatrix}, \tag{3.23}$$

where $\theta_{\boldsymbol{q}} = \arctan\left(q_x/q_y\right)$ is the angle between $\boldsymbol{q}$ and the $y-$axis. We stress that this two-dimensional Hilbert space is that of the pseudo-spin (or lattice) degeneracy, arising from the underlying honeycomb symmetry, and does not account for the electronic spin. The latter constitutes an extra degree of freedom for quasi-particles, which means that electrons carry, along with spin and orbital quantum numbers, an extra lattice-degeneracy quantum number. The vectorial part of the solutions in (3.23) is termed as pseudo-spinors, in a strict analogy with Dirac-spinors. Consequently, a rotation in the pseudo-spinor space is given by $R(\boldsymbol{\theta}) = e^{-i\boldsymbol{\theta}\cdot\boldsymbol{\sigma}/2}$, where $\boldsymbol{\theta} = (\theta_x, \theta_y, \theta_z)$ is a vector of constant angles which parameterises the rotation, and $\boldsymbol{\sigma} = (\sigma_x, \sigma_y, \sigma_z)$ is the 3D vector of Pauli matrices. This property indicates the effective nature of these quasi-particles being that of massless Dirac fermions, where the lattice (pseudo-)spin plays the role of the usual electronic spin.

Next, we shall extend this Hamiltonian to account for a mean-field solution to the Poisson equation, following the same reasoning as for the parabolic case. Hence, we generically write the modified Schrödinger equation as

$$\hat{H}^{\alpha\beta}(\boldsymbol{r}, t) \;=\; -i\hbar v_F \boldsymbol{\sigma}^{\alpha\beta} \cdot \boldsymbol{\nabla} \cdot \; + V(\boldsymbol{r}, t)\delta^{\alpha\beta}, \tag{3.24}$$

where $V(\boldsymbol{r}, t) = -e\phi(\boldsymbol{r}, t)$ is the interacting potential with respect to the electrostatic potential ϕ and electric charge $-e$. Moreover, $V(\boldsymbol{r}, t)$ is governed by the Poisson equation

$$\boldsymbol{\nabla}^2 \, V(\boldsymbol{r}, t) = -\frac{e^2}{\varepsilon} n(\boldsymbol{r}, t), \tag{3.25}$$

with solution

$$V(\boldsymbol{r}, t) = \frac{e^2}{4\pi\varepsilon} \int d\boldsymbol{r'} \, \frac{n(\boldsymbol{r'}, t)}{|\boldsymbol{r} - \boldsymbol{r'}|}, \tag{3.26}$$

and $n(\boldsymbol{r}, t) = n_A(\boldsymbol{r}, t) + n_B(\boldsymbol{r}, t)$ is the total density. Note that, even though the system dynamics is confined to two dimensions, the Poisson equation is written in three dimensions, owing to the dimensionality of the electric fields, which go out of the two-dimensional plane. To construct the Wigner function, we need to ensure the inclusion of the pseudo-spin degrees of freedom, which is done by going from a scalar to a tensorial structure [73–77]. Thus, we define the Wigner matrix components as

$$W^{\alpha\gamma}(\boldsymbol{r}, \boldsymbol{k}, t) = \int \frac{d\boldsymbol{s}}{(2\pi)^2} \, e^{i\boldsymbol{k}\cdot\boldsymbol{s}} \; \Phi^{*\alpha}(\boldsymbol{r} + \boldsymbol{s}/2, t)\Phi^{\gamma}(\boldsymbol{r} - \boldsymbol{s}/2, t). \tag{3.27}$$

where the indices α,γ run over the sublattice set $\{A, B\}$. Let us also define the vector $\boldsymbol{\Phi} = (\Phi^A, \Phi^B)$, such that the total electronic density in (3.26) can be written as $n = \boldsymbol{\Phi}^\dagger\boldsymbol{\Phi}$. The correlation matrix at equal times $C^{\alpha\gamma}(\boldsymbol{r}, \boldsymbol{s}, t) = \Phi^{*\;\alpha}(\boldsymbol{r} + \boldsymbol{s}/2, t)\Phi^{\;\gamma}(\boldsymbol{r} - \boldsymbol{s}/2, t)$ can be found as the inverse Fourier transform of $W^{\alpha\gamma}(\boldsymbol{r}, \boldsymbol{k}, t)$

$$C^{\alpha\gamma}(\boldsymbol{r}, \boldsymbol{s}, t) = \int d\boldsymbol{k} \; e^{-i\boldsymbol{k}\cdot\boldsymbol{s}} \; W^{\;\alpha\gamma}(\boldsymbol{r}, \boldsymbol{k}, t). \tag{3.28}$$

To construct the equation for the phase-space evolution of $W^{\alpha\gamma}$, we use the Schrödinger-Poisson model, which consists in solving the Schrödinger equation

$$i\hbar\frac{\partial}{\partial t}\Phi^{\alpha}(\boldsymbol{r}, t) = \hat{H}^{\alpha\beta}\Phi^{\beta}(\boldsymbol{r}, t), \tag{3.29}$$

together with (3.26). Therefore, for two distinct spatial coordinates, $\boldsymbol{r}_1$ and $\boldsymbol{r}_2$, we write the Schrödinger equation and its hermitian conjugate as[1]

$$-i\hbar\frac{\partial}{\partial t}\Phi^{*\alpha}(\boldsymbol{r_1},t) = \; iv_F\hbar\boldsymbol{\nabla}_{\boldsymbol{r_1}}\cdot\Phi^{*\beta}(\boldsymbol{r_1},t)\;\boldsymbol{\sigma}^{\beta\alpha} + V(\boldsymbol{r_1},t)\Phi^{*\alpha}(\boldsymbol{r_1},t), \tag{3.30}$$

$$i\hbar\frac{\partial}{\partial t}\Phi^{\;\gamma}(\boldsymbol{r_2},t) = -iv_F\hbar\boldsymbol{\nabla}_{\boldsymbol{r_2}}\cdot\boldsymbol{\sigma}^{\gamma\beta}\Phi^{\beta}(\boldsymbol{r_2},t) + V(\boldsymbol{r_2},t)\Phi^{\gamma}(\boldsymbol{r_2},t). \tag{3.31}$$

After multiplying (3.30) by $\Phi^{\;\gamma}(\boldsymbol{r_2},t)$ and subtracting it to (3.31) multiplied by $\Phi^{*\;\alpha}(\boldsymbol{r_1},t)$, we find the l.h.s. of (3.28), provided the coordinate transformation $\boldsymbol{r_{1,2}} = \boldsymbol{r} \pm \boldsymbol{s}/2$. Hence, we get

$$\int d\boldsymbol{k}\,\Big(\,i\hbar\frac{\partial}{\partial t}W^{\alpha\gamma}(\boldsymbol{r},\boldsymbol{k},t)e^{-i\boldsymbol{k}\cdot\boldsymbol{s}} + iv_F\hbar\boldsymbol{\nabla}_{\boldsymbol{r_1}}\cdot\boldsymbol{\sigma}^{\alpha\beta}W^{\beta\gamma}(\boldsymbol{r},\boldsymbol{k},t)e^{-i\boldsymbol{k}\cdot\boldsymbol{s}} + iv_F\hbar\boldsymbol{\nabla}_{\boldsymbol{r_2}}\cdot W^{\alpha\beta}(\boldsymbol{r},\boldsymbol{k},t)\boldsymbol{\sigma}^{\beta\gamma}e^{-i\boldsymbol{k}\cdot\boldsymbol{s}}$$
$$+\,\big[V(\boldsymbol{r_1},t) - V(\boldsymbol{r_2},t)\big]W^{\alpha\gamma}(\boldsymbol{r},\boldsymbol{k},t)e^{-i\boldsymbol{k}\cdot\boldsymbol{s}}\,\Big) = 0. \tag{3.32}$$

The spatial derivatives of the new set of variables are related to the previous ones by

$$\boldsymbol{\nabla}_{\boldsymbol{r}_1} = \frac{1}{2}\boldsymbol{\nabla}_{\boldsymbol{r}} + \boldsymbol{\nabla}_{\boldsymbol{s}}, \tag{3.33}$$

$$\boldsymbol{\nabla}_{\boldsymbol{r}_2} = \frac{1}{2}\boldsymbol{\nabla}_{\boldsymbol{r}} - \boldsymbol{\nabla}_{\boldsymbol{s}}, \tag{3.34}$$

which can be used to simplify (3.32). Then, multiplying (3.32) by $e^{i\boldsymbol{k'}\cdot\boldsymbol{s}}$ and integrating over $d\boldsymbol{s}/(2\pi)^2$, we find[2]

$$i\hbar\frac{\partial}{\partial t}W^{\alpha\gamma} + \frac{i\hbar v_F}{2}\boldsymbol{\nabla}_{\boldsymbol{r}}\cdot\big[\boldsymbol{\sigma}^{\alpha\beta}W^{\beta\gamma} + W^{\alpha\beta}\boldsymbol{\sigma}^{\;\beta\gamma}\big] + v_F\hbar\,\boldsymbol{k}\cdot\big[\boldsymbol{\sigma}^{\alpha\beta}W^{\beta\gamma} - W^{\alpha\beta}\boldsymbol{\sigma}^{\beta\gamma}\big]$$
$$+\int d^2q\; e^{i\boldsymbol{rq}}\;\big[W_+^{\alpha\gamma}\;-\;W_-^{\alpha\gamma}\big]\;V(\boldsymbol{q},t) = \;0, \tag{3.35}$$

where $V(\boldsymbol{q},t)$ is the Fourier transform of the potential, in momentum space, and

$$W_\pm^{\alpha\gamma} = W^{\alpha\gamma}(\boldsymbol{r},\boldsymbol{k}\pm\boldsymbol{q}/2,t). \tag{3.36}$$

We also replaced $V(\boldsymbol{r},t)$ by $\int d\boldsymbol{q}\;\; e^{i\boldsymbol{q}\cdot\boldsymbol{r}}V(\boldsymbol{q},t)$ and $W^{\alpha\gamma}(\boldsymbol{r},\boldsymbol{k},t)$ by $\int d\boldsymbol{s'}\;\; e^{-i\boldsymbol{k}\cdot\boldsymbol{s'}}W^{\alpha\gamma}(\boldsymbol{r},\boldsymbol{s'},t)/(2\pi)^2$ in (3.32). Let us define the following commutator and anti-commutator (with subscripts $\mp$, respectively) between the Wigner matrix and a differential operator $\hat{O}$

$$[\hat{O},W]_\pm^{\kappa\lambda} = \overrightarrow{\hat{O}}^{\kappa\tau}W^{\tau\lambda} \pm W^{\kappa\tau}\overleftarrow{\hat{O}}^{\tau\lambda}. \tag{3.37}$$

The Wigner transport equation can be rewritten as

$$i\hbar\frac{\partial}{\partial t}W^{\alpha\gamma} + \hbar v_F\;[\hat{\boldsymbol{k}},W]_+^{\alpha\gamma} + \frac{i\hbar v_F}{2}[\hat{\boldsymbol{\partial}},W]_-^{\alpha\gamma} = \int d^2q\; e^{i\boldsymbol{rq}}\;\big(W_-^{\alpha\gamma} - W_+^{\alpha\gamma}\big)V(\boldsymbol{q},t) \tag{3.38}$$

[1] We make use of the property $\big(\sigma^{\kappa\lambda}\big)^* = \sigma^{\lambda\kappa}$, valid for the Pauli matrices.

[2] We integrate by parts the term $\sim \boldsymbol{\nabla}_{\boldsymbol{s}}$, and change $\boldsymbol{k'}$ back to $\boldsymbol{k}$, for convenience.

where we defined

$$\hat{\boldsymbol{\partial}} = \begin{pmatrix} 0 & \frac{\partial}{\partial x} - i\frac{\partial}{\partial y} \\ \frac{\partial}{\partial x} + i\frac{\partial}{\partial y} & 0 \end{pmatrix}, \tag{3.39}$$

$$\hat{\boldsymbol{k}} = \begin{pmatrix} 0 & k_x - ik_y \\ k_x + ik_y & 0 \end{pmatrix}. \tag{3.40}$$

Equation (3.38) is similar to (2.29), both in the time derivative and potential term, where the last is adapted to the two-dimensional space. The defining feature has to do with the kinetic term, which is expressed in terms of the commutator and the anti-commutator. This convoluted form results from the linear energy dispersion relation of quasi-particles, introduced in the Schödinger equation as $\sim \boldsymbol{\sigma}^{\alpha\beta} \cdot \boldsymbol{\nabla}$, as we exploit further ahead.

We should now make a side note to distinguish between $\hat{\boldsymbol{k}}$ and $\hat{\boldsymbol{\partial}}$ in (3.38). In fact, $\boldsymbol{q}$ is the conjugate variable of $\boldsymbol{r}$,

$$i\boldsymbol{q} \to \frac{\partial}{\partial \boldsymbol{r}}, \tag{3.41}$$

whereas $\boldsymbol{k}$ is the phase-space variable. We emphasise that equation (3.41) is only true in the distribution sense, *i.e.*, when the functions are being integrated. To clarify the difference between $\boldsymbol{k}$ and $\boldsymbol{q}$, let us compute the Wigner function for a plane wave solution $\Phi_{\boldsymbol{q}}(\boldsymbol{r}) = e^{i\boldsymbol{q}\cdot\boldsymbol{r}}/\sqrt{A}$, where A is the area, corresponding to a solution of (3.20). Hence,

$$W(\boldsymbol{r}, \boldsymbol{k}, t) = \delta(\boldsymbol{q} - \boldsymbol{k})/A. \tag{3.42}$$

This suggests trying a solution of the form

$$W^{\alpha\gamma}(\boldsymbol{r}, \boldsymbol{k}, t) = \int\int d\boldsymbol{q}\, d\omega\, e^{i(\boldsymbol{q}\cdot\boldsymbol{r} - \omega t)} \delta(\boldsymbol{q} - \boldsymbol{k})\, \Lambda^{\alpha\gamma}(\boldsymbol{q}, \omega), \tag{3.43}$$

where $W^{\alpha\gamma}(\boldsymbol{q}, \boldsymbol{k}, \omega) = \delta(\boldsymbol{q} - \boldsymbol{k})\Lambda^{\alpha\gamma}(\boldsymbol{q}, \omega)$ is the double Fourier transform of the Wigner matrix in space and time domains. By plugging (3.43) into (3.38), and integrating over $\boldsymbol{k}$ for the case of free particles ($V = 0$), this leads to a secular equation involving each $\Lambda^{\alpha\gamma}(\boldsymbol{q}, \omega)$

$$\begin{pmatrix} \omega & \frac{3}{2}v_F q_+ & \frac{1}{2}v_F q_- & 0 \\ \frac{3}{2}v_F q_- & \omega & 0 & \frac{1}{2}v_F q_- \\ \frac{1}{2}v_F q_+ & 0 & \omega & \frac{3}{2}v_F q_+ \\ 0 & \frac{1}{2}v_F q_+ & \frac{3}{2}v_F q_- & \omega \end{pmatrix} \begin{pmatrix} \Lambda^{11} \\ \Lambda^{12} \\ \Lambda^{21} \\ \Lambda^{22} \end{pmatrix} = 0, \tag{3.44}$$

where $q_\pm = q_x \pm iq_y$. A non-trivial solution[3] of (3.44) leads to the dispersion relation

$$\omega(\boldsymbol{q}) = \pm v_F \sqrt{q_+ q_-} = \pm v_F |\boldsymbol{q}|. \tag{3.45}$$

[3] *i.e.*, $(\Lambda^{11}, \Lambda^{12}, \Lambda^{21}, \Lambda^{22}) \neq 0$.

This result is the same as (3.18) near the Dirac point, as expected for the free case. We shall now try to take into account the effect of interactions, but before that, a more convenient choice of basis for the wave-functions is employed, which we illustrate next.

3.3 Wigner matrix in the diagonal basis

Henceforth, we will be interested in analysing the phase-space evolution of the Wigner matrix. As it must be clear, such a kinetic equilibrium is quite demanding to guess in the sublattice basis, owning to the fact that quasi-electrons in this basis are merely linear combinations of the true elementary excitations of the Hamiltonian in (3.20). If follows that setting a proper equilibrium configuration in this basis is quite a complex task, and we shall move to a more convenient one. In practise, this task boils down to the diagonalization of (3.24), at the Hamiltonian level, or equivalently, of (3.11), at the operator level. This last seems to be more intuitive. So, following the general (similarity) transformation procedure [78], we define the new operators $\hat{c}_{\boldsymbol{q}}$ and $\hat{v}_{\boldsymbol{q}}$ as

$$\begin{pmatrix} \hat{c}_{\boldsymbol{q}} \\ \hat{v}_{\boldsymbol{q}} \end{pmatrix} = S \begin{pmatrix} \hat{a}_{\boldsymbol{q}} \\ \hat{b}_{\boldsymbol{q}} \end{pmatrix}, \tag{3.46}$$

where S is a unitary matrix. In momentum space, the Schrödinger equation, accounting for the Hamiltonian (3.24) reads

$$i\hbar \frac{\partial}{\partial t} \Phi^{\alpha}(\boldsymbol{q}, t) = \hbar v_F \boldsymbol{q} \cdot \boldsymbol{\sigma}^{\alpha\beta} \Phi^{\beta}(\boldsymbol{q}, t) + \int d\boldsymbol{q'}\ V(\boldsymbol{q'}, t) \Phi^{\alpha}(\boldsymbol{q} - \boldsymbol{q'}, t). \tag{3.47}$$

The present transformation is accomplished with $\boldsymbol{\Psi}(\boldsymbol{q}, t) = S\boldsymbol{\Phi}(\boldsymbol{q}, t)$, where $\boldsymbol{\Psi}$ is a new vector field, with components $\boldsymbol{\Psi}^T(\boldsymbol{q}, t) = (\hat{c}_{\boldsymbol{q}} \ \ \hat{v}_{\boldsymbol{q}})$. Replacing $\boldsymbol{\Phi}$ by $S^{\dagger}\boldsymbol{\Psi}$ in (3.47), and left-acting on both sides with S, we demand the off diagonal term to vanish, *i.e.*, we choose S such that $S\boldsymbol{q} \cdot \boldsymbol{\sigma} S^{\dagger}$ is diagonal. We obtain

$$S = \frac{1}{\sqrt{2}} \begin{pmatrix} -e^{-i\theta(\boldsymbol{q})} & 1 \\ e^{i\theta(\boldsymbol{q})} & 1 \end{pmatrix}, \tag{3.48}$$

where $e^{i\theta(\boldsymbol{q})} = \sqrt{\Delta(\boldsymbol{q})/\Delta^*(\boldsymbol{q})}$. Equation (3.47) then becomes

$$i\hbar \frac{\partial}{\partial t} \Psi^{\alpha}(\boldsymbol{q}, t) = \hbar v_F |\boldsymbol{q}| \sigma_z^{\alpha\beta} \Psi^{\beta}(\boldsymbol{q}, t) + \int d\boldsymbol{q'}\ V(\boldsymbol{q'}, t) \Psi^{\alpha}(\boldsymbol{q} - \boldsymbol{q'}, t), \tag{3.49}$$

which is diagonal, as intended, and

$$\sigma_z = \begin{pmatrix} 1 & 0 \\ 0 & -1 \end{pmatrix}. \tag{3.50}$$

The valence and conduction band operators are found as linear combinations of the previous

$$\hat{c}_{\boldsymbol{q}} = \frac{1}{\sqrt{2}}\left(\hat{b}_{\boldsymbol{q}} - e^{-i\theta(\boldsymbol{q})}\hat{a}_{\boldsymbol{q}}\right), \tag{3.51}$$

$$\hat{v}_{\boldsymbol{q}} = \frac{1}{\sqrt{2}}\left(\hat{b}_{\boldsymbol{q}} + e^{i\theta(\boldsymbol{q})}\hat{a}_{\boldsymbol{q}}\right), \tag{3.52}$$

$$\hat{c}^{\dagger}_{\boldsymbol{q}} = \frac{1}{\sqrt{2}}\left(\hat{b}^{\dagger}_{\boldsymbol{q}} - e^{i\theta(\boldsymbol{q})}\hat{a}^{\dagger}_{\boldsymbol{q}}\right), \tag{3.53}$$

$$\hat{v}^{\dagger}_{\boldsymbol{q}} = \frac{1}{\sqrt{2}}\left(\hat{b}^{\dagger}_{\boldsymbol{q}} + e^{-i\theta(\boldsymbol{q})}\hat{a}^{\dagger}_{\boldsymbol{q}}\right). \tag{3.54}$$

and verify, as before, the anti-commutation relation for fermionic operators

$$\{\hat{c}_{\boldsymbol{q}}, \hat{c}^{\dagger}_{\boldsymbol{q'}}\} = \delta_{\boldsymbol{q}\boldsymbol{q'}}, \tag{3.55}$$

$$\{\hat{v}_{\boldsymbol{q}}, \hat{v}^{\dagger}_{\boldsymbol{q'}}\} = \delta_{\boldsymbol{q}\boldsymbol{q'}}. \tag{3.56}$$

Note that the total density is the same in the two basis, *i.e.*, $\boldsymbol{\Phi}^{\dagger}\boldsymbol{\Phi} = \boldsymbol{\Psi}^{\dagger}\boldsymbol{\Psi}$, which means that the mean field potential V is invariant under the present transformation. This property is a state of the conservation of the number of particles, independently of the basis choosen to count them. Furthermore, this new basis corresponds to that of conduction ($\alpha = 1$) and valence ($\alpha = 2$) bands, with kinetic energies $\pm\xi(\boldsymbol{q})$, and $\xi(\boldsymbol{q})$ being the massless dispersion relation. Hence, $\hat{c}^{\dagger}_{\boldsymbol{q}}(\hat{c}_{\boldsymbol{q}})$ creates (annihilates) an electron with momentum $\boldsymbol{q}$ and energy $+\xi(\boldsymbol{q})$ in the conduction band, and $\hat{v}^{\dagger}_{\boldsymbol{q}}$ ($\hat{v}_{\boldsymbol{q}}$) creates (annihilates) an electron with momentum $\boldsymbol{q}$ and energy $-\xi(\boldsymbol{q})$ in the valence band.

Let us now define the new Wigner matrix in terms of $\boldsymbol{\Psi}$ as[4]

$$W^{\ \alpha\gamma}(\boldsymbol{r}, \boldsymbol{k}, t) = \int \frac{d\boldsymbol{s}}{(2\pi)^2}\, e^{i\boldsymbol{k}\cdot\boldsymbol{s}}\ \Psi^{*\alpha}(\boldsymbol{r} + \boldsymbol{s}/2, t)\Psi^{\gamma}(\boldsymbol{r} - \boldsymbol{s}/2, t), \tag{3.57}$$

and its Fourier transform

$$W^{\alpha\gamma}(\boldsymbol{q}, \boldsymbol{k}, t) = \Psi^{*\alpha}(\boldsymbol{k} - \boldsymbol{q}/2, t)\ \Psi^{\gamma}(\boldsymbol{k} + \boldsymbol{q}/2, t). \tag{3.58}$$

Starting from (3.49), and repeating the same procedure leading to (3.32), we get

$$\begin{aligned} i\hbar\frac{\partial}{\partial t}\Big[\Psi^{*\alpha}(\boldsymbol{q}_2, t)\Psi^{\gamma}(\boldsymbol{q}_1, t)\Big] &= \hbar v_F\Big[|\boldsymbol{q_1}|\Psi^{*\alpha}(\boldsymbol{q}_2, t)\Psi^{\beta}(\boldsymbol{q}_1, t)\sigma_z^{\beta\gamma} - |\boldsymbol{q_2}|\sigma_z^{\alpha\beta}\Psi^{*\beta}(\boldsymbol{q}_2, t)\Psi^{\gamma}(\boldsymbol{q}_1, t)\Big] \\ &+ \int d\boldsymbol{q'}\Big[V(\boldsymbol{q'}, t)\Psi^{*\alpha}(\boldsymbol{q}_2, t)\Psi^{\gamma}(\boldsymbol{q}_1 - \boldsymbol{q'}, t) - V(-\boldsymbol{q'}, t)\Psi^{*\alpha}(\boldsymbol{q}_2 - \boldsymbol{q'}, t)\Psi^{\gamma}(\boldsymbol{q}_1, t)\Big], \end{aligned} \tag{3.59}$$

where we used the fact that $V(\boldsymbol{r}, t)$ is real, which implies $V^*(\boldsymbol{q}, t) = V(-\boldsymbol{q}, t)$. We can rewrite the last

[4] We will be using the same symbol to denote the Wigner matrix in the several basis, which is not problematic because it should be clear from the context which one is what.

term on the r.h.s. of (3.59) using relation (A.8). It leads to

$$\begin{aligned}&\int d\boldsymbol{q}'\Big[V(\boldsymbol{q}',t)\Psi^{*\alpha}(\boldsymbol{q}_2,t)\Psi^{\gamma}(\boldsymbol{q}_1-\boldsymbol{q}',t)-V(-\boldsymbol{q}',t)\Psi^{*\alpha}(\boldsymbol{q}_2-\boldsymbol{q}',t)\Psi^{\gamma}(\boldsymbol{q}_1,t)\Big],\\ &=\int d\boldsymbol{q}'\;V(\boldsymbol{q}',t)\Big(\;e^{-\boldsymbol{q}'\cdot\boldsymbol{\nabla}_{\boldsymbol{q}_1}}-e^{\;\boldsymbol{q}'\cdot\boldsymbol{\nabla}_{\boldsymbol{q}_2}}\Big)\;\Psi^{*\alpha}(\boldsymbol{q}_2,t)\Psi^{\gamma}(\boldsymbol{q}_1,t).\end{aligned}\tag{3.60}$$

By introducing the coordinate transformation $\boldsymbol{q}_1=\boldsymbol{k}+\boldsymbol{q}/2$ and $\boldsymbol{q}_2=\boldsymbol{k}-\boldsymbol{q}/2$ and, accordingly,

$$\boldsymbol{\nabla}_{\boldsymbol{q}_1}=\frac{1}{2}\boldsymbol{\nabla}_{\boldsymbol{k}}+\boldsymbol{\nabla}_{\boldsymbol{q}},\tag{3.61}$$

$$\boldsymbol{\nabla}_{\boldsymbol{q}_2}=\frac{1}{2}\boldsymbol{\nabla}_{\boldsymbol{k}}-\boldsymbol{\nabla}_{\boldsymbol{q}},\tag{3.62}$$

into equation (3.60), we finally obtain

$$\begin{aligned}i\hbar\,\frac{\partial}{\partial t}W^{\alpha\gamma}(\boldsymbol{q},\boldsymbol{k},t)=\xi(\boldsymbol{k}+\boldsymbol{q}/2)\;W^{\alpha\beta}(\boldsymbol{q},\boldsymbol{k},t)\;\sigma_z^{\beta\gamma}-\xi(\boldsymbol{k}-\boldsymbol{q}/2)\;\sigma_z^{\alpha\beta}\;W^{\beta\gamma}(\boldsymbol{q},\boldsymbol{k},t)\\ +\int d\boldsymbol{q}'\;V(\boldsymbol{q}',t)\;\Delta W^{\alpha\gamma}(\boldsymbol{q},\boldsymbol{k},\boldsymbol{q}',t),\end{aligned}\tag{3.63}$$

where

$$\Delta W^{\alpha\gamma}(\boldsymbol{q},\boldsymbol{k},\boldsymbol{q}',t)=W^{\alpha\gamma}(\boldsymbol{q}-\boldsymbol{q}',\boldsymbol{k}-\boldsymbol{q}'/2,t)-W^{\alpha\gamma}(\boldsymbol{q}-\boldsymbol{q}',\boldsymbol{k}+\boldsymbol{q}'/2,t).\tag{3.64}$$

Although the Wigner equation (3.63) will be more useful than its real-space version, as will be shown shortly, we can always Fourier transform it back to real space. However, due to the cumbersome form of the Hamiltonian in real space, it is preferable to work with (3.63), and inverse Fourier transform back to $\boldsymbol{r}$ in the end of the calculations. As we shall see next, the important results will be obtained directly from (3.63), as it contains equivalent information to its real space counterpart. Nevertheless, it is interesting to do it in order to highlight the differences with the more conventional version for the parabolic case of (2.29). Straightforward steps lead to the Fourier transform version of (3.63)

$$i\hbar\frac{\partial}{\partial t}W^{\alpha\gamma}(\boldsymbol{r},\boldsymbol{k},t)+i\hbar\mathcal{K}\{W^{\alpha\gamma}\}=e\int d\boldsymbol{q}\;e^{i\boldsymbol{q}\cdot\boldsymbol{r}}\;\phi(\boldsymbol{q},t)\;\Big(s^{\alpha}W_{-}^{\alpha\gamma}-s^{\gamma}W_{+}^{\alpha\gamma}\Big),\tag{3.65}$$

where we defined $W_{\pm}^{\alpha\gamma}\doteq W^{\alpha\gamma}(\boldsymbol{r},\boldsymbol{k}\pm\boldsymbol{q}/2,t)$. The operator $\mathcal{K}$ represents the kinetic term, which in the present case of 2D-linear dispersion relation has the convoluted form

$$\mathcal{K}\{W^{\alpha\gamma}\}=v_F\int\frac{d\boldsymbol{r}'}{(2\pi)^2}\;\frac{\sin\big(2\boldsymbol{k}\cdot\boldsymbol{r}'\big)}{|\boldsymbol{r}'|^3}\;W^{\alpha\gamma}(\boldsymbol{r}-\boldsymbol{r}',\boldsymbol{k},t).\tag{3.66}$$

The real space version of $\mathcal{K}$ makes it hard to handle, in practice, such that a much simple result is given by the Fourier transformed equations. The off-diagonal terms of (3.65) contain extra information about the two populations, that have symmetric charges, thus symmetric couplings to the electrostatic potential. However, if one considers the equation for the diagonal elements only, $W^{\alpha\alpha}\doteq W^{\alpha}$, and further setting $V^{\alpha}(\boldsymbol{q},t)=s^{\alpha}e\phi(\boldsymbol{q},t)$, the real-space Wigner equation yields (no summation)

$$i\hbar\frac{\partial}{\partial t}W^{\alpha}(\boldsymbol{r},\boldsymbol{k},t)+i\hbar\mathcal{K}\{W^{\alpha}\}=\int d\boldsymbol{q}\;e^{i\boldsymbol{q}\cdot\boldsymbol{r}}\;\Big(W_{-}^{\alpha}-W_{+}^{\alpha}\Big)V^{\alpha}(\boldsymbol{q},t).\tag{3.67}$$

The first and last terms are identical to (2.29), for a single band α. The defining difference appears in the kinetic term, which case of $\xi(\boldsymbol{q}) = \hbar^2\boldsymbol{q}^2/2m$, reduces to the usual convective-like derivative

$$\mathcal{K}_{\rm par}\{W^\alpha\} = \frac{\hbar\boldsymbol{k}}{m}\cdot\boldsymbol{\nabla}\, W^\alpha. \tag{3.68}$$

Equations (3.66) and (3.68) show defining differences, being the first nonlocal on the Wigner components, in opposition to the second. The nonlocality of (3.66) is profoundly related to the relativistic-like nature of the Dirac electrons, and strongly differs from the term appearing in semi-classical equations proposed in the literature,

$$\mathcal{K}\{W^\alpha\} = \boldsymbol{v}_{\boldsymbol{k}}\cdot\boldsymbol{\nabla}W^\alpha, \tag{3.69}$$

with $\boldsymbol{v}_{\boldsymbol{k}} = \partial_{\boldsymbol{k}}\xi(\boldsymbol{k})/\hbar = v_F\boldsymbol{k}/|\boldsymbol{k}|$ [79]. For parabolic particles, on the contrary, the classical limit of the Wigner equation corresponds to the Vlasov equation. However, no classical limit of (3.66) exists (i.e. it diverges as $\hbar \to 0$), which then confers to Dirac particles a purely quantum nature. In the next chapter, we will shown how this particularity introduces further complications in the derivation of the hydrodynamical model.

Besides, the system of equations depicted above contains more information than one actually needs, considering the present approximation for the potential. In fact, the mean field approximation of (3.26) makes the off-diagonal terms of $W^{\alpha\gamma}$ to completely decouple from the diagonal ones, since the potential depends on the latter, only. Explicitly, each component of (3.63) reads

$$\Big[i\hbar\,\frac{\partial}{\partial t} - \Delta\xi^-(\boldsymbol{q},\boldsymbol{k})\Big]W^{11}(\boldsymbol{q},\boldsymbol{k},t) = \int d\boldsymbol{q}'\; V(\boldsymbol{q}',t)\Delta W^{11}(\boldsymbol{q},\boldsymbol{k},\boldsymbol{q}',t), \tag{3.70}$$

$$\Big[i\hbar\,\frac{\partial}{\partial t} - \Delta\xi^+(\boldsymbol{q},\boldsymbol{k})\Big]W^{21}(\boldsymbol{q},\boldsymbol{k},t) = \int d\boldsymbol{q}'\; V(\boldsymbol{q}',t)\Delta W^{21}(\boldsymbol{q},\boldsymbol{k},\boldsymbol{q}',t), \tag{3.71}$$

$$\Big[i\hbar\,\frac{\partial}{\partial t} + \Delta\xi^-(\boldsymbol{q},\boldsymbol{k})\Big]W^{22}(\boldsymbol{q},\boldsymbol{k},t) = \int d\boldsymbol{q}'\; V(\boldsymbol{q}',t)\Delta W^{22}(\boldsymbol{q},\boldsymbol{k},\boldsymbol{q}',t), \tag{3.72}$$

where we defined $\Delta\xi^\pm(\boldsymbol{q},\boldsymbol{k}) = \xi(\boldsymbol{k}+\boldsymbol{q}/2) \pm \xi(\boldsymbol{k}-\boldsymbol{q}/2)$. The transport equation for W^{12} can be found by complex conjugating (3.71). As previously mentioned, the potential $V(\boldsymbol{q},t)$ above is only a function of the density, which allows to express it with respect to the Wigner diagonal elements, *viz.*[5]:

$$n^\alpha(\boldsymbol{q},t) = \int d\boldsymbol{k}\; W^{\alpha\alpha}(\boldsymbol{q},\boldsymbol{k},t), \tag{3.73}$$

with no summation over repeated symbols[6]. The elements W^{11} and W^{22} describe the evolution of the populations of conduction and valence electrons, respectively. Alternatively, W^{12} and W^{21} contain information on inter-band interference, and correlations between the different populations. As can be noted, these two terms evolve independently. Therefore, equations (3.70) and (3.72) form a closed system of equations, in the mean-field approximation. This argument allows to discard (3.71) and its complex conjugate from the calculations.

Another important aspect to mark is that W^{22} is still related to the density of valence electrons (with

[5] If $f(\boldsymbol{r}) = \int d\boldsymbol{k}\; g(\boldsymbol{r},\boldsymbol{k})$, then the same relation holds in Fourier space, *i.e.*, $f(\boldsymbol{q}) = \int d\boldsymbol{k}\; g(\boldsymbol{q},\boldsymbol{k})$.

[6] We will maintain this convention henceforth: whenever we write $O^{\alpha\alpha}$, it means the $\alpha-$diagonal component of the matrix $\hat{O}$.

charge $-e$), and not holes (with charge $+e$), which turn out to be the appropriate quasi-particles involved in the graphene kinetic processes (see Appendix D.1.3). For most of the cases, we will be interested in the pure conducting electron case, for which equation (3.70) alone is well suited, so (3.72) can simply be neglected. Such conditions are found in gated or $n-$doped graphene [80, 81], which will be treated shortly. In these cases, the electronic dynamics is restricted to the conduction band, and the relevant processes include intra-band transitions only, for which the valence band merely plays the role of a filled Fermi sea. However, intrinsic (undoped) graphene exhibits an equal number of conducting electron and holes, in thermal equilibrium. The thermal electron (n^1) and hole (n^2) densities can be calculated using the Fermi-Dirac distribution function, through [82]

$$n^1 = \int_0^{+\infty} dE\ \mathcal{D}(E)\ f_{FD}(E), \tag{3.74}$$

$$n^2 = \int_{-\infty}^{0} dE\ \mathcal{D}(E)\ \Big[1 - f_{FD}(E)\Big], \tag{3.75}$$

where $\mathcal{D}(E) = 2E/\pi\hbar^2 v_F^2$ is the 2D density of states near the Dirac points, and $f_{FD}(E) = \big(1 + e^{(E-E_F)/k_BT}\big)^{-1}$ is the Fermi-Dirac distribution function. We obtain

$$n^1 = n^2 \simeq \frac{(k_BT)^2}{6h^2 v_F^2}. \tag{3.76}$$

The densities in (3.76) are only valid for intrinsic graphene, which arise in the limit of vanishingly small doping. Notwithstanding, when the presence of holes is not negligible, *i.e.*, when E_F is of the order of the thermal energy, its transport is introduced using a modified version of (3.70)$-$(3.72), along with the corresponding change in the Poisson equation, derived and discussed in Appendix D.1.3. Here, we simply present the final result. The complete Wigner-Poisson model for the degenerate electron-hole system reads

$$\Big[i\hbar\,\frac{\partial}{\partial t} - \Delta\xi^-(\boldsymbol{q},\boldsymbol{k})\Big]W^{\alpha\gamma}(\boldsymbol{q},\boldsymbol{k},t) = e\int d\boldsymbol{q'}\ \phi(\boldsymbol{q'},t)\ \Delta W^{\alpha\gamma}(\boldsymbol{q},\boldsymbol{k},\boldsymbol{q'},t), \tag{3.77}$$

where

$$\phi(\boldsymbol{r},t) = \frac{e}{4\pi\varepsilon_0\varepsilon_r}\int d\boldsymbol{r'}\ \frac{n^2(\boldsymbol{r'},t) - n^1(\boldsymbol{r'},t)}{|\boldsymbol{r}-\boldsymbol{r'}|}. \tag{3.78}$$

Above, we redefined the Wigner matrix elements $\Delta W^{\alpha\gamma}(\boldsymbol{q},\boldsymbol{k},\boldsymbol{q'},t)$ to include the band dependence on the charge, as

$$\Delta W^{\alpha\gamma}(\boldsymbol{q},\boldsymbol{k},\boldsymbol{q'},t) = s^\alpha W^{\alpha\gamma}(\boldsymbol{q}-\boldsymbol{q'},\boldsymbol{k}-\boldsymbol{q'}/2,t) - s^\gamma W^{\alpha\gamma}(\boldsymbol{q}-\boldsymbol{q'},\boldsymbol{k}+\boldsymbol{q'}/2,t), \tag{3.79}$$

where $s^\alpha = 2\alpha - 3$ is the sign of the $\alpha-$th charge. The electron and hole densities remain related to the diagonal components of the Wigner matrix *via* the relation (3.73), although W^{22} is now representative of the hole sector. As aforesaid, the system composed by the transport equation for W^{11} and W^{22} evolves independently of W^{12} and W^{21}, as long as the mean-field solution for the potential of (3.78)

is considered. Therefore, it remains solvable without calling for the off-diagonal terms, which can then be discarded. However, a complete kinetic description would imply a different form of the interacting potential, which eventually becomes a function W^{12} and W^{21}, to capture correlations above the mean-field density. Such a detailed description is excluded from the present work, as it plays a minimal role in the regimes of interest, consistent with previous results [83].

3.4 Plasmonic modes in doped graphene

In order to test the Wigner-Poisson system formerly derived, let us start by considering the case a graphene sheet doped with negative charge carriers, of density n_0, which occupy the conduction band. This is also known as n-doped graphene. Doping densities as high as 10^{13} cm^{-2} are achievable within the current doping methods. They are essentially of two kinds: electro-doping [84–86] and electrochemical-doping [87]. The first consists in applying a gate voltage V_g between the graphene layer and a metal gate, akin to the graphene field effect transistors (FET) configuration [88]. The sign of V_g determines the type of carriers (either doping electrons or holes) that accommodates in the band structure. The other method relies on the interaction between the graphene lattice and atoms of different species. The charge transfer from the doping atoms to the graphene layer can occur either by direct transfer or by substitutional doping, in which some carbon atoms are replaced by other atoms with a different valence, that are able to donate electrons or holes to the system. However, for the substitutional method to achieve high doping densities, it may lead to a significant modification of the linear dispersion-relation. Throughout this work, either electro-doping or direct-charge-transfer are adequate methods to produce the necessary doping.

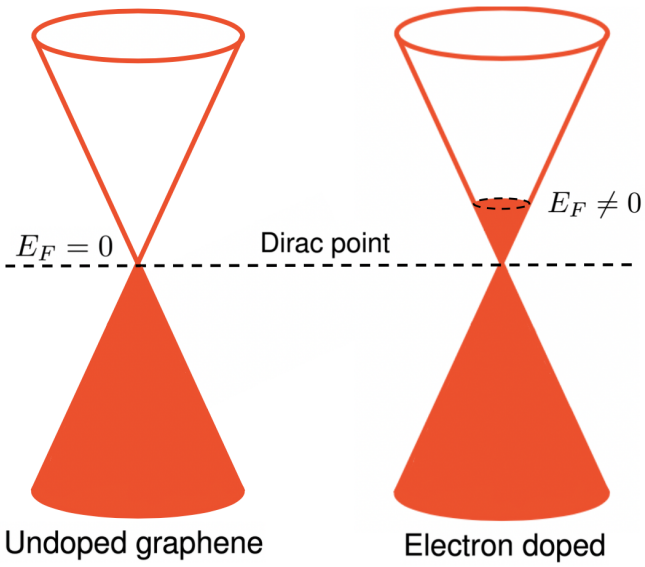

Figure 3.4: Schematic representation of the linear dispersion (Dirac cones) near $\boldsymbol{q} = \boldsymbol{K}$ in the first Brillouin zone, with both bands touching at zero gap. For undoped graphene, at $T = 0K$, the Fermi level lies exactly at the Dirac point, whereas for electron doped graphene, the Fermi level is located in the interior of the conduction band, making it fill up to E_F.

Considering the case of n-doping, the conduction band gets filled with electrons up to the Fermi level, E_F, related to the Fermi wave-number by $E_F = \hbar v_F k_F$. In the momentum-energy space, this is defined by the cone $E(\boldsymbol{k}) = \hbar v_F |\boldsymbol{k}| \Theta(k_F - |\boldsymbol{k}|)$, where $\Theta(x)$ is the Heaviside step function (see Figure 3.4). The Fermi wave-number is related with the doping density by

$$k_F = \sqrt{\frac{4\pi n_0}{g_s g_v}}, \tag{3.80}$$

where $g_s g_v$ accounts for the spin ($g_s = 2$) and valley ($g_v = 2$) degeneracy. The first results from the degeneracy of the spin populations in each energy band, which we have neglected in our treatment so far, and the latter should be incorporated to consistently include the two minima in the first Brillouin zone (BZ) [89]. In n-doped graphene, and for sufficiently high doping densities, the presence of holes is insignificant, even at non-zero temperatures. If, however, $E_F \lesssim k_B T$, some valence electrons can be thermally excited into the conduction band, leaving holes in the valence band. On the contrary, undoped graphene ($n_0 = 0$) exhibits an equal number of conducting electrons and holes, in thermal equilibrium.

Let us consider the case of a pure electron system, such that the Fermi level E_F is located way above the thermal energy, *i.e.*, $E_F \gg k_B T$. As such, the first component of (3.77) suffices to analyse this case,

$$\Big[i\hbar\frac{\partial}{\partial t} - \Delta\xi^-(\boldsymbol{q},\boldsymbol{k})\Big] W = e \int d\boldsymbol{q'}\; \phi(\boldsymbol{q'},t)\Big[W(\boldsymbol{q}-\boldsymbol{q'},\boldsymbol{k}+\boldsymbol{q'}/2,t) - W(\boldsymbol{q}-\boldsymbol{q'},\boldsymbol{k}-\boldsymbol{q'}/2,t)\Big]. \tag{3.81}$$

We have dropped the indices for simplicity, $W \doteq W^{11}$. The electrostatic potential reads

$$\phi(\boldsymbol{r},t) = -\frac{e}{4\pi\varepsilon_0\varepsilon_r} \int d\boldsymbol{r'}\; \frac{n(\boldsymbol{r'},t)}{|\boldsymbol{r}-\boldsymbol{r'}|}, \tag{3.82}$$

where, again, $n \doteq n^1$ is the electron density. The Fourier transform of the above expression is calculated in Appendix D.1, and gives

$$\phi(\boldsymbol{q},t) = -\frac{e}{2\varepsilon_0\varepsilon_r}\frac{n(\boldsymbol{q},t)}{q}. \tag{3.83}$$

Equation (3.83) shows that the Coulomb potential in 2D exhibits a $1/q$ dependence, instead of the usual $1/q^2$ dependence in 3D [78]. Equation (3.81) goes to

$$\Big[i\hbar\frac{\partial}{\partial t} - \Delta\xi^-(\boldsymbol{q},\boldsymbol{k})\Big] W(\boldsymbol{q},\boldsymbol{k},t) = \int d\boldsymbol{q'}\; n(\boldsymbol{q'},t)\, \mathcal{U}(q')\Big[W(\boldsymbol{q}-\boldsymbol{q'},\boldsymbol{k}-\boldsymbol{q'}/2,t) - W(\boldsymbol{q}-\boldsymbol{q'},\boldsymbol{k}+\boldsymbol{q'}/2,t)\Big], \tag{3.84}$$

where we defined

$$\mathcal{U}(q) = \frac{e^2}{2\varepsilon_r\varepsilon_0 q}, \tag{3.85}$$

We can solve last equation perturbatively, for the plasmon dispersion relation. This will lead to the allowed frequencies ω for each mode $\boldsymbol{q}$ of the plasma wave, $\omega = \omega(\boldsymbol{q})$. Therefore, we consider a small perturbation around the equilibrium configuration, *i.e.*, write the Wigner function as

$$W(\boldsymbol{r},\boldsymbol{k},t) = W_0(\boldsymbol{k}) + \tilde{W}(\boldsymbol{r},\boldsymbol{k},t), \tag{3.86}$$

where W_0 represents the static and homogeneous background in equilibrium, and $\tilde{W}$ indicates a per-

turbation around the equilibrium configuration, verifying $|W_0| \gg |\tilde{W}|$. Consistently, the density reads $n(\boldsymbol{r},t) = n_0 + \tilde{n}(\boldsymbol{r},t)$, which are related to (3.86) by integration along $\boldsymbol{k}$. Equation (3.84) requires the Fourier transform of both the Wigner function and the density, which gives

$$W(\boldsymbol{q},\boldsymbol{k},t) = W_0(\boldsymbol{k})\delta(\boldsymbol{q}) + \tilde{W}(\boldsymbol{q},\boldsymbol{k},t), \tag{3.87}$$

$$n(\boldsymbol{q},t) = n_0\delta(\boldsymbol{q}) + \tilde{n}(\boldsymbol{q},t). \tag{3.88}$$

After introducing (3.87) and (3.88) into (3.84), and separating the zero-th and the first order terms, we find two equations. For the lowest order, we get

$$\Delta\xi^{-}(\boldsymbol{q},\boldsymbol{k})W_0(\boldsymbol{k})\delta(\boldsymbol{q}) + n_0\int d\boldsymbol{q'}\ \delta(\boldsymbol{q}-\boldsymbol{q'})\delta(\boldsymbol{q'})\,\mathcal{U}(q')\Big[W_0(\boldsymbol{k}+\boldsymbol{q'}/2) - W_0(\boldsymbol{k}-\boldsymbol{q'}/2)\Big] = 0. \tag{3.89}$$

Using $\delta(\boldsymbol{q'})\delta(\boldsymbol{q}-\boldsymbol{q'}) = \delta(\boldsymbol{q})\delta(\boldsymbol{q}-\boldsymbol{q'})$, and performing the last integration, we obtain

$$W_0(\boldsymbol{k})\Big[\xi(\boldsymbol{k}+\boldsymbol{q}/2) - \xi(\boldsymbol{k}-\boldsymbol{q}/2)\Big]\delta(\boldsymbol{q}) + n_0\,\mathcal{U}(q)\Big[W_0(\boldsymbol{k}+\boldsymbol{q}/2) - W_0(\boldsymbol{k}-\boldsymbol{q}/2)\Big]\delta(\boldsymbol{q}) = 0 \tag{3.90}$$

This equation is trivially verified using the relation $\delta(\boldsymbol{q}-\boldsymbol{q}_0)f(\boldsymbol{q}) = \delta(\boldsymbol{q}-\boldsymbol{q}_0)f(\boldsymbol{q}_0)$, valid for any smooth function f. Therefore, we conclude that the lowest order contributions in (3.63) vanish. Moreover, the first order terms yield

$$\Big[i\hbar\frac{\partial}{\partial t} - \Delta\xi^{-}(\boldsymbol{q},\boldsymbol{k})\Big]\tilde{W}(\boldsymbol{q},\boldsymbol{k},t) = \tilde{n}(\boldsymbol{q},t)\,\mathcal{U}(q)\,\Delta W_0(\boldsymbol{k},\boldsymbol{q}) + n_0\int d\boldsymbol{q'}\,\mathcal{U}(q)\delta(\boldsymbol{q'})\Delta\tilde{W}(\boldsymbol{q},\boldsymbol{k},\boldsymbol{q'},t), \tag{3.91}$$

where the definitions below were used:

$$\Delta W_0(\boldsymbol{k}) = W_0(\boldsymbol{k}-\boldsymbol{q}/2) - W_0(\boldsymbol{k}+\boldsymbol{q}/2), \tag{3.92}$$

$$\Delta\tilde{W}(\boldsymbol{q},\boldsymbol{k},\boldsymbol{q'},t) = \tilde{W}(\boldsymbol{q}-\boldsymbol{q'},\boldsymbol{k}-\boldsymbol{q'}/2,t) - \tilde{W}(\boldsymbol{q}-\boldsymbol{q'},\boldsymbol{k}+\boldsymbol{q'}/2,t). \tag{3.93}$$

Note that the last term in (3.91) vanishes, after the integration in $\boldsymbol{q'}$. After Fourier transforming the time coordinate, we can recast (3.91) into a more familiar form,

$$\tilde{W}(\boldsymbol{q},\boldsymbol{k},\omega) = \tilde{n}(\boldsymbol{q},t)\,\mathcal{U}(q)\,\frac{\Delta W_0(\boldsymbol{k},\boldsymbol{q})}{\hbar\omega - \xi(\boldsymbol{k}+\boldsymbol{q}/2) + \xi(\boldsymbol{k}-\boldsymbol{q}/2)}. \tag{3.94}$$

After integrating both sides in $\boldsymbol{k}$, we can recast the solution to the above equation in the form of a dielectric function $\epsilon(\boldsymbol{q},\omega)$, which reads

$$\epsilon(\boldsymbol{q},\omega) = 1 - \mathcal{U}(q)\Pi(\boldsymbol{q},\omega), \tag{3.95}$$

and the polarizability function $\Pi(\boldsymbol{q},\omega)$ is defined as

$$\Pi(\boldsymbol{q},\omega) = \int d\boldsymbol{k}\,\frac{W_0(\boldsymbol{k}) - W_0(\boldsymbol{k}+\boldsymbol{q})}{\hbar\omega + \xi(\boldsymbol{k}) - \xi(\boldsymbol{k}+\boldsymbol{q})}. \tag{3.96}$$

When written in this manner, the plasmon dispersion relation contained in (3.94) is found as a solution to the equation $\epsilon(\boldsymbol{q},\omega)=0$. Equation (3.95) corresponds to the well-know result of the random phase approximation (RPA) for the polarizability [90]. RPA is valid for small values of the coupling parameter r_s ($\sim$ ratio of average potential energy to average kinetic energy), which can be estimated as $r_s\sim\alpha_s/\varepsilon_r$, where $\alpha_s=e^2/(4\pi\varepsilon_0\hbar v_F)\approx 2.2$ is the graphene structure constant and ε_r is the relative permittivity. As a result, (3.96) is reliable as long as $\varepsilon_r\gtrsim 2.2$. As $r_s\to 0$, RPA becomes exact and the plasmon frequency can be entirely calculated using the noninteracting irreducible polarizability, such that we recover (3.95). In the scope of the present work, the same validity condition is imposed, because (3.91) only accounts for low order excitations. Equation (3.95) could be solved, numerically, in the entire $(\boldsymbol{q},\omega)-$plane, after specifying the equilibrium function $W_0(\boldsymbol{k})$. However, we will find it more instructive to calculate $\epsilon(\boldsymbol{q},\omega)$ analytically, which can be done in the limit of small q. To do so, let us rewrite the polarizability as

$$\Pi(\boldsymbol{q},\omega)=\int d\boldsymbol{k}\; W_0(\boldsymbol{k})\left[\frac{1}{\hbar\omega+\xi(\boldsymbol{k})-\xi(\boldsymbol{k}+\boldsymbol{q})}-\frac{1}{\hbar\omega+\xi(\boldsymbol{k}-\boldsymbol{q})-\xi(\boldsymbol{k})}\right], \tag{3.97}$$

achieved with a coordinate transformation. Then, we align $\boldsymbol{q}$ with the $x-$direction, such that $\boldsymbol{k}\cdot\boldsymbol{q}=k\,q\cos\theta$, for θ being the polar angle of $\boldsymbol{k}$. This procedure allows us to write $|\boldsymbol{k}\pm\boldsymbol{q}|=\sqrt{k^2+q^2\pm 2kq\cos\theta}$. With this in mind, we easily expand the fractions in (3.97) up to $\mathcal{O}\big(q^4\big)$, to obtain

$$\begin{aligned}\frac{1}{\hbar\omega+\xi(\boldsymbol{k})-\xi(\boldsymbol{k}+\boldsymbol{q})}-\frac{1}{\hbar\omega+\xi(\boldsymbol{k}-\boldsymbol{q})-\xi(\boldsymbol{k})}\simeq\;&\frac{v_F^2\sin^2\theta}{\hbar k}\frac{q^2}{\omega^2}+\frac{2v_F^2}{\hbar k}\big(\cos\theta-\cos^3\theta\big)\frac{q^3}{\omega^3}\\&+\frac{3v_F^3}{\hbar k}\big(\cos^2\theta-\cos^4\theta\big)\frac{q^4}{\omega^4}.\end{aligned} \tag{3.98}$$

We can assume the equilibrium configuration to be given by

$$W_0(\boldsymbol{k})=n_0\Theta(k_F-k)/\pi k_F^2, \tag{3.99}$$

i.e., we occupy all $\boldsymbol{k}-$states up to the region[7] $|\boldsymbol{k}|=k_F$, and leave the remaining states unoccupied. This is justified invoking the 2D Fermi model for an electron gas once, in the ultra-cold limit $T\to 0$, we have $\lim\limits_{T\to 0} f_{FD}(\xi_k)=\Theta(\xi_{k_F}-\xi_k)$, where $f_{FD}(x)$ is the previously defined Fermi-Dirac distribution function. In addition, it verifies $\int d\boldsymbol{k}\; W_0(\boldsymbol{k})=n_0$. We stress the fact that the correct form of $f_{FD}(\xi_{\boldsymbol{k}})$ can be introduced as temperature corrections to the Heaviside step function used above, but are found to be negligible in the present case. Introducing the above results into (3.97), we get

$$\Pi(\boldsymbol{q},\omega)=k_F v_F\pi\frac{q^2}{\omega^2}+\frac{3v_F^3k_F\pi}{4}\frac{q^4}{\omega^4} \tag{3.100}$$

Up to $\mathcal{O}\big(q^2\big)$ terms, we obtain the plasmon dispersion relation

$$\omega(q)=\pm\Big(\omega_p^2\frac{q}{k_F}+\frac{3}{4}v_F^2q^2\Big)^{1/2}, \tag{3.101}$$

[7] This region is referred to in the literature as the Fermi sphere.

where ω_p is the characteristic plasmon frequency

$$\omega_p = \left(\frac{e^2 n_0 v_F}{2\hbar \varepsilon_0 \varepsilon_r} \right)^{1/2}, \tag{3.102}$$

which depends on experimental parameters ε_r and n_0, as well as universal constants. By defining the dimensionless variables $\omega' = \omega/\omega_p$, $q' = q/k_F$, we can recast (3.101) as

$$\omega'(q') = \pm \left(q' + \frac{3\varepsilon_r}{8\alpha_s} q'^2 \right)^{1/2}, \tag{3.103}$$

The positive branch of (3.103) is depicted in Figs. 3.5 and 3.6. Each branch corresponds to a different direction of propagation (forward and backward waves) for the longitudinal plasmonic modes. For the typical material values of $\varepsilon_r = 2.5$ and $n_0 \in [5 \times 10^{-6}, 1] \times 10^{12}$ cm^{-2}, ω_p lies in the THz-region, $\omega_p \in [0.3, 234.6]$ THz. The first term in the dispersion relation, $\omega \propto \sqrt{q}$, is the dominant one, being characteristic of 2D electron gases [90]. The most relevant difference, when compared to the characteristic plasmon frequency in the 3-dimensional parabolic case, $\omega_p^{3D} = \sqrt{e^2 n_0/\varepsilon_0 m}$, is the appearance of $\hbar$ in the leading term, revealing its pure quantum nature. Therefore, no classical counterpart exists for the 2-dimensional Dirac plasma. This result was already found in the literature [91, 92], derived within RPA. Both methods are equivalent, but the present one is found to be more practical, leading to severely less convoluted calculations. On the other hand, the present formulation is convenient to describe the system out of equilibrium, and it can be used to construct hydrodynamical models, as we shall see next.

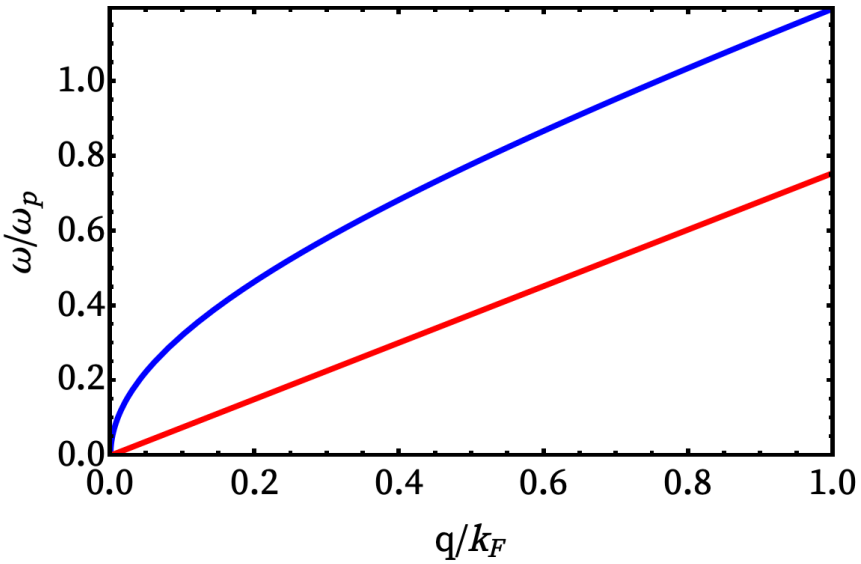

Figure 3.5: Positive solution for the plasmon dispersion relation of (3.103) (in blue), along with the Dirac dispersion relation $\omega = v_F q$ (in red), plotted for $\epsilon_r = 2.5$.

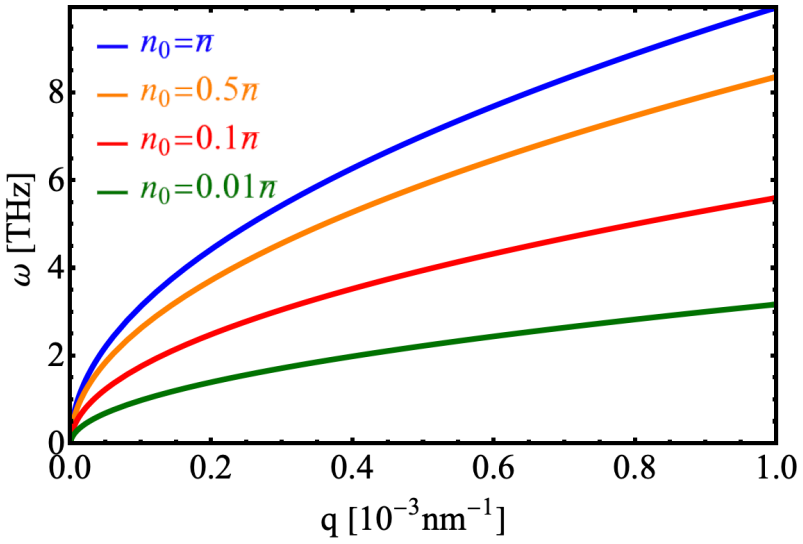

Figure 3.6: Plasmon dispersion relation (positive branch), for $\epsilon_r = 2.5$ and different values of the density, measured in units of $\overline{n} = 10^{12}$ cm^{-2}. The functional dependence is of the form $\omega \propto n^{1/4}$, in contrast with that of 3D parabolic plasmons, where typically $\omega \propto n^{1/2}$. The condition $q \ll k_F$ holds.

Chapter 4

Hydrodynamical model

In this chapter, we use the model derived before to construct the set of hydrodynamical equations governing the charge transport in graphene. Those equations are established after taking the moments of the Wigner equation, to include density and averaged momentum evolution, for the electron-hole system. The linear energy dispersion introduces a peculiar modification, when compared to the more familiar case of parabolic plasmas, being one of differences the constant Fermi velocity of charge carriers, akin to the photons. Despite not having a definite mass, Dirac particles are travelling at a constant speed, and thus the hydrodynamical formulation requires a fluid velocity field to be constructed. As such, the relation between velocity and momentum is used to put forward an effective mass, which is not, in general, momentum-independent. This technicality, as we shall see, makes it more convenient to start entirely with momentum (or wave-vector), which plays the role of the relevant hydrodynamical variable, aside with the density. As usual, when dealing with a quantum hydrodynamical model, the resolvable length scales are restrict to the long wavelength limit, $q \ll k_F$. Besides, we neglect both relativistic and spin effects, which additionally imposes the condition $\omega/q \ll c$. Such a procedure is justified as far as magnetic effects are negligible [83], guaranteeing the invariance between both spin populations. The classical limit of the relevant equations is obtained, retaining the most important features for the case of interest, and a comparison with previous models is settled. In this scope, we derive the non-linear relation between velocity and momentum, and discuss some important issues concerning the effective mass problem [93, 94]. In the end, the first quantum terms are kept in the hydrodynamical equations, and the corresponding quantum corrections are added to the previous plasmon dispersion relation.

4.1 Derivation of the hydrodynamical set of equations

In the previous chapter, we derived the transport equation for the Wigner matrix components,

$$\Big[i\hbar\,\frac{\partial}{\partial t} - \Delta\xi^{-}(\boldsymbol{q},\boldsymbol{k})\Big]W^{\alpha\gamma}(\boldsymbol{q},\boldsymbol{k},t) = e\int d\boldsymbol{q}'\;\phi(\boldsymbol{q}',t)\;\Delta W^{\alpha\gamma}(\boldsymbol{q},\boldsymbol{k},\boldsymbol{q}',t). \tag{4.1}$$

One of the major advantages of kinetic equations is the possibility of calculating the moments out of (4.1). Because we are concerned with the diagonal elements of the Wigner matrix only, let us define W^α as being the diagonal components, *i.e.*, $W^\alpha \doteq W^{\alpha\alpha}$. Similarly to the classical and quantum cases treated in chapter 2, we define the average value of an operator $\hat{\mathcal{G}}$ as

$$\overline{\mathcal{G}}^\alpha = \frac{1}{n^\alpha(\boldsymbol{r},t)} \int d\boldsymbol{k}\; \mathcal{T}\{\hat{\mathcal{G}}\} W^\alpha(\boldsymbol{r},\boldsymbol{k},t) \tag{4.2}$$

where $\mathcal{T}\{\hat{\mathcal{G}}\}$ denotes the Weyl transform of the operator $\hat{\mathcal{G}}$, defined in (2.19). Equation (4.2) is valid for both scalar and vectorial operators, where in the vectorial case, (4.2) holds true for each component.

The cases $\hat{\mathcal{G}} = 1$ and $\hat{\boldsymbol{\mathcal{G}}} = \hat{\boldsymbol{k}}$ define the relevant hydrodynamical variables

$$n^\alpha(\boldsymbol{r},t) = \int d\boldsymbol{k}\; W^\alpha(\boldsymbol{r},\boldsymbol{k},t), \tag{4.3}$$

$$\overline{\boldsymbol{k}}^\alpha(\boldsymbol{r},t) = \frac{1}{n^\alpha(\boldsymbol{r},t)} \int d\boldsymbol{k}\; \boldsymbol{k}\; W^\alpha(\boldsymbol{r},\boldsymbol{k},t), \tag{4.4}$$

Above, we used $\mathcal{T}\{\hat{\boldsymbol{k}}\} = \boldsymbol{k}$, which can be proved by starting with (2.19) and performing the coordinate transformation $\boldsymbol{s} = \boldsymbol{r} - \boldsymbol{z}/2$, together with the relation $\langle \boldsymbol{r}|\, \hat{\boldsymbol{k}}\, |\boldsymbol{r'}\rangle = -i\boldsymbol{\nabla}\, \delta(\boldsymbol{r}-\boldsymbol{r'})$. In fact, a similar relation is found in the case of $\hat{\mathcal{G}}$ being a function of the operator $\hat{\boldsymbol{k}}$, *i.e.*, $\mathcal{T}\{\hat{\mathcal{G}}(\hat{\boldsymbol{k}})\} = \mathcal{G}(\boldsymbol{k})$, which in its turn implies

$$\overline{\mathcal{G}(\boldsymbol{k})}^\alpha(\boldsymbol{r},t) = \frac{1}{n^\alpha(\boldsymbol{r},t)} \int d\boldsymbol{k}\; \mathcal{G}(\boldsymbol{k})\; W^\alpha(\boldsymbol{r},\boldsymbol{k},t), \tag{4.5}$$

Since electrons and holes are massless Dirac fermions, moving at a constant velocity v_F, we can define the averaged currents $\overline{\boldsymbol{j}}^\alpha$ as

$$\overline{\boldsymbol{j}}^\alpha(\boldsymbol{r},t) = n^\alpha \overline{\boldsymbol{v}}^\alpha, \tag{4.6}$$

where $\overline{\boldsymbol{v}}^\alpha$ is the averaged velocity

$$\overline{\boldsymbol{v}}^\alpha = \frac{v_F}{n^\alpha} \int d\boldsymbol{k}\; \frac{\boldsymbol{k}}{|\boldsymbol{k}|}\; W^\alpha(\boldsymbol{r},\boldsymbol{k},t). \tag{4.7}$$

We will see that (4.7) is the correct velocity field, after identifying the classical limit of the hydrodynamical equations.

In order to obtain the hydrodynamical equations from the kinetic model of (3.63), one must differentiate (4.3) and (4.4)[1] with respect to time, and replace $\partial_t W^\alpha(\boldsymbol{r},\boldsymbol{k},t)$ by $\int d\boldsymbol{q}\; e^{i\boldsymbol{q}\cdot\boldsymbol{r}}\; \partial_t W^\alpha(\boldsymbol{q},\boldsymbol{k},t)$, given that (4.1) only provides time derivatives of the Wigner matrix components in the Fourier space. Then, the

[1] Timed n^α.

quantum continuity and momentum equations are

$$
\begin{aligned}
i\hbar\frac{\partial}{\partial t}n^{\alpha} &= \int d\boldsymbol{k}\; d\boldsymbol{q}\; e^{i\boldsymbol{r}\cdot\boldsymbol{q}}\;\Delta\xi^{-}(\boldsymbol{q},\boldsymbol{k})\;W^{\alpha}(\boldsymbol{q},\boldsymbol{k},t) \\
&\quad + e\int d\boldsymbol{q}\; d\boldsymbol{q}'\; e^{i\boldsymbol{q}\cdot\boldsymbol{r}}\;\phi(\boldsymbol{q}',t)\int d\boldsymbol{k}\;\Delta W^{\alpha\alpha}(\boldsymbol{q},\boldsymbol{k},\boldsymbol{q}',t), \qquad (4.8)\\
i\hbar\frac{\partial}{\partial t}\big(n^{\alpha}\overline{\boldsymbol{k}}^{\alpha}\big) &= \int d\boldsymbol{k}\; d\boldsymbol{q}\; e^{i\boldsymbol{r}\cdot\boldsymbol{q}}\;\boldsymbol{k}\;\Delta\xi^{-}(\boldsymbol{q},\boldsymbol{k})\;W^{\alpha}(\boldsymbol{q},\boldsymbol{k},t) \\
&\quad + e\int d\boldsymbol{q}\; d\boldsymbol{q}'\; e^{i\boldsymbol{q}\cdot\boldsymbol{r}}\;\phi(\boldsymbol{q}',t)\int d\boldsymbol{k}\;\boldsymbol{k}\;\Delta W^{\alpha\alpha}(\boldsymbol{q},\boldsymbol{k},\boldsymbol{q}',t). \qquad (4.9)
\end{aligned}
$$

where $n^{\alpha}\equiv n^{\alpha}(\boldsymbol{r},t)$ and $\overline{\boldsymbol{k}}^{\alpha}\equiv\overline{\boldsymbol{k}}^{\alpha}(\boldsymbol{r},t)$. It is convenient to rewrite

$$
\Delta W^{\alpha\gamma}(\boldsymbol{q},\boldsymbol{k},\boldsymbol{q}',t) = -2s^{\alpha}e^{-\boldsymbol{q}'\cdot\boldsymbol{\nabla}_{\boldsymbol{q}}}\Big[\sinh\Big(\frac{\boldsymbol{q}'}{2}\cdot\boldsymbol{\nabla}_{\boldsymbol{k}}\Big)\delta^{\alpha\gamma}+\cosh\Big(\frac{\boldsymbol{q}'}{2}\cdot\boldsymbol{\nabla}_{\boldsymbol{k}}\Big)(\delta^{\alpha\gamma}-1)\Big]W^{\alpha\gamma}(\boldsymbol{q},\boldsymbol{k},t), \quad (4.10)
$$

as well as

$$
\Delta\xi^{-}(\boldsymbol{q},\boldsymbol{k}) = 2\sinh\Big(\frac{\boldsymbol{q}}{2}\cdot\boldsymbol{\nabla}_{\boldsymbol{k}}\Big)\xi(\boldsymbol{k}). \qquad (4.11)
$$

Therefore, starting with (4.8), we get

$$
\begin{aligned}
i\hbar\frac{\partial}{\partial t}n^{\alpha} &= 2\int d\boldsymbol{k}\; d\boldsymbol{q}\; e^{i\boldsymbol{r}\cdot\boldsymbol{q}}\;\left[\sinh\Big(\frac{\boldsymbol{q}}{2}\cdot\boldsymbol{\nabla}_{\boldsymbol{k}}\Big)\xi(\boldsymbol{k})\right]\;W^{\alpha}(\boldsymbol{q},\boldsymbol{k},t) \\
&\quad - 2\mathcal{Q}^{\alpha}\int d\boldsymbol{q}\; d\boldsymbol{q}'\; e^{i\boldsymbol{q}\cdot\boldsymbol{r}}\;\phi(\boldsymbol{q}',t)\;e^{-\boldsymbol{q}'\cdot\boldsymbol{\nabla}_{\boldsymbol{q}}}\int d\boldsymbol{k}\;\sinh\Big(\frac{\boldsymbol{q}'}{2}\cdot\boldsymbol{\nabla}_{\boldsymbol{k}}\Big)W^{\alpha}(\boldsymbol{q},\boldsymbol{k},t), \qquad (4.12)
\end{aligned}
$$

In 2D, the differential operator $\sinh\Big(\frac{\boldsymbol{q}'}{2}\cdot\boldsymbol{\nabla}_{\boldsymbol{k}}\Big)$ reads

$$
\begin{aligned}
\sinh\Big(\frac{\boldsymbol{q}'}{2}\cdot\boldsymbol{\nabla}_{\boldsymbol{k}}\Big) &= \sum_{n=0}^{+\infty}\sum_{m=0}^{2n+1}\;\theta_{nm}\;\Big(\frac{q'_x}{2}\frac{\partial}{\partial_{k_x}}\Big)^{m}\Big(\frac{q'_y}{2}\frac{\partial}{\partial_{k_y}}\Big)^{2n+1-m}, \\
&= \frac{q'_x}{2}\frac{\partial}{\partial_{k_x}}+\frac{q'_y}{2}\frac{\partial}{\partial_{k_y}}+\frac{1}{3!}\Big(\frac{q'_y}{2}\frac{\partial}{\partial_{k_y}}\Big)^{3}+\frac{1}{3!}\Big(\frac{q'_x}{2}\frac{\partial}{\partial_{k_x}}\Big)^{3}+ \\
&\quad \frac{1}{2!}\Big(\frac{q'_x}{2}\frac{\partial}{\partial_{k_x}}\Big)\Big(\frac{q'_y}{2}\frac{\partial}{\partial_{k_y}}\Big)^{2}+\frac{1}{2!}\Big(\frac{q'_x}{2}\frac{\partial}{\partial_{k_x}}\Big)^{2}\Big(\frac{q'_y}{2}\frac{\partial}{\partial_{k_y}}\Big)+\;... \qquad (4.13)
\end{aligned}
$$

where $\theta_{nm}=1/m!(2n+1-m)!$. This expansion is useful because it allows us to simplify the second term on r.h.s of (4.12). Giving that the remaining integrand is $\boldsymbol{k}-$independent, the integral can be calculated through partial integration, which yields vanishing surface contributions, *i.e.*

$$
\begin{aligned}
&\int d\boldsymbol{k}\;\sinh\Big(\frac{\boldsymbol{q}'}{2}\cdot\boldsymbol{\nabla}_{\boldsymbol{k}}\Big)W^{\alpha}(\boldsymbol{q},\boldsymbol{k},t) = \\
&= \sum_{n=0}^{+\infty}\sum_{m=1}^{2n+1}\;\theta_{nm}\int dk_y\;\Big(\frac{q'_y}{2}\frac{\partial}{\partial_{k_y}}\Big)^{2n+1-m}\Big(\frac{q'_x}{2}\frac{\partial}{\partial_{k_x}}\Big)^{m-1}\;\Big[W^{\alpha}(\boldsymbol{q},+\infty,k_y,t)-W^{\alpha}(\boldsymbol{q},-\infty,k_y,t)\Big] \\
&+\sum_{n=0}^{+\infty}\theta_{n0}\int dk_x\;\Big(\frac{q'_y}{2}\frac{\partial}{\partial_{k_y}}\Big)^{2n}\;\Big[W^{\alpha}(\boldsymbol{q},k_x,+\infty,t)-W^{\alpha}(\boldsymbol{q},k_x,-\infty,t)\Big]=0, \qquad (4.14)
\end{aligned}
$$

under the assumption that the matrix elements and all order $\boldsymbol{k}-$derivatives go to zero as $k_i\to\pm\infty$.

Then, we are led to the continuity equation

$$i\hbar\frac{\partial}{\partial t}n^{\alpha}(\boldsymbol{r},t)=2\int d\boldsymbol{k}\;d\boldsymbol{q}\;e^{i\boldsymbol{r}\cdot\boldsymbol{q}}\left[\sinh\Big(\frac{\boldsymbol{q}}{2}\cdot\boldsymbol{\nabla}_{\boldsymbol{k}}\Big)\xi(\boldsymbol{k})\right]W^{\alpha}(\boldsymbol{q},\boldsymbol{k},t). \tag{4.15}$$

We stress the fact that our continuity equation is modified by the linear dispersion relation for Dirac particles. If compared to (2.42), for the case of parabolic plasmas, we observe a more complex structure for the second term arising, instead of the usual form $\sim\boldsymbol{\nabla}\cdot\overline{j}^{\alpha}$. This stems from the fact that the parabolic kinetic term is classical, *i.e.*, it is the same as its classical version. On the contrary, the form of (4.15) is a direct manifestation of the kinetic operator of (3.66), which is not quadratic in $\boldsymbol{k}$, and has no classical counterpart. The quantum nature of (3.66) explicitly modifies the continuity equation (for which we leave a more convenient treatment to the next chapter). Now, we turn our attention to the averaged momentum equation in (4.9). Following a similar procedure, we found

$$\begin{aligned}i\hbar\frac{\partial}{\partial t}\big(n^{\alpha}\overline{\boldsymbol{k}}^{\alpha}\big)=2\int d\boldsymbol{k}\;d\boldsymbol{q}\;e^{i\boldsymbol{r}\cdot\boldsymbol{q}}\;\boldsymbol{k}\left[\sinh\Big(\frac{\boldsymbol{q}}{2}\cdot\boldsymbol{\nabla}_{\boldsymbol{k}}\Big)\xi(\boldsymbol{k})\right]W^{\alpha}(\boldsymbol{q},\boldsymbol{k},t)\\-2\mathcal{Q}^{\alpha}\int d\boldsymbol{q}\;d\boldsymbol{q}'\;e^{i\boldsymbol{q}\cdot\boldsymbol{r}}\;\phi(\boldsymbol{q}',t)\;e^{-\boldsymbol{q}'\cdot\boldsymbol{\nabla}_{\boldsymbol{q}}}\int d\boldsymbol{k}\;\boldsymbol{k}\;\sinh\Big(\frac{\boldsymbol{q}'}{2}\cdot\boldsymbol{\nabla}_{\boldsymbol{k}}\Big)W^{\alpha}(\boldsymbol{q},\boldsymbol{k},t).\end{aligned} \tag{4.16}$$

The second term on the r.h.s. can be simplified. To do that, we use (4.13) to perform the $\boldsymbol{k}-$integration. However, because of the extra $\boldsymbol{k}-$factor inside the integral, some of the terms in the expansion yield non-zero contributions, apart from the vanishing surface terms. Given that the remaining integrand is linear in $\boldsymbol{k}$, the non-zero contributions come from the first two derivatives in (4.13). Hence,

$$\begin{aligned}\int d\boldsymbol{k}\;\boldsymbol{k}\;\sinh\Big(\frac{\boldsymbol{q}'}{2}\cdot\boldsymbol{\nabla}_{\boldsymbol{k}}\Big)W^{\alpha}(\boldsymbol{q},\boldsymbol{k},t)&=-\frac{\boldsymbol{q}'}{2}\int d\boldsymbol{k}\;W^{\alpha}(\boldsymbol{q},\boldsymbol{k},t)\;+\;\cancel{\text{surface terms}},\\&=-\frac{\boldsymbol{q}'}{2}n^{\alpha}(\boldsymbol{q},t)\\&=-\frac{\boldsymbol{q}'}{2}\int\frac{d\boldsymbol{r}'}{(2\pi)^2}\;e^{-i\boldsymbol{q}\cdot\boldsymbol{r}'}n^{\alpha}(\boldsymbol{r}',t).\end{aligned} \tag{4.17}$$

Inserting the above result into the second term on the r.h.s. of (4.16), we finally have

$$\begin{aligned}\mathcal{Q}^{\alpha}\int d\boldsymbol{q}\;d\boldsymbol{q}'\;\frac{d\boldsymbol{r}'}{(2\pi)^2}\;\boldsymbol{q}'\;e^{i\boldsymbol{q}\cdot\boldsymbol{r}}\;\phi(\boldsymbol{q}',t)\;e^{-\boldsymbol{q}'\cdot\boldsymbol{\nabla}_{\boldsymbol{q}}}\;e^{-i\boldsymbol{q}\cdot\boldsymbol{r}'}\;n^{\alpha}(\boldsymbol{r}',t),\\=\mathcal{Q}^{\alpha}\int d\boldsymbol{q}\;d\boldsymbol{q}'\;\frac{d\boldsymbol{r}'}{(2\pi)^2}\;\boldsymbol{q}'\;e^{i\boldsymbol{q}\cdot\boldsymbol{r}}\;\phi(\boldsymbol{q}',t)\;e^{i\boldsymbol{q}'\cdot\boldsymbol{r}'}\;e^{-i\boldsymbol{q}\cdot\boldsymbol{r}'}\;n^{\alpha}(\boldsymbol{r}',t),\\=\mathcal{Q}^{\alpha}\int d\boldsymbol{r}'\;d\boldsymbol{q}'\;\boldsymbol{q}'\;\delta(\boldsymbol{r}-\boldsymbol{r}')\;\phi(\boldsymbol{q}',t)\;e^{i\boldsymbol{q}'\cdot\boldsymbol{r}'}\;n^{\alpha}(\boldsymbol{r}',t),\\=-i\mathcal{Q}^{\alpha}n^{\alpha}(\boldsymbol{r},t)\boldsymbol{\nabla}\phi(\boldsymbol{r},t).\end{aligned} \tag{4.18}$$

In the first step, we used $e^{-\boldsymbol{q}'\cdot\boldsymbol{\nabla}_{\boldsymbol{q}}}\;e^{-i\boldsymbol{q}\cdot\boldsymbol{r}'}=e^{i\boldsymbol{q}'\cdot\boldsymbol{r}'}\;e^{-i\boldsymbol{q}\cdot\boldsymbol{r}'}$, while in the last $\boldsymbol{q}'\;e^{i\boldsymbol{q}'\cdot\boldsymbol{r}}=-i\boldsymbol{\nabla}\;e^{i\boldsymbol{q}'\cdot\boldsymbol{r}}$. In terms of the average momentum $\overline{\boldsymbol{p}}^{\alpha}=\hbar\overline{\boldsymbol{k}}^{\alpha}$, equation (4.16) becomes

$$\frac{\partial}{\partial t}(n^{\alpha}\overline{\boldsymbol{p}}^{\alpha})=\;-2i\int d\boldsymbol{k}\;d\boldsymbol{q}\;e^{i\boldsymbol{r}\cdot\boldsymbol{q}}\;\boldsymbol{p}\left[\sinh\Big(\frac{\boldsymbol{q}}{2}\cdot\boldsymbol{\nabla}_{\boldsymbol{k}}\Big)\xi(\boldsymbol{k})\right]W^{\alpha}(\boldsymbol{q},\boldsymbol{k},t)-\mathcal{Q}^{\alpha}n^{\alpha}\boldsymbol{\nabla}\phi. \tag{4.19}$$

When compared to the momentum equation for parabolic particles in (2.43), the above equation introduces a new term, which is interpreted as a quantum pressure. We examine it in more detail next.

4.2 Classical and semi-classical limits

In order to clarify the meaning of some of the terms in (4.15) and (4.29), it is instructive to obtain the classical limit $\hbar \to 0$, which can be done by replacing $\boldsymbol{k}$ with $\boldsymbol{p}/\hbar$ and neglecting $\mathcal{O}(\hbar)$ terms. The semi-classical limits are derived by keeping higher orders of $\hbar$. By Taylor expanding the $\sinh$ operator in (4.15), we have

$$\frac{\partial}{\partial t} n^{\alpha}(\boldsymbol{r},t) = -2i \int d\boldsymbol{q}\, d\boldsymbol{k}\, e^{i\boldsymbol{q}\cdot\boldsymbol{r}}\, W^{\alpha}(\boldsymbol{q},\boldsymbol{k},t) \sum_{n=0}^{+\infty} \frac{\hbar^{2n}}{(2n+1)!} \Big(\frac{\boldsymbol{q}}{2}\cdot\boldsymbol{\nabla}_{\boldsymbol{p}}\Big)^{2n+1} \xi(\boldsymbol{p})\ , \tag{4.20}$$

The same holds for (4.29)

$$\begin{aligned}\frac{\partial}{\partial t} n^{\alpha}(\boldsymbol{r},t)\overline{\boldsymbol{p}}^{\alpha}(\boldsymbol{r},t) = &-2i \int d\boldsymbol{q}\, d\boldsymbol{k}\, e^{i\boldsymbol{q}\cdot\boldsymbol{r}}\, \boldsymbol{p}\, W^{\alpha}(\boldsymbol{q},\boldsymbol{k},t) \sum_{n=0}^{+\infty} \frac{\hbar^{2n}}{(2n+1)!} \Big(\frac{\boldsymbol{q}}{2}\cdot\boldsymbol{\nabla}_{\boldsymbol{p}}\Big)^{2n+1} \xi(\boldsymbol{p}) \\ &- \mathcal{Q}^{\alpha} n^{\alpha}(\boldsymbol{r},t)\boldsymbol{\nabla}\phi(\boldsymbol{r},t).\end{aligned} \tag{4.21}$$

These expressions allow for the classical and semi-classical limits to be readly evaluated, by keeping the orders of $\hbar$ to our desire. Separating the sum into the classical ($\hbar-$independent) and quantum ($\hbar-$dependent) terms, it yields

$$\frac{\partial}{\partial t} n^{\alpha} + \boldsymbol{\nabla}\cdot\vec{\boldsymbol{j}}^{\alpha} = \hbar \int d\boldsymbol{k}\, \mathcal{N}\{W^{\alpha}\}, \tag{4.22}$$

$$\frac{\partial}{\partial t}(n^{\alpha}\overline{\boldsymbol{p}}^{\alpha}) + \boldsymbol{\nabla} P^{\alpha} + \mathcal{Q}^{\alpha} n^{\alpha}\boldsymbol{\nabla}\phi = \hbar \int d\boldsymbol{k}\, \boldsymbol{p}\, \mathcal{N}\{W^{\alpha}\}, \tag{4.23}$$

where $\vec{\boldsymbol{j}}^{\alpha}$ are the density currents defined in (4.6) and P^{α} is the pressure tensor[2]

$$P^{\alpha}(\boldsymbol{r},t) = v_F \int d\boldsymbol{k}\, \frac{1}{|\boldsymbol{p}|} \begin{pmatrix} p_x^2 & p_x p_y \\ p_y p_x & p_y^2 \end{pmatrix} W^{\alpha}(\boldsymbol{r},\boldsymbol{k},t). \tag{4.24}$$

The kernel $\mathcal{N}\{W^{\alpha}\}$ represents the quantum corrections to the classical hydrodynamical equations, which depend on the particular configuration of the system

$$\mathcal{N}\{W^{\alpha}\} = \sum_{n=1}^{+\infty} \frac{2\hbar^{2n-1}}{(2n+1)!\, i} \int d\boldsymbol{q}\, e^{i\boldsymbol{q}\cdot\boldsymbol{r}}\, W^{\alpha}(\boldsymbol{q},\boldsymbol{k},t) \Big(\frac{\boldsymbol{q}}{2}\cdot\boldsymbol{\nabla}_{\boldsymbol{p}}\Big)^{2n+1} \xi(\boldsymbol{p}). \tag{4.25}$$

Note that, in the case of parabolic dispersion relation, $\xi(\boldsymbol{p}) = \boldsymbol{p}^2/2m$, $\mathcal{N}$ vanishes. However, in the massless case, all order derivatives of $\xi(\boldsymbol{p})$ exist. Contrary to the parabolic case, for which the pressure

[2]The latin indices are spatial indices, which run over the spatial components x and y. This notation is used henceforth. The term $\boldsymbol{\nabla} P^{\alpha}$ is a vector, with the $i-$th component being given by $(\sum_j)\partial P_{\alpha ij}/\partial x_j$. It can be interpret as the action of a row vector on a matrix, yielding a column vector. Einstein's convention is also applied, so the summation symbol is discarded.

was the correlation function between velocity components, we conclude that, in the 2-dimensional case of Dirac particles, it is modified to be the average value of the product of one momentum component and one velocity coordinate. In other words, we have

$$P_{ij}^{\alpha}(\boldsymbol{r},t) = n^{\alpha}\overline{p_i v_j}^{\alpha} \, . \tag{4.26}$$

The classical limit applied to equations (4.22)−(4.23) is thus established by neglecting the quantum corrections $\mathcal{N}$. Therefore, setting the r.h.s. of both equations to zero, it is possible to rewrite the momentum equation, like in the parabolic case. To do that, we define the fluctuations around the equilibrium configuration of function $g(\boldsymbol{k})$ as

$$\delta g^{\alpha} = g - \overline{g}^{\alpha}. \tag{4.27}$$

Notice that the fluctuations hold a dependence on the band index since the average value may be different when calculated with each one of the diagonal components of the Wigner matrix. An immediate consequence of the definition (4.27) is $\overline{\delta g^{\alpha}} = 0$. Using this property, the pressure tensor can be rewritten as

$$P_{ij}^{\alpha}(\boldsymbol{r},t) = n^{\alpha}\overline{p_i}^{\alpha}\overline{v_j}^{\alpha} + n^{\alpha}\overline{\delta p_i^{\alpha}\delta v_j^{\alpha}}^{\alpha}. \tag{4.28}$$

Replacing (4.28) into (4.23) with $\mathcal{N} = 0$, we get

$$n^{\alpha}\Big(\frac{\partial}{\partial t} + \overline{\boldsymbol{v}}^{\alpha}\cdot\boldsymbol{\nabla}\Big)\,\overline{\boldsymbol{p}}^{\alpha} = -\boldsymbol{\nabla}\mathcal{P}^{\alpha} - \mathcal{Q}^{\alpha}n^{\alpha}\boldsymbol{\nabla}\phi, \tag{4.29}$$

where $\overline{\boldsymbol{v}}^{\alpha}$ is the velocity field in (4.7) and $\mathcal{P}^{\alpha}$ is the dynamical pressure tensor

$$\mathcal{P}_{ij}^{\alpha}(\boldsymbol{r},t) = n^{\alpha}\Big(\overline{p_i v_j}^{\alpha} - \overline{p_i}^{\alpha}\overline{v_j}^{\alpha}\Big). \tag{4.30}$$

Up to this point, we have just considered the density and averaged momentum as hydrodynamical variables. Higher order variables could be defined, being the averaged energy density $n^{\alpha}\overline{\xi}^{\alpha}$ the next in the chain, for which new transport equations would be settled, coupling the new to the previous variables. However, within the current scope, equations (4.22) and (4.23) suffice to describe the system accurately, as they form a closed set, thus higher order equations in the hydrodynamical hierarchy will be discarded. To go beyond the classical limit, we can include a quantum correction in the above equations, by considering the first term of $\mathcal{N}\{W^{\alpha}\}$, which leads to the semi-classical hydrodynamical model. Therefore, neglecting $\mathcal{O}\big(\hbar^2\big)$ terms in (4.25) we obtain, after straightforward algebra

$$\mathcal{N}\{W^{\alpha}\} \simeq \frac{\hbar}{24}\left[\frac{\partial^3}{\partial x^3}\Big(J_{xxx}W^{\alpha}\Big) + \frac{\partial^3}{\partial y^3}\Big(J_{yyy}W^{\alpha}\Big) + 3\frac{\partial^2}{\partial x^2}\frac{\partial}{\partial y}\Big(J_{xxy}W^{\alpha}\Big) + 3\frac{\partial}{\partial x}\frac{\partial^2}{\partial y^2}\Big(J_{yyx}W^{\alpha}\Big)\right], \tag{4.31}$$

where $W^{\alpha} \equiv W^{\alpha}(\boldsymbol{r},\boldsymbol{k},t)$ and J_{ijl} is a new dispersive tensor, defined as

$$J_{ijl} = v_F\left(\frac{3p_ip_jp_l}{|\boldsymbol{p}|^5} - \frac{\delta_{ij}p_l + \delta_{jl}p_i + \delta_{li}p_j}{|\boldsymbol{p}|^3}\right). \tag{4.32}$$

As mentioned before, $\mathcal{N}$ is $x-y$ symmetric. Equations (4.22)$-$(4.23) then read

$$\frac{\partial}{\partial t}n^\alpha + \boldsymbol{\nabla}\cdot\overline{\boldsymbol{j}}^\alpha = \frac{\hbar^2}{24}\left[\frac{\partial^3}{\partial x^3}\left(n^\alpha\overline{J_{xxx}}^\alpha\right) + \frac{\partial^3}{\partial y^3}\left(n^\alpha\overline{J_{yyy}}^\alpha\right) + 3\frac{\partial^2}{\partial x^2}\frac{\partial}{\partial y}\left(n^\alpha\overline{J_{xxy}}^\alpha\right) + 3\frac{\partial^2}{\partial y^2}\frac{\partial}{\partial x}\left(n^\alpha\overline{J_{yyx}}^\alpha\right)\right] + \mathcal{O}(\hbar^4), \tag{4.33}$$

$$\frac{\partial}{\partial t}(n^\alpha\overline{\boldsymbol{p}}^\alpha) + \boldsymbol{\nabla}P^\alpha + \mathcal{Q}^\alpha n^\alpha\boldsymbol{\nabla}\phi = \frac{\hbar^2}{24}\left[\frac{\partial^3}{\partial x^3}\left(n^\alpha\overline{\boldsymbol{T}_{xxx}}^\alpha\right) + \frac{\partial^3}{\partial y^3}\left(n^\alpha\overline{\boldsymbol{T}_{yyy}}^\alpha\right) + 3\frac{\partial^2}{\partial x^2}\frac{\partial}{\partial y}\left(n^\alpha\overline{\boldsymbol{T}_{xxy}}^\alpha\right) + 3\frac{\partial^2}{\partial y^2}\frac{\partial}{\partial x}\left(n^\alpha\overline{\boldsymbol{T}_{yyx}}^\alpha\right)\right] + \mathcal{O}(\hbar^4), \tag{4.34}$$

and $\boldsymbol{T}_{ijl} = \boldsymbol{p}J_{ijl}$, whose components we denote by $\boldsymbol{T}_{ijl} = (T^x_{ijl}, T^y_{ijl}) = (p_xJ_{ijl}, p_yJ_{ijl})$. The inclusion of the tensors J_{ijl} and $\boldsymbol{T}_{ijl}$ makes our model much harder to solve, as we now need a closure equation relating the average values of the tensors J_{ijl} and $\boldsymbol{T}_{ijl}$ with the previous hydrodynamical variables n^α and $\overline{\boldsymbol{p}}^\alpha$, which in turn requires knowledge of the diagonal components W^α. This problem is overcome with the help of a generic *ansatz* for the Wigner function, valid in the ultra-cold limit $T\to 0$, which will provide a closure relation for the first quantum corrections in the hydrodynamical equations. Before that, it is crucial to relate the fluid velocity to the fluid momentum, $\overline{\boldsymbol{v}}$ and $\overline{\boldsymbol{p}}$, which is the subject of the next chapter.

4.3 Mass transport

Having set the relevant transport equations, we shall move now to a more detailed discussion concerning the fluid momentum and velocity fields. In Ref. [33], an equation similar to (4.29) has been proposed to model a ballistic transport regime in graphene. In that work, a continuity and momentum equation were established, from a Boltzmann model for the classical distribution function. The authors discussed the validity limit of the proportionality relation, and used $\overline{\boldsymbol{p}}^1 = \mathcal{M}\overline{\boldsymbol{v}}^1$, where $\mathcal{M}$ is the Drude mass, $\mathcal{M} = \hbar k_F/v_F$. Furthermore, a modified Fermi wave-vector $k_F(\boldsymbol{r},t) = \sqrt{\pi n(\boldsymbol{r},t)}$ was used to define the local Drude mass via $\mathcal{M}(\boldsymbol{r},t) = \hbar k_F(\boldsymbol{r},t)/v_F$, so that the constant of proportionality between momentum and velocity becomes density dependent (and thus, implicitly spatial and time dependent). Any dependence on momentum was neglected.

To star this discussion in the scope of the present work, let us also consider the pure conducting electron system in (4.29), and restrict ourselves to one-dimensional motion, say, in the x direction. Note that there is, in principle, no loss of generality with this choice, given that no term was included that explicitly breaks the original conical symmetry. We also drop the band index, to condense notation. Equation (4.29) becomes

$$\left(\frac{\partial}{\partial t} + \overline{v}_x\frac{\partial}{\partial x}\right)\overline{p}_x = -\frac{1}{n}\frac{\partial\mathcal{P}}{\partial x} + F_x. \tag{4.35}$$

where $F_x = e\partial\phi/\partial x$ is the force acting on the carriers and $\mathcal{P} \doteq \mathcal{P}^1_{xx}$. On the other hand, the force

equation of Ref. [33] reads

$$\left(\frac{\partial}{\partial t}+\frac{1}{2}\overline{v}_x\frac{\partial}{\partial x}\right)\overline{v}_x=-\frac{1}{\mathcal{M}n}\frac{\partial\mathcal{P}}{\partial x}+\frac{1}{\mathcal{M}}F_x, \tag{4.36}$$

which is different from (4.35). With the present formalism, we found $\overline{\boldsymbol{p}}$ to be the good hydrodynamical variable to proceed; on the contrary, the procedure in Ref. [33] is applied to the classical velocity field instead, which justifies the main differences between (4.35) and (4.36). Additionally, the linear relation $\overline{\boldsymbol{p}}=\mathcal{M}(n)\overline{\boldsymbol{v}}$ was proposed to link $\overline{\boldsymbol{p}}$ to $\overline{\boldsymbol{v}}$, which is not generically valid for massless carriers [93]. Such fact is clearly supported by the present results, and should be evident after examining (4.4) and (4.7). Accordingly, in Ref. [94], it is pointed out that the mass content of the continuity and momentum equations is different, such that two quantities $n(\boldsymbol{r},t)$ and $\rho(\boldsymbol{r},t)$ naturally arise, respectively, in those two equations, denoting the density and mass density. Moreover, the (hydrodynamical) local mass $m(\boldsymbol{r},t)=\rho(\boldsymbol{r},t)/n(\boldsymbol{r},t)$ is, in its turn, not constant. The present results of (4.22) and (4.23) can be interpreted in the same manner, by defining the local mass $m(x,t)$, using

$$m(x,t)=\frac{\overline{p}_x(x,t)}{\overline{v}_x(x,t)}, \tag{4.37}$$

which is also not a constant, as we shall see next.

In equilibrium, *i.e.*, using (3.99), we find that

$$m=\Gamma\mathcal{M}, \tag{4.38}$$

where $\Gamma=2/3$ is a numerical factor. This result remains valid whenever the distribution admits the separable form $W(\boldsymbol{r},\boldsymbol{k},t)=w(\boldsymbol{r},t)W_0(\boldsymbol{k})$. However, for a generic solution, we indeed obtain a space and time dependent mass. Recalling the generic 2D model, the mass must be introduced with a tensorial form m_{ij}, which linearly relates two vectorial fields $\overline{\boldsymbol{p}}$ and $\overline{\boldsymbol{v}}$, as

$$\begin{aligned} m_{ij}(\boldsymbol{r},t)&=\frac{\overline{p}_i}{\overline{v}_i}\delta_{ij},\\ &=\frac{\hbar}{v_F}\frac{\displaystyle\int d\boldsymbol{k}\; k_i\; W(\boldsymbol{r},\boldsymbol{k},t)}{\displaystyle\int d\boldsymbol{k}\; k_i\; W(\boldsymbol{r},\boldsymbol{k},t)/|\boldsymbol{k}|}\delta_{ij}, \end{aligned} \tag{4.39}$$

The meaning of such fields should be clear: despite the charge carriers have no mass, the fluid velocity and momentum fields can be used to construct a fictitious mass, motivated by the usual parabolic case. Nevertheless, the value of the mass at each point in space and time does not correspond to the actual mass of carriers, but rather to what would the mass be if the two fields were indeed proportional to each other. It should, thus, be interpreted as a mathematical trick to provide more handy equations. Moreover, the tensorial structure for the mass should be included to contemplate the most generic case, for which the rotational symmetry in real space can be broken. Additionally, the mass density ρ becomes a tensor, $\rho_{ij}(\boldsymbol{r},t)=m_{ij}(\boldsymbol{r},t)n(\boldsymbol{r},t)$ Nonetheless, up to this point, no rotational-symmetry breaking terms have

been included, and m_{ij} should, thus, become proportional to the identity matrix, $m_{ij}(\boldsymbol{r},t) = m(\boldsymbol{r},t)\delta_{ij}$ and $\rho_{ij}(\boldsymbol{r},t) = \rho(\boldsymbol{r},t)\delta_{ij}$. Under such conditions, making $\hbar = 0$ in (4.22)−(4.23) leads to

$$\frac{\partial n}{\partial t} + \frac{\partial (n\overline{v}_j)}{\partial x_j} = 0, \tag{4.40}$$

$$\frac{\partial (\rho\overline{v}_i)}{\partial t} + \frac{\partial P_{ij}}{\partial x_j} - en\frac{\partial \phi}{\partial x_i} = 0, \tag{4.41}$$

thus recovering the results of [94] for the classical limit.

Moving forward, we aim at getting some insight on the hydrodynamic mass term, given in (4.39), which provides a closure relation between velocity and momentum. This tasks ultimately boils down to finding the correct form for the Wigner function. To avoid calculating the complete solution of (3.77), we follow the philosophy presented in Ref. [95], where, based on the incompressibility of the phase fluid, a shifted Fermi-Dirac distribution function has been proposed to describe the equilibrium. It is of the form

$$W(\boldsymbol{r},\boldsymbol{k},t) = \frac{n_0}{\pi k_F^2}\Theta\left(k_F - n_0\left|\frac{\boldsymbol{k} - \overline{\boldsymbol{k}}(\boldsymbol{r},t)}{n(\boldsymbol{r},t)}\right|\right), \tag{4.42}$$

where n and $\overline{\boldsymbol{k}} = (\overline{k}_x, \overline{k}_y)$ are the electron density and average wave-vector, respectively. This particular function guarantees equations (4.3) and (4.4) to be satisfied. For simplicity, we also strict the motion to be along the $x-$axis, and set $\overline{k}_y(\boldsymbol{r},t) = 0$. Introducing (4.42) into the $x-$component of (4.7), yields

$$\overline{v}_x(\boldsymbol{r},t) = \frac{v_F}{\pi k_F n'(\boldsymbol{r},t)}\int_{-\infty}^{+\infty} dk_y \int_{-\infty}^{+\infty} dk_x\, \frac{k_x}{\sqrt{k_x^2+k_y^2}}\,\Theta\left(k_F - \sqrt{\frac{\left[k_x - \overline{k}_x(\boldsymbol{r},t)\right]^2}{n'(\boldsymbol{r},t)^2} - k_y^2}\right), \tag{4.43}$$

where $n'(\boldsymbol{r},t) = n(\boldsymbol{r},t)/n_0$. The Heaviside step function defines the region of integration to lie inside an ellipse centred in $(\overline{k}_x, 0)$. Explicitly, we can derive the following result for a general function $g(\boldsymbol{r},\boldsymbol{k},t)$

$$\int d\boldsymbol{k}\; g(\boldsymbol{r},\boldsymbol{k},t)\,\Theta\left(k_F - \sqrt{\frac{\left[k_x - \overline{k}_x(\boldsymbol{r},t)\right]^2}{n'(\boldsymbol{r},t)^2} - k_y^2}\right) = \int_{-k_F}^{+k_F} dk_y \int_{k_-}^{k_+} dk_x\; g(\boldsymbol{r},\boldsymbol{k},t) \tag{4.44}$$

where

$$k_\pm(\boldsymbol{r},k_y,t) = \overline{k}_x(\boldsymbol{r},t) \pm n'(\boldsymbol{r},t)\sqrt{k_F^2 - k_y^2}. \tag{4.45}$$

Using this property to perform the integral in (4.39) along k_x and defining dimensionaless variables $k'_\pm = k_\pm/k_F$, $\overline{k}'_x = \overline{k}_x/k_F$, $k'_y = k_y/k_F$, it leads to

$$\overline{v}_x = \frac{v_F}{\pi n'}\int_{-1}^{+1} dk'_y\, \frac{4n'\,\overline{k}'_x\sqrt{1-{k'_y}^2}}{\sqrt{{k'_-}^2+{k'_y}^2}+\sqrt{{k'_+}^2+{k'_y}^2}}. \tag{4.46}$$

This relation can be evaluated numerically, and the result is depicted in Fig. 4.2. It is, however, instructive to obtain analytic expressions for certain limits of interest. We start by recasting the above equation into

the familiar form

$$\overline{v}_x(\boldsymbol{r},t) = \frac{\overline{p}_x(\boldsymbol{r},t)}{m(\boldsymbol{r},t)}, \tag{4.47}$$

where $m(\boldsymbol{r},t) = \mathcal{M}\gamma(\boldsymbol{r},t)$ and $\gamma(\boldsymbol{r},t)$ is a Lorentz-like factor, which depends on the position and time merely through the hydrodynamical variables $n(\boldsymbol{r},t)$ and $\overline{p}_x(\boldsymbol{r},t) = \hbar\,\overline{k}_x(\boldsymbol{r},t)$, as

$$\gamma^{-1}(n,\overline{p}_x) = \frac{8}{\pi}\int_0^1 dy\,\frac{\sqrt{1-y^2}}{\sqrt{f_+}+\sqrt{f_-}}\,, \tag{4.48}$$

where

$$f_\pm = \left(p' \pm n'\sqrt{1-y^2}\right)^2 + y^2. \tag{4.49}$$

Although the integral of (4.48) has no analytic solution, it reduces to simple expressions, in the limiting cases of small and large average momentum. We can verify that $(\partial\gamma/\partial\overline{p}_x)_{\overline{p}_x=0} = 0$, thus in the limit of small fluid momentum $\overline{p}_x/p_F \ll 1$, γ becomes momentum independent

$$\gamma(n) \simeq \frac{\pi}{4}\,\frac{1-n^2/n_0^2}{K_1(1-n^2/n_0^2) - K_2(1-n^2/n_0^2)}, \tag{4.50}$$

where $K_1(x) = \int_0^{\pi/2} d\theta\ (1-x^2\sin^2\theta)^{-1/2}$ and $K_2(x) = \int_0^{\pi/2} d\theta\ (1-x^2\sin^2\theta)^{1/2}$ are the complete elliptic integrals of the first and second kind. Accordingly, the quantities $\overline{p}_x$ and $\overline{v}_x$ become proportional to each other, ensuring a relation of the form $\overline{p}_x = m(n)\overline{v}_x$. However, only for the case $n = n_0$ the mass converges to the Drude mass, *i.e.*, the asymptotic expression of (4.50) verifies $\gamma(n_0) = 1$. For general out-of-equilibrium conditions with small averaged momentum, we have $m(n) = \gamma(n)\mathcal{M}$, with $\gamma(n)$ depicted in Fig. 4.1.

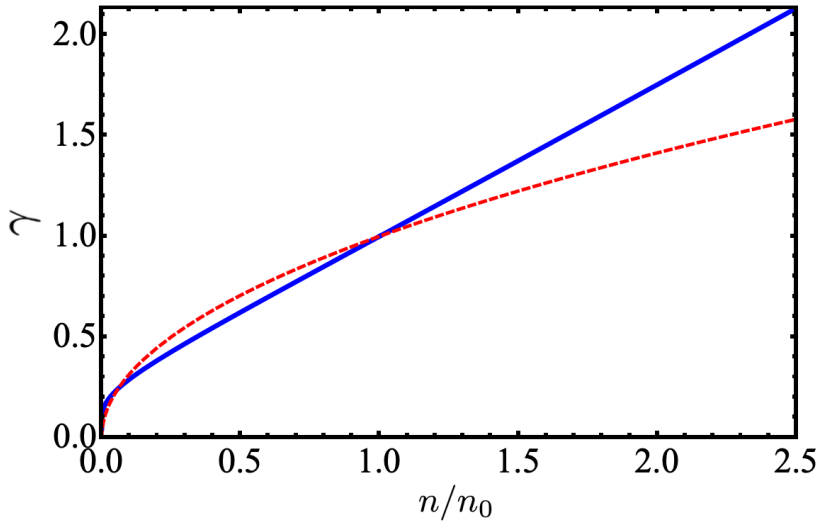

Figure 4.1: Graphical representation of equation (4.50), where γ is the (dimensionless) Lorentz factor, evaluated in the limit $\overline{p}_x/p_F \ll 1$. γ is independent of $\overline{p}_x$, and depends only on the electron density, with asymptotic behaviour $\gamma(n') \sim \pi n'/4n$ for $n' \gg 1$; $\gamma(n') = \sqrt{n'}$ (dashed red).

In Fig. 4.1, we also plot the commonly adopted expression $\gamma(n') = \sqrt{n'}$, for comparison. This form of γ leads to the effective mass

$$m(n') = \mathcal{M}\sqrt{n'}, \tag{4.51}$$

which is based on the local approximation for the Fermi wave-vector, $k_F = \sqrt{\pi n_0} \to \sqrt{\pi n(\boldsymbol{r}, t)}$ [2, 93, 94]. Equation (4.50) results in significant changes, when compared to the latter, with a functional dependence on n which strongly differs from proposed $\sqrt{n}$ behaviour, specially in the case of $n' \gg 1$.

Conversely, for the limiting case of $\overline{p}_x/p_F \gg 1$ we find

$$\gamma \simeq \frac{|\overline{p}_x|}{v_F \mathcal{M}}, \tag{4.52}$$

which implies $\overline{v}_x \simeq v_F \, \mathrm{sign}(\overline{p}_x)$, where $\mathrm{sign}(x)$ returns the sign of x. Then, for large fluid momentum, the fluid velocity approaches the Fermi velocity, never overcoming it, and becomes independent of the density and absolute value of $\overline{p}_x$, retaining only the momentum sign. In Fig. 4.2, we can see how changes on the density affect this relation. For increasing values of the density, the linear region becomes larger. On the contrary, for vanishingly small density, the relation is rapidly non-linear with increasing $\overline{p}_x$. Therefore, in low-density systems, knowledge of the equilibrium Wigner function is mandatory to reveal the relation between fluid momentum and velocity. In the generic 2D case, a relation of the form $\overline{\boldsymbol{v}} = \overline{\boldsymbol{p}}/m(\boldsymbol{r}, t)$ is expected, as in the case of relativistic dynamics. Without loss of generality, we must be able to arrive at a vectorial relation by starting from our one-dimensional simplification, as the symmetry between different directions still holds[3]. In that case, the form of $m(\boldsymbol{r}, t)$ is still given by $\mathcal{M}\gamma(\boldsymbol{r}, t)$, where γ is that of (4.48). Explicitly, γ only depends on the hydrodynamical variables n and $\overline{\boldsymbol{p}}$, thus holding an implicit spatial and time dependence, once $n = n(\boldsymbol{r}, t)$ and $\overline{\boldsymbol{p}} = \overline{\boldsymbol{p}}(\boldsymbol{r}, t)$. The relation between velocity and momentum is, thus, highly non-linear, as indicated in Fig. 4.1. We stress the fact that the expression of (4.48) is indicated to describe the transport of Dirac particles, as it encloses the correct relation from the low to the high density and momentum regimes. As such, the inclusion of (4.48) in the hydrodynamical model will certainly contribute towards a more rigours description.

To finalise, we should also comment on the particular choice of (4.42). As mentioned in [95], the incompressibility of the phase-space fluid, in a quantum picture, is violated by phenomena like tunneling, which would lead to a change in the amplitude of W, along a particle trajectory. Such behaviour is clearly not casted by (4.42). Nevertheless, (4.42) is correct to first order, and gets more accurate as the temperature decreases. Since graphene effective Fermi temperature, $T_F = E_F/k_B$, is very high ($\sim 1300K$ for $n_0 \sim 10^{12}\mathrm{cm}^{-2}$), then the present low-temperature approximation should be valid for room temperature conditions.

[3]This would not be so if a preferred direction was chosen, *e.g.*, by applying an external electric or magnetic field in the $x - y$ plane.

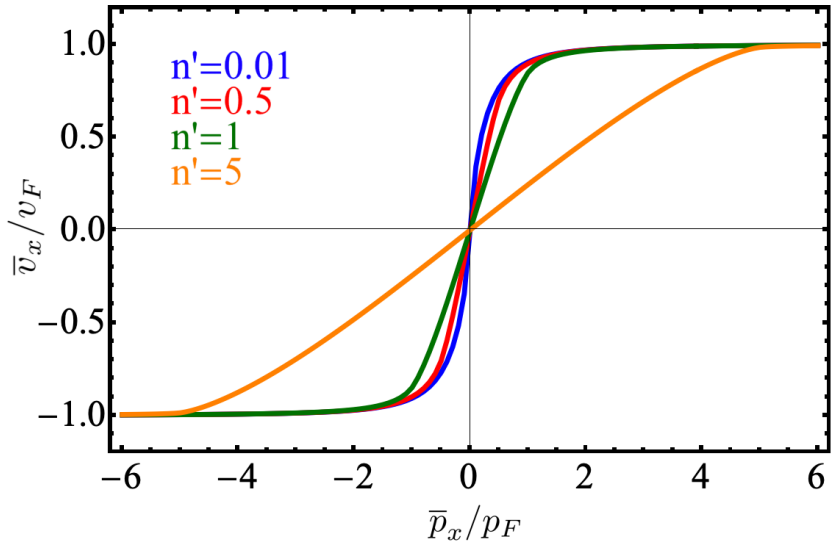

Figure 4.2: Graphical representation of (4.46). Near the origin, we find a linear relation between both variables, while for large momentum, the velocity converges, in absolute value, to the Fermi velocity, becoming only a function of the sign of $\overline{p}_x$.

4.4 Hydrodynamical plasmon dispersion relation

We now turn our attention to the quantum corrections present in the hydrodynamical equations. Up to $\mathcal{O}(\hbar^4)$, we saw that the continuity and averaged momentum equations acquire contributions described by the tensors J_{ijl} and $\boldsymbol{T}_{ijl}$, which can be interpreted as new pressure-like tensors, arising from the linear single-particle dispersion. Remember that, in the case of parabolic systems, those corrections were absent, which makes the models easier to solve.

The *ansatz* of (4.42) allows to evaluate the expectation value of the tensors J_{ijl}, $\boldsymbol{T}_{ijl}$ and P^{α}_{ij} as a function of the hydrodynamical variables n^{α} and $\overline{\boldsymbol{p}}^{\alpha}$. First, let us simplify the calculations by restricting, yet again, the variations to the $x-$direction, and drop the band index, to keep notation compact. We are led to

$$\frac{\partial}{\partial t}n + \frac{\partial}{\partial x}(n\overline{v}_x) = \frac{\hbar^2}{24}\frac{\partial^3}{\partial x^3}\left(n\overline{J_{xxx}}\right), \tag{4.53}$$

$$\frac{\partial}{\partial t}(n\overline{p}_x) + \frac{\partial}{\partial x}P_{xx} + \mathcal{Q}n\frac{\partial}{\partial x}\phi = \frac{\hbar^2}{24}\frac{\partial^3}{\partial x^3}\left(n\overline{T^x_{xxx}}\right), \tag{4.54}$$

together with the closure relation found in the previous chapter

$$\overline{p}_x = \gamma\mathcal{M}\overline{v}_x. \tag{4.55}$$

We recall the explicit form of the relevant tensorial components we aim to calculate

$$\overline{J_{xxx}} = \frac{3v_F}{n\hbar^2}\int d\boldsymbol{k}\ \left(\frac{k_x^2}{k}-1\right)\frac{k_x}{k^3}\ W(\boldsymbol{r},\boldsymbol{k},t), \tag{4.56}$$

$$\overline{T^x_{xxx}} = \frac{3v_F}{n\hbar^2}\int d\boldsymbol{k}\,\left(\frac{k_x^2}{k}-1\right)\frac{k_x^2}{k^3}\,W(\boldsymbol{r},\boldsymbol{k},t), \tag{4.57}$$

$$P_{xx} = \hbar v_F \int d\boldsymbol{k}\,\frac{k_x^2}{k}\,W(\boldsymbol{r},\boldsymbol{k},t), \tag{4.58}$$

where $k=\sqrt{k_x^2+k_y^2}$. Using (4.42) and the relation of (4.44), (4.56) gives

$$\overline{J_{xxx}} = \frac{v_F n_0}{\pi p_F^2 n}\int_{-k_F}^{k_F} dk_y\; k_y^2\left[\frac{1}{(k_+^2+k_y^2)^{1/2}}-\frac{1}{(k_-^2+k_y^2)^{1/2}}\right], \tag{4.59}$$

where we performed the integration over k_x. Doing the same for (4.57) and (4.58), it yields

$$\overline{T^x_{xxx}} = \frac{\hbar v_F n_0}{\pi p_F^2 n}\int_{-k_F}^{k_F} dk_y\left[\frac{k_-^3}{(k_-^2+k_y^2)^{3/2}}-\frac{k_+^3}{(k_+^2+k_y^2)^{1/2}}\right], \tag{4.60}$$

$$P_{xx} = \frac{\hbar v_F n_0}{2\pi k_F^2}\int_{-k_F}^{k_F} dk_y\left[k_+(k_+^2+k_y^2)^{1/2}-k_-(k_-^2+k_y^2)^{1/2}-k_y^2\log\left(\frac{k_+(k_-^2+k_y^2)^{1/2}}{k_-(k_+^2+k_y^2)^{1/2}}\right)\right]. \tag{4.61}$$

The integrands admit no analytic primitive. Nevertheless, we will be ultimately interested in solving the linearised versions of (4.53)−(4.54), which is valid for small amplitude fluctiations. Therefore, we shall rewrite the fluid momentum as

$$\overline{p}_x(x,t) = \overline{p}_{x,0} + \tilde{\overline{p}}_x(x,t), \tag{4.62}$$

where $\overline{p}_{x,0}$ is the background value and $\tilde{\overline{p}}_x$ is a first-order correction, verifying $|\tilde{\overline{p}}_x|/p_F \ll 1$. For the equilibrium configuration, we expect to have $\overline{p}_{x,0}=0$, such that only the first order term contributes. Expanding (4.59)−(4.64) and neglecting $\mathcal{O}\left(\tilde{\overline{p}}_x^2/p_F^2\right)$ terms, it leads to

$$\overline{J_{xxx}} \simeq \frac{4v_F}{\pi p_F^3}\frac{n_0/n}{(n^2/n_0^2-1)^2}\left[2K_1\left(1-\frac{n_0^2}{n^2}\right)-\left(1+\frac{n^2}{n_0^2}\right)K_2\left(1-\frac{n_0^2}{n^2}\right)\right]\tilde{\overline{p}}_x, \tag{4.63}$$

$$\overline{T^x_{xxx}} \simeq \frac{4v_F}{\pi p_F}\frac{n/n_0}{(n^2/n_0^2-1)^2}\left[2K_1\left(1-\frac{n_0^2}{n^2}\right)-\left(1+\frac{n^2}{n_0^2}\right)K_2\left(1-\frac{n_0^2}{n^2}\right)\right], \tag{4.64}$$

$$P_{xx} \simeq \frac{4p_F v_F n_0}{3\pi}\frac{1}{n^2/n_0^2-1}\left[\frac{n^4}{n_0^4}K_2\left(1-\frac{n_0^2}{n^2}\right)-\frac{n^2}{n_0^2}K_1\left(1-\frac{n_0^2}{n^2}\right)\right], \tag{4.65}$$

The linearised $\overline{T^x_{xxx}}$ and P_{xx} are momentum independent, given that changes in $\tilde{\overline{p}}_x$ only contribute quadratically, which we neglect. For small fluctuations, the pressure is only density-dependent, as usual. In its turn, the linearised $\overline{J_{xxx}}$ is proportional to $\tilde{\overline{p}}_x$. Provided the relations (4.63)−(4.65), the system of equations (4.53)−(4.55) is formally closed, with the three equations involving three variables, n, $\overline{p}_x$ and $\overline{v}_x$. An additional linearisation with respect to the density is necessary, so we rewrite

$$n(x,t) = n_0 + \tilde{n}(x,t), \tag{4.66}$$

with $|\tilde{n}|/n_0 \ll 1$. Up to first order in momentum, we have

$$\overline{v}_x = \frac{\overline{p}_x}{\gamma(n)\mathcal{M}} \tag{4.67}$$

where $\gamma(n)$ is given by (4.50). Therefore, after applying the expansion in (4.66) and keeping only $\mathcal{O}(\tilde{n})$ terms, we find

$$\overline{v}_x \simeq \frac{\overline{p}_x}{\mathcal{M}}\left(1 - \frac{3}{4}\frac{\tilde{n}}{n_0}\right). \tag{4.68}$$

Above, we used the following properties for the elliptical integrals:

$$\frac{dK_1(x)}{dx} = \frac{K_2(x) - (1-x)K_1(x)}{2x(1-x)}, \tag{4.69}$$

$$\frac{dK_2(x)}{dx} = \frac{K_2(x) - K_1(x)}{2x}, \tag{4.70}$$

$$K_i(0) = \frac{\pi}{2}. \tag{4.71}$$

Those properties can also be used to linearise (4.63)−(4.65), with respect to the density, which yields

$$\overline{J_{xxx}} \simeq -\frac{3v_F}{4p_F^3}\tilde{\overline{p}}_x, \tag{4.72}$$

$$\overline{T^x_{xxx}} \simeq \frac{3v_F}{p_F}\left(\frac{1}{4} - \frac{1}{8}\frac{\tilde{n}}{n_0}\right), \tag{4.73}$$

$$P_{xx} \simeq p_F v_F n_0 \left(\frac{1}{3} + \frac{3}{4}\frac{\tilde{n}}{n_0}\right). \tag{4.74}$$

Finally, using (4.62), (4.66), (4.68) and (4.72)−(4.74) into the hydrodynamical equations of (4.53)−(4.54), and neglecting second order terms, leads to the linearised hydrodynamical model

$$\frac{\partial}{\partial t}\tilde{n} + \frac{\partial}{\partial x}\Big(n_0\frac{\tilde{\overline{p}}_x}{\mathcal{M}}\Big) = -\frac{\hbar^2}{24}\frac{\partial^3}{\partial x^3}\Big(n_0\frac{3v_F}{4p_F^3}\tilde{\overline{p}}_x\Big), \tag{4.75}$$

$$\frac{\partial}{\partial t}(n_0\tilde{\overline{p}}_x) + \frac{\partial}{\partial x}\Big(\frac{3}{4}p_F v_F\tilde{n}\Big) + \mathcal{Q}n_0\frac{\partial}{\partial x}\tilde{\phi} = \frac{\hbar^2}{24}\frac{\partial^3}{\partial x^3}\Big(\frac{3v_F}{8p_F}\tilde{n}\Big), \tag{4.76}$$

where $\tilde{\phi}(\boldsymbol{r}, t)$ is the first order electrostatic potential with respect to the perturbed density

$$\tilde{\phi}(\boldsymbol{r}, t) = \frac{\mathcal{Q}}{4\pi\varepsilon_0\varepsilon_r}\int d\boldsymbol{r'}\ \frac{\tilde{n}(x,t)}{|\boldsymbol{r} - \boldsymbol{r'}|}. \tag{4.77}$$

By Fourier transforming the linearised equations in both position and time, we are led to

$$-i\omega\ \tilde{n}(q,\omega) + iqn_0\frac{\tilde{\overline{p}}_x(q,\omega)}{\mathcal{M}} = i\hbar^2 q^3 n_0\frac{v_F}{32p_F^3}\ \tilde{\overline{p}}_x(q,\omega), \tag{4.78}$$

$$-i\omega n_0\ \tilde{\overline{p}}_x(q,\omega) + iq_x\frac{3}{4}p_F v_F\ \tilde{n}(q,\omega) + iq\mathcal{Q}n_0\ \tilde{\phi}(q,\omega) = -i\hbar^2 q^3\frac{v_F}{64p_F}\ \tilde{n}(q,\omega). \tag{4.79}$$

where we relabelled q_x as q, because of rotational invariance. Using $\tilde{\phi}(q,\omega) = \mathcal{Q}\tilde{n}(q,\omega)/2\varepsilon_0\varepsilon_r q$ (see Appendix D.1) and $\mathcal{Q} = -|e|$ we can solve the system (4.78)−(4.79), which gives the plasmon dispersion

relation

$$\omega(q) = \pm\left(\omega_p^2 \frac{q}{k_F} + \frac{3}{4} v_F^2 q^2 - \frac{\omega_p^2}{32}\frac{q^3}{k_F^3} + \nu \frac{\hbar^2 q^4}{4\mathcal{M}^2}\right)^{1/2}. \tag{4.80}$$

where $\nu = -1/32$ results from the contributions of both $\overline{J_{xxx}}$ and $\overline{T^x_{xxx}}$. The $\pm$ sign refers to each plasmon branch for forward and backward propagation. The two first terms are the classical contributions to the plasmon dispersion, in agreement with the result already found in (3.101), while the third term corresponds to a classical ($\hbar$ independent) correction. The quantum correction ($\sim \hbar^2$) is contained in the last term, which represents the Bohm term. It is of the same form as the one proportional to q^4, found in (2.37) for longitudinal plasma oscillations, despite being multiplied by a negative factor ν. This difference should be attributed to the linear dispersion relation of the Dirac electrons, which reduces the energy of those longitudinal modes. Since the absolute value of ν is rather small, such correction only becomes important for intermediate wave-number values, as can be seen in Fig. 4.3.

To summarise, the first quantum corrections have been obtained for the plasmonic dispersion relation in graphene, which, to the best of our knowledge, had not been given anywhere else. These came after the inclusion of the novel quantum corrections $\mathcal{N}$, given in (4.25), which we naturally found from our *ab-initio* kinetic formulation. In the parabolic case, $\xi(\boldsymbol{p}) = \boldsymbol{p}^2/2m$, described in chapter 2.3, $\mathcal{N}$ vanished, owning to the parabolic dependence of the kinetic energy on the momentum coordinate. In fact, even with a full quantum treatment in terms of the Wigner function, the kinetic term of parabolic particles remains identical to its classical counterpart, which in turn adds no corrections to the hydrodynamical equations, when compared to their classical versions. Nevertheless, for a kinetic term of the form $\xi(\boldsymbol{p}) = v_F|\boldsymbol{p}|$, infinite number of terms appeared, in powers of $\hbar$, and the lowest orders were included. These contributions allowed to derive a corrected expression for the plasmonic dispersion relation, such that a Bohm-like term $\sim \hbar^2 q^4/4\mathcal{M}^2$ was found. Moreover, we also showed how a non-linear relation between velocity and momentum can be settled, starting from the kinetic equation.

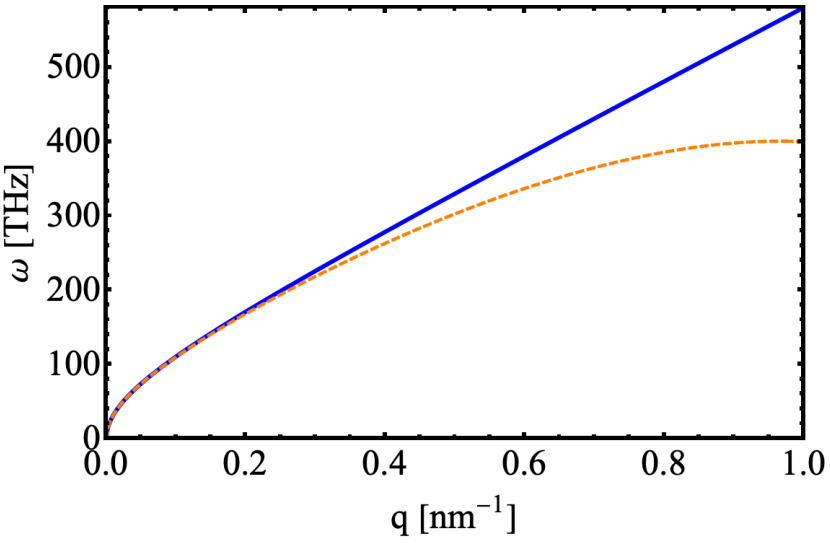

Figure 4.3: Positive branch of the semi-classical plasmon dispersion relation in (4.80) (orange dashed), together with its classical counterpart, given by (3.101) (blue), with $\varepsilon_r = 2.5$.

Chapter 5

Streaming instability

Under certain conditions, both damping and growth (instability) of plasma waves may occur, whenever the dispersion relation renders an imaginary part for the frequency. Considering the case of a single $\boldsymbol{q}-$mode, the density excitation (or plasmon) reads[1]

$$\tilde{n}(\boldsymbol{r},t) = \tilde{n}(\boldsymbol{q})\, e^{i[\boldsymbol{q}\cdot\boldsymbol{r}-\omega(\boldsymbol{q})t]}. \tag{5.1}$$

Writing[2] $\omega(\boldsymbol{q}) = \omega_r(\boldsymbol{q}) + i\omega_i(\boldsymbol{q})$, we indeed find the condition $\omega_i(\boldsymbol{q}) < 0$ to correspond to a decay of the amplitude in time (or damping), whereas for $\omega_i(\boldsymbol{q}) > 0$, the mode amplitude will grow, leading to an instability. We also define the phase and group velocity $\boldsymbol{v}_p$ and $\boldsymbol{v}_g$ by

$$\boldsymbol{v}_p = \frac{\omega(\boldsymbol{q})}{\boldsymbol{q}}, \tag{5.2}$$

$$\boldsymbol{v}_g = \boldsymbol{\nabla}_{\boldsymbol{q}}\, \omega(\boldsymbol{q}). \tag{5.3}$$

The first is related with the rate at which a given phase of the wave travels in a given medium, while the second, in its turn, denotes the velocity of the overall envelope shape that encloses the amplitude modulations. Both are a function of $\boldsymbol{q}$, and are independent quantities, for generic dispersion relations.

While damping is generally unwanted in graphene-based devices, instabilities can be used in our favour, such as in the construction of THz radiation emitters. Therefore, in this chapter, we go back to the kinetic equations developed in chapter 3, and look for possible regimes of plasmonic instabilities, using a specific configuration consisting in two parallel graphene sheets separated by a distance d (see Fig. 5.1). In one of the layers (also called the active layer), a beam of electrons is injected by applying a potential difference to its edges. The drifting current that is formed, against the steady background electronic system, provides a mechanism of instability that is similar to that of two stream instability, extensively

[1] The symbol $\sim$ denotes, as before, the fluctuations of the density relatively to its equilibrium value n_0, $\tilde{n} = n - n_0$.

[2] Notice that we should regard $\boldsymbol{q}$ as a discrete value, chosen from the first Brillouin zone, *i.e.*, $\mathbf{q}_{\boldsymbol{n}} = 2\pi(n_x, n_y)/A$, where A is the 2D area and $\boldsymbol{n}$ is a vector whose components span the set of natural values $[1, \sqrt{N}]$, N is the number of lattice points. Therefore, rigorously speaking, $\boldsymbol{q}-$integrations should be understood as summations over the first Brillouin zone. However, in the limit of large surface areas, the wave-vector spacing becomes negligible, and we eventually replace it by a continuous variable. Additionally, summations may be replaced by integrals, which are much easier to perform, in accordance with what we have been doing in previous chapters, $\frac{1}{A}\sum_{\boldsymbol{q}} \to \int d\boldsymbol{q}$.

studied in the context of parabolic [96, 97] and solid-state plasmas [98–100]. Two-stream instability can be understood as the opposite effect of damping, which relies on wave-particle interaction. While a plasma density wave can transfer momentum to individual charged particles, leading to a decrease in amplitude of the corresponding mode, the reverse can also happen, provided that enough individual particles populate a specific mode. Such conditions holds for a beam of energetic particles travelling through the plasma.

Recently, the case of current injection in doped graphene was also considered [32, 101], and indeed a similar type of instability has been described. In those works, the equilibrium configuration for the injected beam has the form $W_0(\boldsymbol{k}) = n_b\delta(\boldsymbol{k} - \boldsymbol{k}_b)$, which peaks at some constant wave-vector $\boldsymbol{k}_b$. In the long wavelength limit, it was found that the polarizability becomes proportional to $\sin^2\theta_b$, where θ_b is the angle between the plasmon wave-vector $\boldsymbol{q}$ and the beam wave-vector $\boldsymbol{k}_b$, thus vanishing for parallel injection. This result is rather counterintuitive, as one would expect an enhanced instability for such configuration. However, this result boils down to the Dirac nature of charge carriers in graphene.

In this chapter, we investigate two-stream instability in the Coulomb drag configuration (see Fig. 5.1). We consider d to be such to avoid tunneling between the different layers. Thus, we must ensure that $d \gg d_c$, where d_c is the carbon-carbon distance in graphene, $d_c \approx 0.15\,\mathrm{nm}$. In one of the layers (active layer), a beam of electrons is injected, leaving the other (passive layer) with zero average current. These conditions shall mimic that of two stream instability in conventional parabolic systems, for which one or more unstable solutions are expected. Because of the linear dispersion relation, it is possible to excite large drift velocities in the active layer, without needing to use large voltages. For this reason, graphene Dirac spectrum is ideal for unstable regimes of this kind. On the other hand, high voltages lead to undesired electron/hole inelastic scattering, which entails the suppression of instabilities.

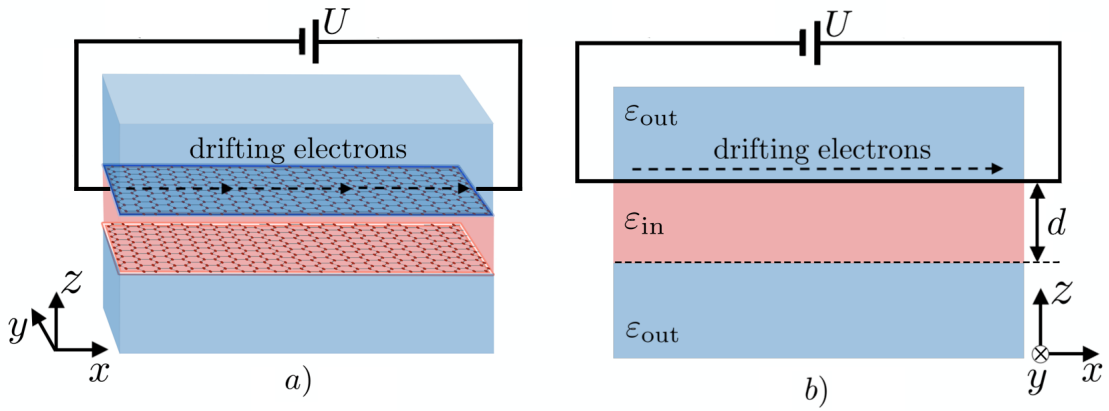

Figure 5.1: Schematic representation of the Coulomb drag configuration, composed by two parallel graphene sheets lying in the $x - y$ plane, separated by a distance d along the $z-$axis. The top and bottom layers are known as the active and passive layers, respectively. The active layer is subjected to an external static voltage, such that a drift current is formed. The injected electrons have energy $E = eU$, which gives an average wave-number $k_b = eU/\hbar v_F$ to the beam. The effective relative permittivity of the system is $\varepsilon = (\varepsilon_{\mathrm{in}} + \varepsilon_{\mathrm{out}})/2$. a) Perspective view; b) Front view.

5.1 Kinetic description of the Coulomb drag instability

Unstable plasmon modes may exhibit arbitrarily large values of $\omega_i(\boldsymbol{q})$, even surpassing the corresponding real part $\omega_r(\boldsymbol{q})$. This particularity unables the treatment of the imaginary part of the frequency as a perturbation, which is common approach in the derivation of the well-known result in linear response theory

$$\omega_i(\boldsymbol{q}) \simeq -\left(\epsilon_i(\mathbf{q},\omega_r)\left[\frac{\partial\epsilon_r(\mathbf{q},\omega)}{\partial\omega}\right]^{-1}\right)_{\omega=\omega_r(\boldsymbol{q})}, \tag{5.4}$$

relating the imaginary part of the frequency with the real and imaginary parts of the dielectric function, $\epsilon(\boldsymbol{q},\omega) = \epsilon_r(\boldsymbol{q},\omega) + i\epsilon_i(\boldsymbol{q},\omega)$. This formula is extensively used to describe damping of plasma waves. Notwithstanding, in the present case, we need to regard the full model derived in chapter 3, which comprises the transport equation for the Wigner matrix components

$$\Big[i\hbar\,\frac{\partial}{\partial t} - \Delta\xi^{-}(\boldsymbol{q},\boldsymbol{k})\Big]W^{\alpha\gamma}(\boldsymbol{q},\boldsymbol{k},t) = e\int d\boldsymbol{q}'\;\phi(\boldsymbol{q}',t)\;\Delta W^{\alpha\gamma}(\boldsymbol{q},\boldsymbol{k},\boldsymbol{q}',t). \tag{5.5}$$

together with the Poisson equation. As formulated in chapter 3, we consider the pure electron system, valid for $E_F \gg k_BT$, and for which only the $(\alpha\gamma) = (11)$ component of the above equations is relevant. We shall drop the band index, as before, by defining $W^{11} \doteq W$ and $n_1 \doteq n$. To describe the configuration shown in Fig. 5.1, let us denote the Wigner function for the active and passive layers as $W_\uparrow$ and $W_\downarrow$, respectively. Due to the long range nature of the Coulomb interaction, the electrostatic potential $\phi(\boldsymbol{q},t)$ in (5.5) must be modified to include the mean-field effect of both layers. Thus, the potential at each layer reads

$$-e\phi_\tau(\boldsymbol{r},t) = \frac{e^2}{4\pi\varepsilon_0\varepsilon_r}\int d\boldsymbol{r}'\left(\frac{n_\tau(\boldsymbol{r}',t)}{|\boldsymbol{r}-\boldsymbol{r}'|} + \frac{n_{\overline{\tau}}(\boldsymbol{r}',t)}{|\boldsymbol{r}-\boldsymbol{r}'+d\hat{\boldsymbol{z}}|}\right), \tag{5.6}$$

where $\tau = \{\uparrow,\downarrow\}$ denote the active and passive layers, respectively, $\hat{\boldsymbol{z}}$ is the unit vector pointing in the $z-$direction, and $\overline{\tau}$ indicates the layers complementary to τ. Equation (5.6) corresponds to the mean-field approximation for the potential, $V_\tau = -e\phi_\tau$. The densities are connected to each Wigner function by the usual relation $n_\tau = \int d\boldsymbol{k}\; W_\tau$. Fourier transforming (5.6) leads to (see Appendix D.1)

$$-e\phi_\tau(\boldsymbol{q},t) = \mathcal{U}(q)\Big[n_\tau(\boldsymbol{q},t) + n_{\overline{\tau}}(\boldsymbol{q},t)e^{-qd}\Big], \tag{5.7}$$

where d is the inter-layer distance. Moreover, we assume that the out of equilibrium configuration is described by adding a small contribution to the equilibrium Wigner function. In its turn, the equilibrium will be different depending on the layer, due to the asymmetric conditions. Expanding each Wigner function as $W_\tau(\boldsymbol{r},\boldsymbol{k},t) = W_{\tau 0}(\boldsymbol{k}) + \tilde{W}_\tau(\boldsymbol{r},\boldsymbol{k},t)$ and introducing it into (5.5), it can be shown, following a similar procedure to the one described in 3.4, that the first order quantity $\tilde{W}(\boldsymbol{q},\boldsymbol{k},\omega)$ evolves according to

$$\hbar\omega\tilde{W}_\tau(\boldsymbol{q},\boldsymbol{k},\omega) = \Big[\xi(\boldsymbol{k}+\boldsymbol{q}/2) - \xi(\boldsymbol{k}-\boldsymbol{q}/2)\Big]\tilde{W}_\tau(\boldsymbol{q},\boldsymbol{k},\omega) + \mathcal{U}(q)\Big[\tilde{n}_\tau(\boldsymbol{q},\omega) + \tilde{n}_{\overline{\tau}}(\boldsymbol{q},\omega)e^{-qd}\Big]\Delta W_{\tau 0}, \tag{5.8}$$

where $\Delta W_{\tau 0}(\boldsymbol{q},\boldsymbol{k}) = W_{\tau 0}(\boldsymbol{k}-\boldsymbol{q}/2) - W_{\tau 0}(\boldsymbol{k}+\boldsymbol{q}/2)$ and $\tilde{n}_\tau = \int d\boldsymbol{k}\ \tilde{W}_\tau$. Above, we have neglected second order quantities. Further manipulation of (5.8) yields

$$n_\tau(\boldsymbol{q},\omega) = \mathcal{U}(q)\Big[n_\tau(\boldsymbol{q},\omega) + n_{\overline{\tau}}(\boldsymbol{q},\omega)e^{-qd}\Big]\Pi_\tau(\boldsymbol{q},\omega), \tag{5.9}$$

where the polarizability function $\Pi_\tau(\boldsymbol{q},\omega)$ has the usual form

$$\Pi_\tau(\boldsymbol{q},\omega) = \int d\boldsymbol{k}\ \frac{\Delta W_{\tau 0}(\boldsymbol{q},\boldsymbol{k})}{\hbar\omega + \xi(\boldsymbol{k}-\boldsymbol{q}/2) - \xi(\boldsymbol{k}+\boldsymbol{q}/2)}. \tag{5.10}$$

Equation (5.9) represents a system of two coupled equations, which can be rewritten in matrix form as

$$\begin{pmatrix} \mathcal{U}(q)\Pi_\uparrow(\boldsymbol{q},\omega) - 1 & \mathcal{U}(q)\Pi_\uparrow(\boldsymbol{q},\omega)e^{-qd} \\ \mathcal{U}(q)\Pi_\downarrow(\boldsymbol{q},\omega)e^{-qd} & \mathcal{U}(q)\Pi_\downarrow(\boldsymbol{q},\omega) - 1 \end{pmatrix} \begin{pmatrix} \tilde{n}_\uparrow(\boldsymbol{q},\omega) \\ \tilde{n}_\downarrow(\boldsymbol{q},\omega) \end{pmatrix} = 0. \tag{5.11}$$

The existence of a non-trivial solution for the perturbed density elements $\tilde{n}_\tau$ requires the determinant of the above matrix to vanish. Hence, we find the dielectric function to be given by

$$\epsilon(\boldsymbol{q},\omega) = 1 + [\mathcal{U}(q)]^2\Pi_\uparrow(\boldsymbol{q},\omega)\Pi_\downarrow(\boldsymbol{q},\omega)(1-e^{-2qd}) - \mathcal{U}(q)\Big[\Pi_\uparrow(\boldsymbol{q},\omega) + \Pi_\downarrow(\boldsymbol{q},\omega)\Big], \tag{5.12}$$

such that the dispersion relation corresponds to the solutions of $\epsilon(\boldsymbol{q},\omega) = 0$. As we shall see, the present relation results in instability ($\omega_i(\boldsymbol{q}) > 0$) for some of the roots of (5.12), in a certain region of the $\boldsymbol{q}-$space and for a given set of experimental parameters. These will arise after a proper choice for the equilibrium of both the active and passive layers, $W_{\uparrow 0}(\boldsymbol{k})$ and $W_{\downarrow 0}(\boldsymbol{k})$.

5.1.1 Polarizability and equilibrium Wigner functions for $q \to 0$.

Let us denote the doping densities of each layer by $n_{0\uparrow}$ and $n_{0\downarrow}$. Each of these doping densities yield a different Fermi wave-vector at each of the layers, $k_{F\uparrow}$ and $k_{F\downarrow}$. As we shall see, keeping different doping densities will allow to study the relevant case of $n_{0\uparrow} = 0$, such that all the electrons participate in the beam current.

The most natural choice to describe the equilibrium in the passive layer is the zero-temperature limit of the Fermi distribution function, as before. Then, we set

$$W_{\downarrow 0}(\boldsymbol{k}) = \frac{n_{\downarrow 0}}{\pi k_{F\downarrow}^2}\ \Theta(k_F - k), \tag{5.13}$$

where $\boldsymbol{k} \doteq k$. The active layer equilibrium must account for the doping electrons, plus the contribution from the injected current. If we denote by n_b the density of injected electrons, then the equilibrium function $W_{\uparrow 0}(\boldsymbol{k})$ reads

$$W_{\uparrow 0}(\boldsymbol{k}) = \frac{n_{\uparrow 0}}{\pi k_{F\uparrow}^2}\ \Theta(k_F - k) + n_b\delta(\boldsymbol{k}-\boldsymbol{k}_b). \tag{5.14}$$

The validity of these equilibrium distributions is subjected to certain constrains, namely, regarding the last term on the r.h.s. of (5.14). In fact, immediately after the beam being injected into the active layer,

collisions start to thermalise the $\delta-$function, making it to spread around $\boldsymbol{k}_b$, such that we expect it to acquire a spatial (and temporal) dependence. Here, we assume this function to be valid through the entire length of the system, which is accurate in the limit $T \to 0$, where collisions are increasingly negligible. It remains valid for temperatures below the Fermi temperature, which for reasonable doping densities, $n_0 \approx 10^{12}\text{cm}^{-2}$, is considerably high, $T_F \approx 886°\text{C}$. Also, we are neglecting other sources of scattering, namely, that with phonons and impurities. Those are described by localised wave-functions, and thus should be of less importance in the long-wavelength limit, $q \to 0$, for which sharp spatial fluctuations of the equilibrium are of small account. This justifies the choice of (5.14).

To solve the dispersion relation, we start by plugging (5.13) and (5.14) into (5.10). First, notice that a more convenient arrangement of (5.10) proceeds after a change of variables

$$\Pi_\tau(\boldsymbol{q},\omega) = \int d\boldsymbol{k}\; W_{\tau 0}(\boldsymbol{k}) \left(\frac{1}{\hbar\omega + \xi(\boldsymbol{k}) - \xi(\boldsymbol{k}+\boldsymbol{q})} - \frac{1}{\hbar\omega + \xi(\boldsymbol{k}-\boldsymbol{q}) - \xi(\boldsymbol{k})} \right). \tag{5.15}$$

Applying the approximation of (3.98), and retaining terms up to $\mathcal{O}(q^2)$, we obtain for the polarizability of the passive layer

$$\Pi_\downarrow(\boldsymbol{q},\omega) \simeq \frac{v_F k_{F\downarrow}}{\hbar\pi} \frac{q^2}{\omega^2}. \tag{5.16}$$

For the active layer, the equilibrium function is composed by two terms, being the first representative of the doping electrons. Given that we are assuming the same doping for both layers, then the first term of $\Pi_\uparrow(\boldsymbol{q},\omega)$ is equal to that in (5.16). The remaining part is obtained after a trivially integration of the $\delta-$function. Therefore, we get

$$\Pi_\uparrow(\boldsymbol{q},\omega) \simeq \frac{v_F k_{F\uparrow}}{\hbar\pi} \frac{q^2}{\omega^2} + \frac{n_b}{\hbar\omega + \xi(\boldsymbol{k}_b) - \xi(\boldsymbol{k}_b+\boldsymbol{q})} - \frac{n_b}{\hbar\omega + \xi(\boldsymbol{k}_b-\boldsymbol{q}) - \xi(\boldsymbol{k}_b)}\,. \tag{5.17}$$

It should be noted that the above expression depends only on the relative angle between $\boldsymbol{q}$ and $\boldsymbol{k}_b$, as already pointed out in [101], by resorting to the relation

$$|\boldsymbol{k} \pm \boldsymbol{q}|^2 = k^2 + q^2 \pm 2\boldsymbol{k}\cdot\boldsymbol{q}. \tag{5.18}$$

Hence, after aligning $\boldsymbol{q}$ with the $x-$direction, we get, without loss of generality

$$\xi(\boldsymbol{k}_b \pm \boldsymbol{q}) = \hbar v_F \sqrt{k_b^2 + q^2 \pm 2qk_b\cos\theta_b}, \tag{5.19}$$

where θ_b is the angle between $\boldsymbol{k}_b$ and $\boldsymbol{q}$ (or simply the polar angle of $\boldsymbol{k}_b$, as $\boldsymbol{q}$ lies in the $x-$direction). This feature is expected, as can be noted by taking $\boldsymbol{k}_b = n_b = 0$, for which we must recover our initial conic symmetry. Going further, to keep consistency with the approximation of (3.98), it is important to expand the denominators in (5.17) for small q, beyond first order, using

$$\xi(\boldsymbol{k}_b) - \xi(\boldsymbol{k}_b+\boldsymbol{q}) \simeq -\hbar\boldsymbol{v}_b\cdot\boldsymbol{q} - \frac{\hbar v_F \sin^2\theta_b}{2k_b} q^2, \tag{5.20}$$

$$\xi(\boldsymbol{k}_b) - \xi(\boldsymbol{k}_b+\boldsymbol{q}) \simeq -\hbar\boldsymbol{v}_b\cdot\boldsymbol{q} + \frac{\hbar v_F \sin^2\theta_b}{2k_b} q^2, \tag{5.21}$$

where $\boldsymbol{v}_b = v_F \boldsymbol{k}_b / k_b$ is the beam velocity. Equation (5.17) thus becomes

$$\Pi_\uparrow(\boldsymbol{q}, \omega) \simeq \frac{v_F k_{F\uparrow}}{\hbar \pi} \frac{q^2}{\omega^2} + \frac{v_F n_b}{\hbar k_b} \frac{q^2 \sin^2 \theta_b}{(\omega - \boldsymbol{v}_b \cdot \boldsymbol{q})^2 - \frac{v_F^2}{4k_b^2} q^4 \sin^4 \theta_b}. \tag{5.22}$$

5.1.2 Dispersion relation

In order to solve the dispersion relation of interest, which is achieved by equating (5.12) to zero, let us define the following dimensionless variables

$$q' = \frac{q}{k_{F\downarrow}}, \tag{5.23}$$

$$\omega' = \frac{\omega}{\omega_p}, \tag{5.24}$$

$$\Pi'_\tau = \frac{\Pi_\tau}{\Pi_0}, \tag{5.25}$$

$$\mathcal{U}' = \frac{\mathcal{U}}{\mathcal{U}_0}, \tag{5.26}$$

where $\Pi_0 = \varepsilon_0 k_{F\downarrow}/e^2$, $\mathcal{U}_0 = e^2/\varepsilon_0 k_{F\downarrow}$. Replacing (5.23)−(5.26) into the dielectric function of (5.12), we obtain

$$\epsilon(\boldsymbol{q}, \omega) = 1 + \mathcal{U}'^2 \Pi'_\uparrow \Pi'_\downarrow (1 - e^{-4\pi q' x}) - \mathcal{U}' \left(\Pi'_\uparrow + \Pi'_\downarrow \right), \tag{5.27}$$

where

$$\mathcal{U}'(q') = \frac{1}{2\varepsilon_r q'}, \tag{5.28}$$

$$\Pi'_\downarrow(q', \omega') = 2\varepsilon_r \frac{q'^2}{\omega'^2}, \tag{5.29}$$

$$\Pi'_\uparrow(q', \omega') = w \Pi'_\downarrow(q', \omega') + \sin^2 \theta_b \frac{4\alpha_s y}{z} \; q'^2 \left[\left(\sqrt{\frac{2\alpha_s}{\varepsilon_r}} \; \omega' - q' \cos \theta_b \right)^2 - \frac{q'^4 \sin^2 \theta_b}{4z^2} \right]^{-1}. \tag{5.30}$$

Above, $\alpha_s \approx 2.2$ is the graphene structure constant, $x = d/\lambda_{F\downarrow}$ is the inter-layer distance normalised to the Fermi wavelength of the passive layer, and $w = k_{F\uparrow}/k_{F\downarrow}$ is the ratio between the Fermi wave-numbers of each layer. Additionally, we defined the beam variables $y = n_b/n_{\downarrow 0}$ and $z = k_b/k_{F\downarrow}$. Within the current approximation, the second term of the polarizability in the active layer verifies $\Pi_\uparrow \sim \sin^2 \theta_b$, which vanishes for $\theta_b = 0$, in agreement with what previous works have found, regarding the single layer configuration [101]. Hence, the configuration for which the plasmon direction is parallel to the direction of the beam is equivalent to removing the beam from the system, yielding no instability.

5.2 Numerical results

We now proceed to numerically solve the dispersion relation, obtained from

$$\epsilon(\boldsymbol{q}, \omega) = 0, \tag{5.31}$$

where $\epsilon(\boldsymbol{q}, \omega)$ is the dielectric function of (5.27).

5.2.1 Equally doped layers

First, let us consider a situation in which both layers are doped, implying $w \neq 0$. In that case, (5.31) turns out to be a sextic equation, which gives six roots of the form $\omega(\boldsymbol{q}) = \omega_r(\boldsymbol{q}) + i\omega_i(\boldsymbol{q})$. Four of them verify $\omega_i(\boldsymbol{q}) = 0$, while the remaining two have a non-zero imaginary part. The real roots represent the optical and acoustic modes, with well-known behaviour $\omega_{\text{op}}^2 = 2r_s v_F^2(k_{F\uparrow} + k_{F\downarrow})q$ and $\omega_{\text{ac}}^2 = 4r_s v_F^2 k_{F\uparrow} k_{F\downarrow} dq^2/(k_{F\uparrow} + k_{F\downarrow})$, in the long wavelength limit $q \to 0$ [102]. The first comprises out-of-phase electronic displacements, whilst the second is made out of electrons oscillating in phase. Moreover, the two complex frequencies are necessarily complex conjugate of each other, due to the coefficients of (5.31) being real, thus making ω^* a solution whenever ω is a solution. One of the complex roots represents a plasmon which is growing in time ($\omega_i > 0$), while the other is decaying ($\omega_i < 0$). In addition, these solutions have degenerate real parts and symmetric imaginary parts. However, for $q > q_{\max}$, the imaginary part of the unstable modes vanishes, and consequently, they become stable, while their corresponding real parts become non-degenerate.

Figures 5.2 and 5.3 show the real part of the stable optical and acoustic modes, respectively, for the forward and backward directions of propagation. We used the same density of doping, $n_{\uparrow 0} = n_{\downarrow 0} = 10^{12}$ cm^{-2}, which gives a Fermi energy of $E_F \approx 0.1$eV and a Fermi wavelength of $\lambda_F \approx 35$nm for both layers, corresponding to the case $w = 1$. The injected electrons energy is related to the Fermi energy by $E_b = zE_F$. The corresponding forward and backward propagating waves are not frequency-symmetric, which is clearly indicated in (5.31), not invariant under $\omega \to -\omega$. Hence, we observe a slight difference in the two branches, apart from the sign, as represented in Figs. 5.2 and 5.3. Physically, this happens because the beam propagating in the active layers breaks the previous invariance under the transformation $\boldsymbol{r} \to -\boldsymbol{r}$, by fixing a preferred direction, and consequently, the dispersion relation holds a dependence on θ_b.

Figures 5.4 and 5.5 show, respectively, the real and imaginary parts of the unstable roots of (5.31). The phase velocity of these modes, $v_p = \omega/q$, verifies $v_p < v_F$, which makes their real parts lying in the inter-band excitation region. By conservation of energy and momentum, this condition implies a non-zero imaginary part [103]. Near the origin, both modes have the same real frequency, and symmetric imaginary frequencies. While the imaginary frequencies are non-zero, the real part grows linearly, and starts to separate from the moment they become stable ($\omega_i = 0$). The instability is, thus, bounded between 0 and $q_{\max}$, with $q_{\max}$ depending on the experimental parameters n_b and k_b, and material parameter ε_r. The simulation determined that $q_{\max} = q_{\max}(n_b, k_b)$ is a growing function of both n_b and k_b.

The factor $\sin^2\theta_b$, that we also find for the single-layer configuration, leads to the conclusion that the instability is suppressed for parallel plasmon and beam direction. This strange behaviour is explained by the linear dispersion relation. In the described conditions, the exponential growing of the unstable mode happens because the charge fluctuations caused by the plasmon produce a net force, which feeds

back the fluctuations. However, this arguments fails when the plasmon direction of propagation is the same as the direction of the beam. Remember that Dirac electrons have a constant speed (v_F), and velocity align with momentum, *i.e.*, $\boldsymbol{v} = v_F \boldsymbol{p}/|\boldsymbol{p}|$. The momentum, in turn, can take any value. Therefore, for the parallel case, the charge fluctuations around the equilibrium only change the magnitude of the momentum, which does not affect the velocity, and the feedback does not occur. On the contrary, when both directions are not aligned, the fluctuations on the charge density are able to affect the direction of momentum, thus changing particles' velocities and allowing for a exponential growing of the wave. Following this argument, we should not expect unstable solutions when the direction of the plasmon is perpendicular to that of the beam, $\theta_b = \pi/2$. As a result, we expect a maximum growing for θ_b in the interval $[0, \pi/2]$. In Fig. 5.6 we show the maximum instability growth rate as a function of the angle θ_b. The maximisation of the growth rate was performed in the entire interval of instability, $q \in [0, q_{max}]$. The maximum is shifted to the right, as we increase the momentum of the beam, and a similar behaviour is found by increasing the density n_b. In Fig. 5.7, we plot the maximum growth rate, as a function of the distance between the layers. Additionally, we restrict ourselves to $d > 0.3\text{nm}$, to avoid tunnelling. We found, for the case of equally doped layers, that increasing the distance favours the instability. In fact, the growth of the waves depends on the ratio between injected and doping electrons. When the layers are brought closer, the effect is similar to that of an increase in the density of equilibrium (doping) electrons, against the same density of injected electrons, once the passive layer has no applied current. This, consequently, decreases the maximum growth rate of the instability. In the limit $d \to +\infty$, we recover the previous results [32, 101].

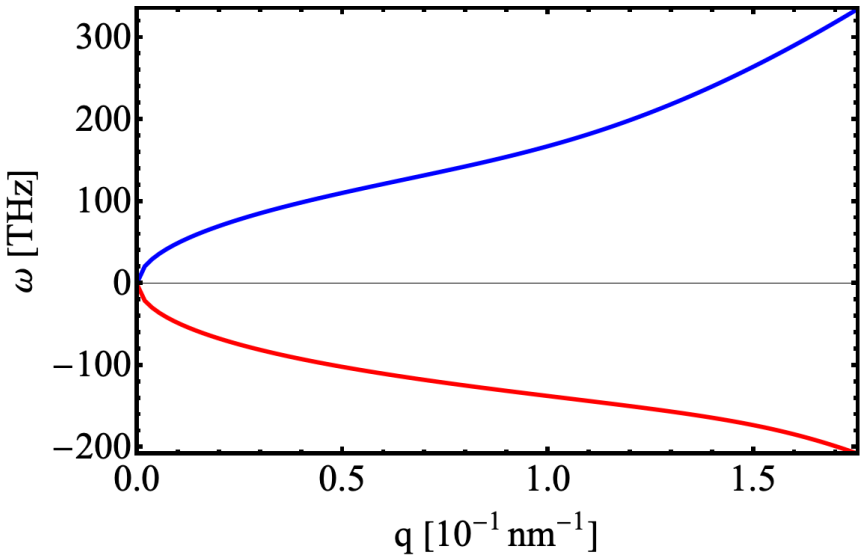

Figure 5.2: Forward (blue) and backward (red) plasmons, in the optical mode. These modes behave as $\omega \sim \pm\sqrt{q}$ near the origin. Fixed simulating parameters: $x = 0.15$, $y = 0.1$, $z = 0.1$, $w = 1$, $\theta_b = \pi/4$ and $\varepsilon_r = 2.5$.

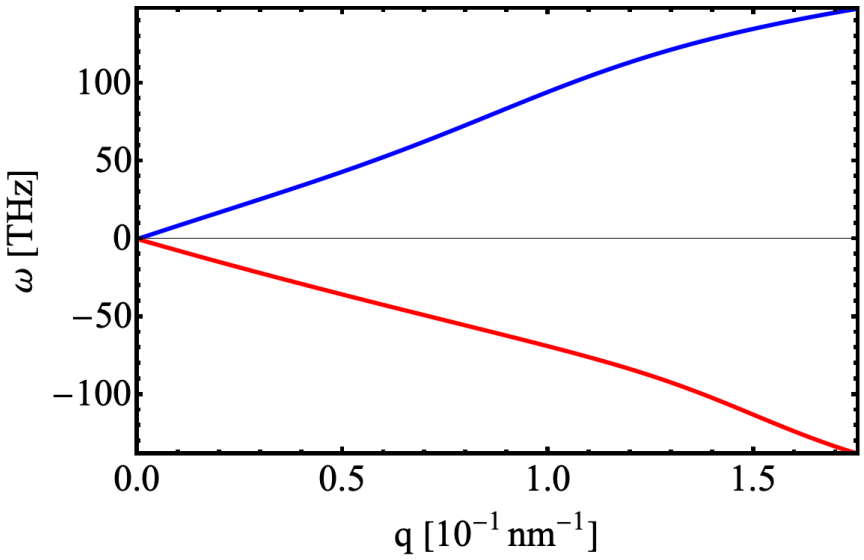

Figure 5.3: Forward (orange) and backward (green) plasmons, in the acoustic mode. These modes behave as $\omega \sim \pm q$ near the origin. Fixed simulating parameters: $x = 0.15$, $y = 0.1$, $z = 0.1$, $w = 1$, $\theta_b = \pi/4$ and $\varepsilon_r = 2.5$.

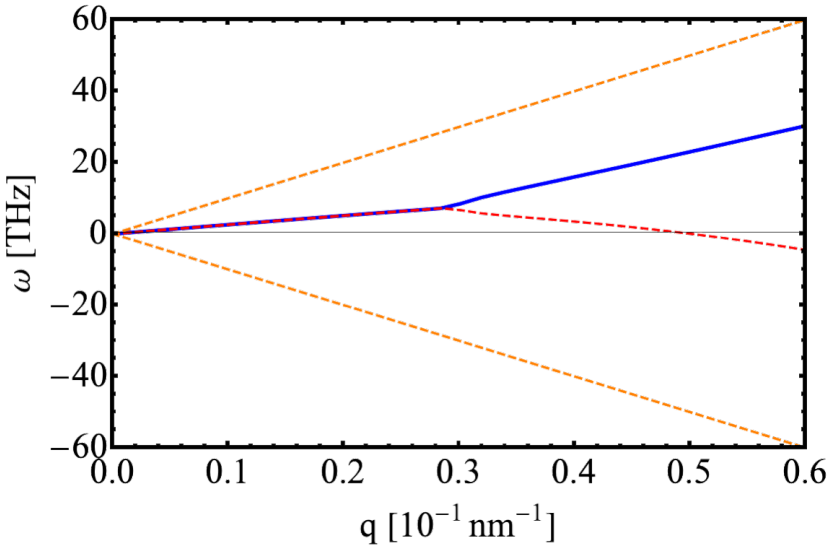

Figure 5.4: Real part of the frequency, for forward (blue) and backward (dashed red) unstable plasmons. The single particle dispersion relation $\omega = \pm v_F q$ is also shown (dashed orange). As expected, the unstable modes lie inside the electron-hole continuum, thus have a non-zero imaginary part. Fixed simulating parameters: $x = 0.15$, $y = 0.1$, $z = 0.1$, $w = 1$, $\theta_b = \pi/4$ and $\varepsilon_r = 2.5$.

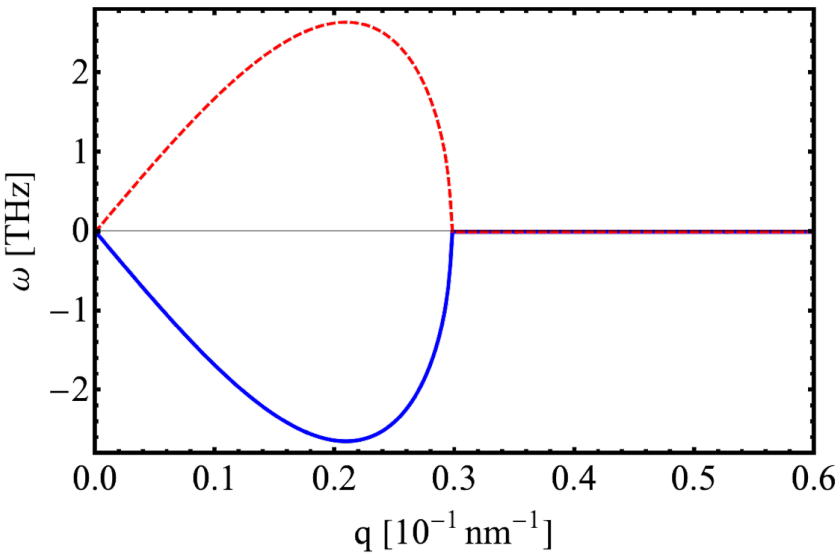

Figure 5.5: Imaginary part of the frequency. The dashed red line corresponds to the backward plasmon, which is growing in time; the blue line is the forward plasmon, which decays in time. Fixed simulating parameters: $x = 0.15$, $y = 0.1$, $z = 0.1$, $w = 1$, $\theta_b = \pi/4$ and $\varepsilon_r = 2.5$.

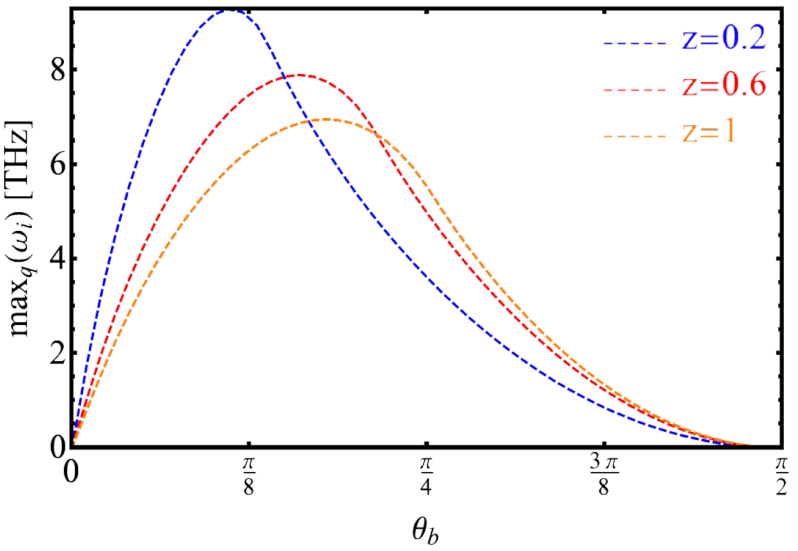

Figure 5.6: Maximum growth rate as a function of the beam angle θ_b, for several values of the normalised beam wave-number, $y = k_b/k_F$. Fixed simulating parameters: $x = 0.15$, $z = 0.1$, $w = 1$ and $\varepsilon_r = 2.5$.

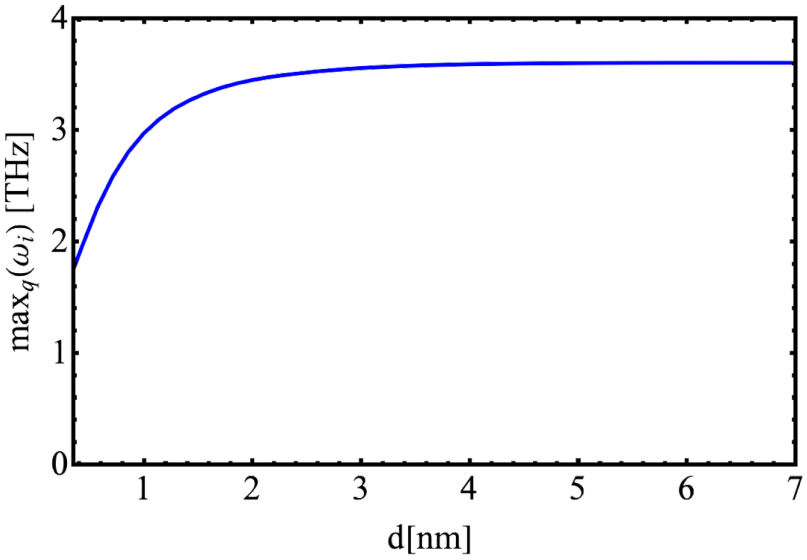

Figure 5.7: Maximum growth rate as a function of the distance between layers, for the case of equal doping. The horizontal axis is restricted to $d > 0.3$ nm. For $d < 0.3$ nm, the distance between carbon atoms in different layers is comparable to the distance between nearest-neighbour atoms in the same layer, and hopping between layers might occur. Fixed simulating parameters: $y = 0.1$, $z = 0.1$, $w = 1$, $\theta_b = \pi/4$ and $\varepsilon_r = 2.5$.

5.2.2 Doped passive layer and undoped active layer

In this section, we treat the equally relevant case of zero doping in the active layer, which is achieved by taking $w = 0$ in (5.30). In that case, the system is described by a quartic equation. The solutions represent two counter propagating plasmons, plus two extra unstable modes, which grow and decay in time, respectively. The previous acoustic and optical modes do not appear, as they require two parallel layers of doped graphene [102]. A similar analysis applies in this case: the real part of the unstable modes is degenerate up to some q_{max}, which depends upon k_b and n_b; the imaginary part exists for $q \in [0, q_{max}]$; for $q > q_{max}$, the real part breaks into different branches, as depicted in Fig. 5.8.

What strongly distinguishes this case from the previous is the dependence of the instability region on the distance between the layers. As shown in Fig. 5.7, for typical simulation parameters, the significant variations of the maximum instability growth rate happened for $d \in [0, 2]$ nm, whereas for larger distances, the instability became saturated in a maximum value, which corresponds to the isolated active layer with injected current. For undoped and doped layers, two stream instability only occurs for sufficiently close graphene sheets, as the isolated undoped active layer can't sustain any instability by itself. Figure 5.9 shows the distance-dependent growth rate for the unstable mode with positive imaginary part. The decaying mode has symmetric imaginary part. We clearly observe the expected decrease of the instability with increasing distance. The simulation shows that, for typical experimental parameters $y \in [0.1, 1]$, $z \in [0.1, 2]$ and $\varepsilon_r \in [2, 10]$, the system becomes stable at $d \gtrsim 8$nm, as the coupling between plasmons and drifting electrons is ineffective to produce the feedback mechanism necessary to sustain the instability.

Comparing both configurations, it can be seen that the second case delivers a stronger instability mechanism, with growth rates that can reach tens of terahertz. On the one hand, we verify that for a

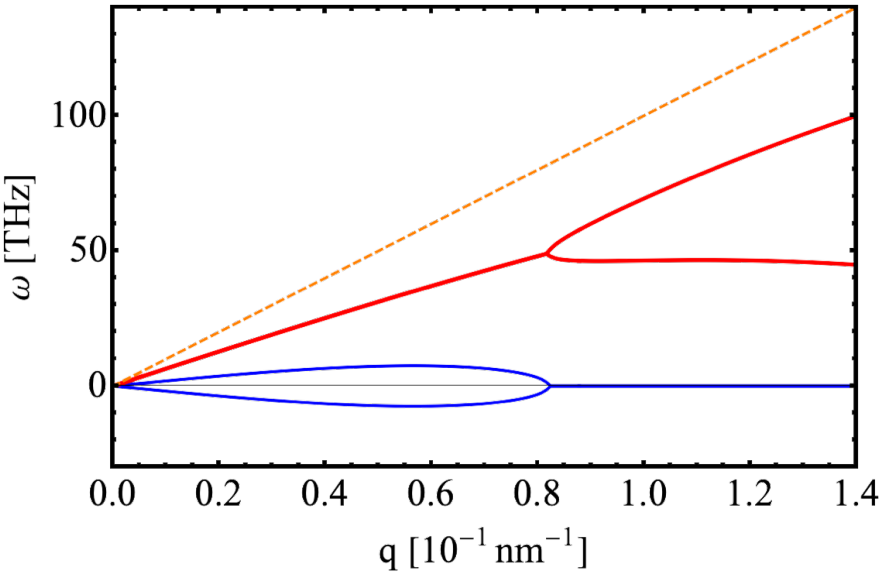

Figure 5.8: Real part (red lines) and imaginary part (blue lines) of the unstable modes. The dashed orange line is the single-particle dispersion relation, $\omega = v_F q$. Fixed simulating parameters: $y = 0.1$, $z = 0.5$, $w = 0$, $\theta_b = \pi/4$ and $\varepsilon_r = 8$.

Coulomb drag configuration, with both layers consisting of doped graphene, disfavours higher growth rates, as the passive layer decreases the effective ratio n_b/n_0 that controls the onset of the instability. This justifies the behaviour as a function of the inter-layers distance d. On the other hand, the doped passive and undoped active layers configuration proved to be more efficient in the promotion of the instability, with growth rates reaching $20 - 30$ THz for realistic experimental values of k_b and n_b. The present growth rates are at least one order of magnitude higher, when compared to other instability mechanisms reported in graphene, as the Dyakonov-Shur (DS) instability [33]. The DS mechanism comprises a hydrodynamical instability, which develops under asymmetric boundary conditions for the electronic density and current. Such conditions are responsible for the formation of successive reflections of the fluid at the edges of the sample, leading to an enhancement of the density fluctuations. Those boundary restrictions are achievable with a graphene field-effect transistor, which allows to fix the injected injected at the drain, while maintaining the electronic density of the source constant. Nonetheless, this effect requires a hydrodynamical regime for the fluid, which in turn implies high electron-electron scattering, so that local thermodynamic equilibrium takes place throughout the system. On the contrary, the present two stream instability is a bulk out-of-equilibrium effect, which neglects the boundary conditions (as they play a minimal role), while requiring small electron-electron scattering rates, so that the sharp $\delta-$distribution for the injected current can be preserved.

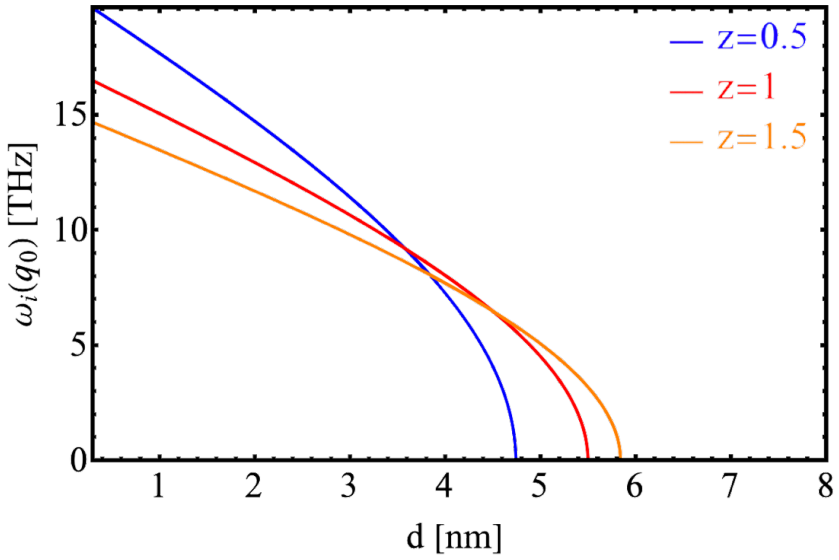

Figure 5.9: Imaginary part of the frequency, as a function of the distance between layers. The results are shown for a fixed wave-number $q_0 = 0.07\text{nm}^{-1}$, and growing values of the drifting wave-vector k_b. The horizontal axis is restricted to $d > 0.3\text{nm}$. Fixed simulating parameters: $y = 0.5$, $w = 0$, $\theta_b = \pi/8$ and $\varepsilon_r = 8$.

Chapter 6

Conclusions

The dynamics of many-body charged systems remains one of the most challenging problems in theoretical physics, with an extensive literature and a variety of mathematical techniques developed over the last years to tackle it. In the present thesis, we relied on a quantum kinetic formalism, based on the definition of phase-space functions through the Weyl transform, and derived a kinetic equation for the evolution of the Wigner function for graphene quasi-particles.

We developed this formalism because it proves to be ideal to examine both the quantum and the semi-classical limits, hence allowing for the construction of a set of hydrodynamical equations. Therefore, starting from the microscopic Hamiltonian, we were able to introduce the graphene kinetic term into the Schödinger equation, at low energies. The single particle contributions were introduced *via* a quantum version of the Liouville theorem based on the Wigner representation, while the interacting potential was given in the mean-field (or Hartree) approximation. The two-body (and higher) interactions could be, in principle, stored in the collisional integral $\mathcal{S}$, written as a functional of the Wigner function.This turns out to be a rigorous approximation for the case of graphene since the coupling constant is density independent, thus r_s is held constant from low to high densities conditions. Additionally, we have $r_s \sim \alpha_s/\varepsilon_r \ll 1$ for sufficiently high relative permittivity (*e.g*, $r_s \approx 0.5$ for a SiO_2 substrate) leading to a weakly-coupled plasma regime, with exchange (Fock) contributions playing a secondary role.

Having set the relevant kinetic equations, we proceeded towards the construction of a hydrodynamical model, by taking the moments of the transport equation. The present formulation allowed to consistently include all quantum corrections in both the continuity and force equations. Those terms are usually neglected because the classical version of the Wigner equation (also known as the Vlasov equation) is commonly adopted. By keeping only the first of those contributions, a closed set of hydrodynamical equations was established. The closure relation came after a particular *ansatz* for the diagonal elements of the Wigner matrix, interpreted as a shifted Fermi-sphere in momentum space, which depended explicitly on the hydrodynamical variables.

Furthermore, the hydrodynamical set of equations enabled us to study the relation between velocity and momentum more profoundly. Despite being quite consensual that those two (fluid) variables are not proportional to each other, in the case of Dirac fluids, a quantitative description has been necessary.

Here, we found a relation of the form $\overline{\boldsymbol{p}} = m(\boldsymbol{r}, t)\overline{\boldsymbol{v}}$, where the local mass $m(\boldsymbol{r}, t)$ was given by the Drude mass $\mathcal{M}$, corrected by a Lorentz-like factor, as $m(\boldsymbol{r}, t) = \mathcal{M}\gamma(\boldsymbol{r}, t)$. In the limiting cases of small and large averaged momentum, $\gamma(\boldsymbol{r}, t)$ was given analytically.

In the end, we returned to the kinetic equation to examine an unstable plasmonic regime, in a Coulomb drag configuration of two graphene sheets, where a beam of electrons was injected in one of them. To do that, we considered the pure electronic case, for which the role of holes is negligible. Instability and damping, which rely on wave-particle interactions, are not possible to treat within the hydrodynamical approach, because those phenomena do not developed under hydrodynamical equilibrium, for which electron-electron scattering guarantees a thermalisation of the distribution. On the contrary, these are purely out-of-equilibrium effects, which oblige to use the full kinetic equations, instead. Moreover, two distinct situations were studied, namely, that consisting of two doped parallel graphene layers, and other where only the passive layer was doped. A similar regime of instability was found in both situations, with similar dependences on the experimental parameters. Notwithstanding, a crucial difference showed up by varying the distance between layers, which disfavoured the instability in the first case. By comparing the results with the Dyakonov-Shur instability [33], which has been proposed for circumventing the THz-gap problem, we concluded that the present two stream instability could deliver growth rates an order of magnitude higher, $\omega_i \in [0, 20]$ THz, for realistic experimental parameters. The real part of the frequency is also located in the THz range, conferring great pertinence to this line of research.

6.1 Achievements

In this work, several important milestone were attained. First, we showed that the Wigner model was equivalent to the RPA formalism for the irreducible polarizability, providing a self-contained method to calculate the plasmonic dispersion relation for the cumbersome case of graphene linear dispersion. This method facilitated the inclusion of those results in a self-consistent theory of quantum transport, that regarded for the Dirac-like kinetic term and had not been treated in this manner anywhere else, to the best of our knowledge.

The second, and probably most notable achievement dwells on the hydrodynamical model, that was properly construct, and whose results were validated when the final dispersion relation was put forward. Such a careful treatment was possible because, despite the real-space version of the Dirac kinetic term being difficult to deal with, we realised that nothing prevents us from starting in Fourier space (for which the kinetic term is simply $\xi(\boldsymbol{q}) = \hbar v_F|\boldsymbol{q}|$), and transforming it back to real space in the end. That idea opened the possibility of including all quantum corrections.

Yet another fulfilled objective regards the relation between momentum and velocity, in the hydrodynamical limit. With the continuity equation unveiling the true form of the velocity field, we were able to relate it with the averaged momentum. We found a non-linear relation with two clearly distinct limiting cases, and an effective mass was given in terms of a Lorentz-like factor, making the bridge with the case of relativistic physics. This relation allowed to clarify an important opened question in the field

of graphene plasmonics, and most prominently, provided us with analytical expressions to use in the hydrodynamical equations and formally close the system.

Finally, we concluded this work by probing an unstable regime involving two graphene layers disposed in a Coulomb drag configuration. In our perspective, the results will help to pave the way towards a future THz emitter.

6.2 Future Work

The work developed under the course of this thesis opened a line of research that should be followed in the future. By having successfully constructed a kinetic theory, based on a microscopic formalism, to model quantum transport in graphene, we have in hands a powerful tool to treat plasmonics within general scenarios. In future research, this formalism should allow to include:

- interaction with lattice phonons and impurities, which are known to play a significant role out of the limit of zero-temperature [104]. These excitations will manifestly introduce losses, which can jeopardise the efficiency of the instabilities;
- interaction with magnetic fields. Our novel strategy of constructing the Wigner matrix by starting in Fourier space should easily allow to further include magnetic effects, through minimal coupling $\boldsymbol{p} \rightarrow \boldsymbol{p} - \mathcal{Q}\boldsymbol{A}$, where $\boldsymbol{A}$ is the vector potential [105]. Moreover, the Maxwell equations should provide a closure relation, linking $\boldsymbol{A}$ to the hydrodynamical variables n and $\overline{\boldsymbol{p}}$, as done previously for the electrostatic potential ϕ.
- correlations and other beyond mean-field effects. The present model enables to treat quantum correlations between particles, namely through the inclusion of the off-diagonal terms of the Wigner matrix in the relevant equations. We showed that the mean-field approximation for the potential implies that the off-diagonal elements completely decouple from the evolution of the diagonal ones. Thus, the information contained in the discarded matrix elements will become important once those elements are included in the interacting potential. Although more challenging, the inclusion of such contributions will probably reveal interesting effects.

Additionally, treating the Dyakonov-Shur instability within this framework is planned for the future. Being a boundary effect, the treatment of this instability will require a set of boundary conditions, that are easily introduced with our complete hydrodynamical model. Particularly, our novel relation between velocity and momentum will probably play a crucial key in studying and understanding this effect, as it allows not only for analytical analysis, but also provides a useful tool for numerical simulations.

Bibliography

[1] K. S. Novoselov, A. K. Geim, S. V. Morozov, D. Jiang, Y. Zhang, S. V. Dubonos, I. V. Grigorieva, and A. A. Firsov. Electric field effect in atomically thin carbon films. *Science*, 306(5696):666–669, 2004. ISSN 0036-8075. doi: 10.1126/science.1102896.

[2] A. H. Castro Neto, F. Guinea, N. M. R. Peres, K. S. Novoselov, and A. K. Geim. The electronic properties of graphene. *Rev. Mod. Phys.*, 81:109–162, Jan 2009. doi: 10.1103/RevModPhys.81.109.

[3] M. Buscema, M. Barkelid, V. Zwiller, H. S. J. van der Zant, G. A. Steele, and A. Castellanos-Gomez. Large and tunable photothermoelectric effect in single-layer mos2. *Nano Letters*, 13(2):358–363, 2013. doi: 10.1021/nl303321g. PMID: 23301811.

[4] S. Das Sarma, S. Adam, E. H. Hwang, and E. Rossi. Electronic transport in two-dimensional graphene. *Rev. Mod. Phys.*, 83:407–470, May 2011. doi: 10.1103/RevModPhys.83.407.

[5] Y. Zhang, Y.-W. Tan, H. L. Stormer, and P. Kim. Experimental observation of the quantum hall effect and berry's phase in graphene. *Nature*, 438(7065):201–204, Nov 2005. ISSN 1476-4687. doi: 10.1038/nature04235.

[6] K. S. Novoselov, A. K. Geim, S. V. Morozov, D. Jiang, M. I. Katsnelson, I. V. Grigorieva, S. V. Dubonos, and A. A. Firsov. Two-dimensional gas of massless dirac fermions in graphene. *Nature*, 438(7065):197–200, Nov 2005. ISSN 1476-4687. doi: 10.1038/nature04233.

[7] E. H. Hwang and S. Das Sarma. Dielectric function, screening, and plasmons in two-dimensional graphene. *Phys. Rev. B*, 75:205418, May 2007. doi: 10.1103/PhysRevB.75.205418.

[8] S. Reich, J. Maultzsch, C. Thomsen, and P. Ordejón. Tight-binding description of graphene. *Phys. Rev. B*, 66:035412, Jul 2002. doi: 10.1103/PhysRevB.66.035412.

[9] P. R. Wallace. The band theory of graphite. *Phys. Rev.*, 71:622–634, May 1947. doi: 10.1103/PhysRev.71.622.

[10] F. H. L. Koppens, D. E. Chang, and F. J. García de Abajo. Graphene plasmonics: A platform for strong light–matter interactions. *Nano Letters*, 11(8):3370–3377, 2011. doi: 10.1021/nl201771h. PMID: 21766812.

[11] A. Geim and K. Novoselov. The rise of graphene. *Nature materials*, 6:183–91, 04 2007. doi: 10.1038/nmat1849.

[12] Y. Yang, Z. Shi, J. Li, and Z.-Y. Li. Optical forces exerted on a graphene-coated dielectric particle by a focused gaussian beam. *Photonics Research*, 4:65, 04 2016. doi: 10.1364/PRJ.4.000065.

[13] F. Wang, Y. Zhang, C. Tian, C. Girit, A. Zettl, M. Crommie, and Y. R. Shen. Gate-variable optical transitions in graphene. *Science*, 320(5873):206–209, 2008. doi: 10.1126/science.1152793.

[14] L. B. N. Laboratory, U. S. D. of Energy. Office of Scientific, and T. Information. *Dirac Charge Dynamics in Graphene by Infrared Spectroscopy*. Lawrence Berkeley National Laboratory, 2008. URL `https://books.google.pt/books?id=G8AtngAACAAJ`.

[15] A. K. Geim. Graphene: Status and prospects. *Science*, 324(5934):1530–1534, 2009. ISSN 0036-8075. doi: 10.1126/science.1158877.

[16] R. W. Wood. On a Remarkable Case of Uneven Distribution of Light in a Diffraction Grating Spectrum. *Proceedings of the Physical Society of London*, 18(1):269–275, June 1902. doi: 10.1088/1478-7814/18/1/325.

[17] L. Rayleigh. On the Dynamical Theory of Gratings. *Proceedings of the Royal Society of London Series A*, 79(532):399–416, Aug. 1907. doi: 10.1098/rspa.1907.0051.

[18] A. Sommerfeld. Ueber die fortpflanzung elektrodynamischer wellen längs eines drahtes. *Annalen der Physik*, 303(2):233–290, 1899. doi: 10.1002/andp.18993030202.

[19] J. Zenneck. Über die fortpflanzung ebener elektromagnetischer wellen längs einer ebenen leiterfläche und ihre beziehung zur drahtlosen telegraphie. *Annalen der Physik*, 328(10):846–866, 1907. doi: 10.1002/andp.19073281003.

[20] U. Fano. The theory of anomalous diffraction gratings and of quasi-stationary waves on metallic surfaces (Sommerfeld's waves). *J. Opt. Soc. Am.*, 31(3):213–222, Mar 1941. doi: 10.1364/JOSA.31.000213.

[21] R. H. Ritchie. Plasma losses by fast electrons in thin films. *Phys. Rev.*, 106:874–881, Jun 1957. doi: 10.1103/PhysRev.106.874.

[22] H. e. a. Lu. Flexibly tunable high-quality-factor induced transparency in plasmonic systems. *Scientific Reports*, 8(1):1558, Jan 2018. ISSN 2045-2322. doi: 10.1038/s41598-018-19869-y.

[23] S. et. al. Roadmap on plasmonics. *Journal of Optics*, 20(4), Apr. 2018. ISSN 2040-8978. doi: 10.1088/2040-8986/aaa114.

[24] J. Lee, S. Shim, B. Kim, and H. S. Shin. Surface-enhanced raman scattering of single- and few-layer graphene by the deposition of gold nanoparticles. *Chemistry – A European Journal*, 17(8):2381–2387, 2011. doi: 10.1002/chem.201002027.

[25] A. Agarwal, M. Vitiello, L. Viti, A. Cupolillo, and A. Politano. Plasmonics with two-dimensional semiconductors: From basic research to technological applications. *Nanoscale*, 10, 04 2018. doi: 10.1039/C8NR01395K.

[26] Y. Li, Z. Li, C. Chi, H. Shan, L. Zheng, and Z. Fang. Plasmonics of 2d nanomaterials: Properties and applications. *Advanced Science*, 4(8):1600430, 2017. doi: 10.1002/advs.201600430.

[27] B. Radisavljevic, A. Radenovic, J. Brivio, V. Giacometti, and A. Kis. Single-layer mos2 transistors. *Nature nanotechnology*, 6:147–50, 01 2011. doi: 10.1038/nnano.2010.279.

[28] R. A. Lewis. A review of terahertz sources. *Journal of Physics D: Applied Physics*, 47(37): 374001, aug 2014. doi: 10.1088/0022-3727/47/37/374001. URL https://doi.org/10.1088%2F0022-3727%2F47%2F37%2F374001.

[29] Y.-S. Lee. *Principles of Terahertz Science and Technology*. Springer Publishing Company, Incorporated, 1st edition, 2008. ISBN 038709539X.

[30] A. Y. Pawar, D. D. Sonawane, K. B. Erande, and D. V. Derle. Terahertz technology and its applications. *Drug Invention Today*, 5(2):157 – 163, 2013. ISSN 0975-7619. doi: https://doi.org/10.1016/j.dit.2013.03.009. URL http://www.sciencedirect.com/science/article/pii/S0975761913000264.

[31] M. Dyakonov and M. Shur. Shallow water analogy for a ballistic field effect transistor: New mechanism of plasma wave generation by dc current. *Phys. Rev. Lett.*, 71:2465–2468, Oct 1993. doi: 10.1103/PhysRevLett.71.2465.

[32] D. Svintsov. Fate of an electron beam in graphene: Coulomb relaxation or plasma instability? *Phys. Rev. B*, 101:235440, Jun 2020. doi: 10.1103/PhysRevB.101.235440. URL https://link.aps.org/doi/10.1103/PhysRevB.101.235440.

[33] P. Cosme and H. Terças. Terahertz laser combs in graphene field-effect transistors. *ACS Photonics*, 7(6):1375–1381, 2020. doi: 10.1021/acsphotonics.0c00313.

[34] V. Ryzhii, A. Satou, and T. Otsuji. Plasma waves in two-dimensional electron-hole system in gated graphene heterostructures. *Journal of Applied Physics - J APPL PHYS*, 101, 01 2007. doi: 10.1063/1.2426904.

[35] R. Bistritzer and A. H. MacDonald. Hydrodynamic theory of transport in doped graphene. *Phys. Rev. B*, 80:085109, Aug 2009. doi: 10.1103/PhysRevB.80.085109.

[36] D. Svintsov, V. Vyurkov, S. Yurchenko, T. Otsuji, and V. Ryzhii. Hydrodynamic model for electron-hole plasma in graphene. *Journal of Applied Physics*, 111(8):083715, Apr 2012. ISSN 1089-7550. doi: 10.1063/1.4705382.

[37] H. Smith and . Jensen, H. Højgaard (Henning Højgaard). *Transport phenomena*. Oxford [England] : Clarendon Press ; New York : Oxford University Press, 1989. ISBN 0198519850. URL http://www.loc.gov/catdir/enhancements/fy0636/88028230-t.html.

[38] S. Khan and M. Bonitz. *Quantum Hydrodynamics*, pages 103–152. 04 2014. ISBN 978-3-319-05437-7. doi: 10.1007/978-3-319-05437-7_4.

[39] E. Wigner. On the quantum correction for thermodynamic equilibrium. *Phys. Rev.*, 40:749–759, Jun 1932. doi: 10.1103/PhysRev.40.749.

[40] H. Groenewold. On the principles of elementary quantum mechanics. *Physica*, 12(7):405 – 460, 1946. ISSN 0031-8914. doi: https://doi.org/10.1016/S0031-8914(46)80059-4.

[41] J. E. Moyal. Quantum mechanics as a statistical theory. *Proc. Cambridge Phil. Soc.*, 45:99–124, 1949.

[42] H. Weyl. Gruppentheorie und quantenmechanik. *Z. Phys.*, 46, 2002.

[43] D. V. Karlovets and V. G. Serbo. Possibility to probe negative values of a Wigner function in scattering of a coherent superposition of electronic wave packets by atoms. *Physical Review Letters*, 119(17), Oct 2017. ISSN 1079-7114. doi: 10.1103/physrevlett.119.173601.

[44] M. Hillery, R. F. O'Connell, M. O. Scully, and E. P. Wigner. *Distribution Functions in Physics: Fundamentals*, pages 273–317. Springer Berlin Heidelberg, Berlin, Heidelberg, 1997. doi: 10.1007/978-3-642-59033-7_28.

[45] F. Haas, G. Manfredi, and M. Feix. Multistream model for quantum plasmas. *Phys. Rev. E*, 62: 2763–2772, Aug 2000. doi: 10.1103/PhysRevE.62.2763. URL `https://link.aps.org/doi/10.1103/PhysRevE.62.2763`.

[46] D. Bohm and D. Pines. A collective description of electron interactions: Iii. Coulomb interactions in a degenerate electron gas. *Phys. Rev.*, 92:609–625, Nov 1953. doi: 10.1103/PhysRev.92.609. URL `https://link.aps.org/doi/10.1103/PhysRev.92.609`.

[47] D. Bohm and E. P. Gross. Theory of plasma oscillations. a. origin of medium-like behavior. *Phys. Rev.*, 75:1851–1864, Jun 1949. doi: 10.1103/PhysRev.75.1851. URL `https://link.aps.org/doi/10.1103/PhysRev.75.1851`.

[48] J. T. Mendonça, J. E. Ribeiro, and P. K. Shukla. Wave kinetic description of quantum pair plasmas. *Journal of Plasma Physics*, 74(1):91–97, 2008. doi: 10.1017/S0022377807006587.

[49] J. Mendonça, A. Serbeto, and P. Shukla. Wave kinetic description of Bogoliubov oscillations in the bose–einstein condensate. *Physics Letters A*, 372(13):2311 – 2314, 2008. ISSN 0375-9601. doi: https://doi.org/10.1016/j.physleta.2007.11.021.

[50] H. Terças, J. T. Mendonça, and G. R. M. Robb. Two-stream instability in quasi-one-dimensional Bose-Einstein condensates. *Phys. Rev. A*, 79:065601, Jun 2009. doi: 10.1103/PhysRevA.79.065601.

[51] G. Manfredi and F. Haas. Self-consistent fluid model for a quantum electron gas. *Phys. Rev. B*, 64:075316, Jul 2001. doi: 10.1103/PhysRevB.64.075316. URL https://link.aps.org/doi/10.1103/PhysRevB.64.075316.

[52] P. K. Shukla and B. Eliasson. Novel attractive force between ions in quantum plasmas. *Phys. Rev. Lett.*, 108:165007, Apr 2012. doi: 10.1103/PhysRevLett.108.165007. URL https://link.aps.org/doi/10.1103/PhysRevLett.108.165007.

[53] M. R. Amin. Quantum effect on modulational instability of laser radiation in a semiconductor plasma. *Journal of Applied Physics*, 107(2):023307, 2010. doi: 10.1063/1.3295917. URL https://doi.org/10.1063/1.3295917.

[54] N. Crouseilles, P.-A. Hervieux, and G. Manfredi. Quantum hydrodynamic model for the nonlinear electron dynamics in thin metal films. *Phys. Rev. B*, 78:155412, Oct 2008. doi: 10.1103/PhysRevB.78.155412. URL https://link.aps.org/doi/10.1103/PhysRevB.78.155412.

[55] F. Haas, G. Manfredi, P. K. Shukla, and P.-A. Hervieux. Breather mode in the many-electron dynamics of semiconductor quantum wells. *Phys. Rev. B*, 80:073301, Aug 2009. doi: 10.1103/PhysRevB.80.073301. URL https://link.aps.org/doi/10.1103/PhysRevB.80.073301.

[56] R. Maroof, A. Mushtaq, and A. Qamar. Quantum dust magnetosonic waves with spin and exchange correlation effects. *Physics of Plasmas*, 23(1):013704, 2016. doi: 10.1063/1.4939807. URL https://doi.org/10.1063/1.4939807.

[57] J. López and J. Montejo-Gámez. A hydrodynamic approach to multidimensional dissipation-based Schrödinger models from quantum Fokker–Planck dynamics. *Physica D: Nonlinear Phenomena*, 238:622–644, 2009.

[58] P. Shukla and B. Eliasson. Nonlinear aspects of quantum plasma physics. *Physics-uspekhi - PHYS-USP*, 53:51–76, 01 2010. doi: 10.3367/UFNe.0180.201001b.0055.

[59] E. Madelung. Hydrodynamical form of quantum theory. *Annales de la Fondation Louis de Broglie*, 15(1):91–96, 1990. ISSN 0182-4295. URL http://inis.iaea.org/search/search.aspx?orig_q=RN:22005322.

[60] F. Haas. *Quantum plasmas: an hydrodynamic approach*. Springer, New York, 2011. URL http://www.springer.com/physics/atomic,+molecular,+optical+%26+plasma+physics/book/978-1-4419-8200-1.

[61] Z. A. Moldabekov, M. Bonitz, and T. S. Ramazanov. Theoretical foundations of quantum hydrodynamics for plasmas. *Physics of Plasmas*, 25(3):031903, 2018. doi: 10.1063/1.5003910. URL https://doi.org/10.1063/1.5003910.

[62] D. B. Melrose and A. Mushtaq. Quantum recoil and bohm diffusion. *Physics of Plasmas*, 16(9):094508, 2009. doi: 10.1063/1.3242726. URL https://doi.org/10.1063/1.3242726.

[63] M.-J. Lee and Y.-D. Jung. Bohm potential effect on the propagation of electrostatic surface wave in semi-bounded quantum plasmas. *Physics Letters A*, 381(6):636 – 638, 2017. ISSN 0375-9601. doi: https://doi.org/10.1016/j.physleta.2016.12.025. URL http://www.sciencedirect.com/science/article/pii/S0375960116312968.

[64] J. Hurst, O. Morandi, G. Manfredi, and P.-A. Hervieux. Semiclassical Vlasov and fluid models for an electron gas with spin effects. *The European Physical Journal D*, 68, 05 2014. doi: 10.1140/epjd/e2014-50205-5.

[65] R. Balescu and W. Y. Zhang. Kinetic equation, spin hydrodynamics and collisional depolarization rate in a spin-polarized plasma. *Journal of Plasma Physics*, 40(2):215–234, 1988. doi: 10.1017/S0022377800013234.

[66] L. Brey, J. Dempsey, N. F. Johnson, and B. I. Halperin. Infrared optical absorption in imperfect parabolic quantum wells. *Phys. Rev. B*, 42:1240–1247, Jul 1990. doi: 10.1103/PhysRevB.42.1240. URL https://link.aps.org/doi/10.1103/PhysRevB.42.1240.

[67] K. Ourabah and M. Tribeche. Quantum ion-acoustic solitary waves: The effect of exchange correlation. *Phys. Rev. E*, 88:045101, Oct 2013. doi: 10.1103/PhysRevE.88.045101. URL https://link.aps.org/doi/10.1103/PhysRevE.88.045101.

[68] I. Zeba, M. Yahia, P. Shukla, and W. Moslem. Electron–hole two-stream instability in a quantum semiconductor plasma with exchange-correlation effects. *Physics Letters A*, 376(34):2309 – 2313, 2012. ISSN 0375-9601. doi: https://doi.org/10.1016/j.physleta.2012.05.049. URL http://www.sciencedirect.com/science/article/pii/S0375960112006743.

[69] S.-H. Mao and J.-K. Xue. Collective dynamics of the electron gas in an anharmonic quantum well. *Physica Scripta*, 84(5):055501, oct 2011. doi: 10.1088/0031-8949/84/05/055501. URL https://doi.org/10.1088%2F0031-8949%2F84%2F05%2F055501.

[70] W. Wang, J. Shao, and Z. Li. The exchange–correlation potential correction to the vacuum potential barrier of graphene edge. *Chemical Physics Letters*, 522:83 – 85, 2012. ISSN 0009-2614. doi: https://doi.org/10.1016/j.cplett.2011.12.002. URL http://www.sciencedirect.com/science/article/pii/S0009261411014825.

[71] J. Mendonca, H. Terças, and A. Gammal. Quantum Landau damping in dipolar bose-einstein condensates. *Physical Review A*, 97, 01 2018. doi: 10.1103/PhysRevA.97.063610.

[72] A. Geim and A. MacDonald. Graphene: Exploring carbon flatland. *Physics Today*, 60(8):35–41, 2007. ISSN 0031-9228. doi: https://doi.org/10.1063/1.2774096.

[73] J. P. Santos and L. O. Silva. Wigner-Moyal description of free variable mass Klein-Gordon fields. *Journal of Mathematical Physics*, 46(10):102901, 2005. doi: 10.1063/1.2049169. URL https://doi.org/10.1063/1.2049169.

[74] J. Zamanian, M. Marklund, and G. Brodin. Scalar quantum kinetic theory for spin-1/2 particles: mean field theory. *New Journal of Physics*, 12(4):043019, apr 2010. doi: 10.1088/1367-2630/12/4/043019. URL https://doi.org/10.1088%2F1367-2630%2F12%2F4%2F043019.

[75] C. Brif and A. Mann. Phase-space formulation of quantum mechanics and quantum-state reconstruction for physical systems with Lie-group symmetries. *Phys. Rev. A*, 59:971–987, Feb 1999. doi: 10.1103/PhysRevA.59.971. URL https://link.aps.org/doi/10.1103/PhysRevA.59.971.

[76] D. Dragoman. Wigner distribution function in nonlinear optics. *Appl. Opt.*, 35(21):4142–4146, Jul 1996. doi: 10.1364/AO.35.004142. URL http://ao.osa.org/abstract.cfm?URI=ao-35-21-4142.

[77] O. T. Serimaa, J. Javanainen, and S. Varró. Gauge-independent Wigner functions: General formulation. *Phys. Rev. A*, 33:2913–2927, May 1986. doi: 10.1103/PhysRevA.33.2913. URL https://link.aps.org/doi/10.1103/PhysRevA.33.2913.

[78] C. Kittel. *Quantum Theory of Solids*. John Wiley and Sons, Inc, 1963. ISBN 0471825638.

[79] T. Stauber, N. M. R. Peres, and F. Guinea. Electronic transport in graphene: A semiclassical approach including midgap states. *Phys. Rev. B*, 76:205423, Nov 2007. doi: 10.1103/PhysRevB.76.205423. URL https://link.aps.org/doi/10.1103/PhysRevB.76.205423.

[80] T. Fang, A. Konar, H. Xing, and D. Jena. Carrier statistics and quantum capacitance of graphene sheets and ribbons. *Applied Physics Letters*, 91(9):092109, 2007. doi: 10.1063/1.2776887. URL https://doi.org/10.1063/1.2776887.

[81] Z. Zheng, W. Wang, T. Ma, Z. Deng, Y. Ke, R. Zhan, Q. Zou, W. Ren, J. Chen, J. She, Y. Zhang, F. Liu, H. Chen, S. Deng, and N. Xu. Chemically-doped graphene with improved surface plasmon characteristics: an optical near-field study. *Nanoscale*, 8:16621–16630, 2016. doi: 10.1039/C6NR04239B. URL http://dx.doi.org/10.1039/C6NR04239B.

[82] F. Giubileo and A. Di Bartolomeo. The role of contact resistance in graphene field-effect devices. *Progress in Surface Science*, 92:143–175, 06 2017. doi: 10.1016/j.progsurf.2017.05.002.

[83] R. Jasiak, G. Manfredi, P.-A. Hervieux, and M. Haefele. Quantum–classical transition in the electron dynamics of thin metal films. *New Journal of Physics*, 11:063042, 06 2009. doi: 10.1088/1367-2630/11/6/063042.

[84] R. R. Nair, P. Blake, A. N. Grigorenko, K. S. Novoselov, T. J. Booth, T. Stauber, N. M. R. Peres, and A. K. Geim. Fine structure constant defines visual transparency of graphene. *Science*, 320(5881):1308–1308, 2008. ISSN 0036-8075. doi: 10.1126/science.1156965. URL https://science.sciencemag.org/content/320/5881/1308.

[85] K. S. Novoselov, A. K. Geim, S. V. Morozov, D. Jiang, M. I. Katsnelson, I. V. Grigorieva, S. V. Dubonos, and A. A. Firsov. Two-dimensional gas of massless Dirac fermions in graphene. *Nature*,

438(7065):197–200, Nov 2005. ISSN 1476-4687. doi: 10.1038/nature04233. URL https://doi.org/10.1038/nature04233.

[86] C. Lee, X. Wei, J. W. Kysar, and J. Hone. Measurement of the elastic properties and intrinsic strength of monolayer graphene. *Science*, 321(5887):385–388, 2008. ISSN 0036-8075. doi: 10.1126/science.1157996. URL https://science.sciencemag.org/content/321/5887/385.

[87] H. Liu, Y. Liu, and D. Zhu. Chemical doping of graphene. *J. Mater. Chem.*, 21:3335–3345, 2011. doi: 10.1039/C0JM02922J. URL http://dx.doi.org/10.1039/C0JM02922J.

[88] D. Reddy, L. F. Register, G. D. Carpenter, and S. K. Banerjee. Graphene field-effect transistors. *Journal of Physics D: Applied Physics*, 44(31):313001, jul 2011. doi: 10.1088/0022-3727/44/31/313001. URL https://doi.org/10.1088%2F0022-3727%2F44%2F31%2F313001.

[89] S. Das Sarma, E. Hwang, and Q. Li. Valley-dependent many-body effects in two-dimensional semiconductors. *Phys. Rev. B*, 80, 04 2009. doi: 10.1103/PhysRevB.80.121303.

[90] S. Das Sarma and E. H. Hwang. Collective modes of the massless Dirac plasma. *Physical Review Letters*, 102(20), May 2009. ISSN 1079-7114. doi: 10.1103/physrevlett.102.206412.

[91] B. Wunsch, T. Stauber, F. Sols, and F. Guinea. Dynamical polarization of graphene at finite doping. *New Journal of Physics*, 8(12):318–318, dec 2006. doi: 10.1088/1367-2630/8/12/318.

[92] Y. Liu, R. Willis, K. Emtsev, and T. Seyller. Plasmon dispersion and damping in electrically isolated two-dimensional charge sheets. *Phys. Rev. B*, 78, 11 2008. doi: 10.1103/PhysRevB.78.201403.

[93] A. J. Chaves, N. M. R. Peres, G. Smirnov, and N. A. Mortensen. Hydrodynamic model approach to the formation of plasmonic wakes in graphene. *Physical Review B*, 96(19), Nov 2017. ISSN 2469-9969. doi: 10.1103/physrevb.96.195438.

[94] D. Svintsov, V. Vyurkov, V. Ryzhii, and T. Otsuji. Hydrodynamic electron transport and nonlinear waves in graphene. *Physical Review B*, 88(24), Dec 2013. ISSN 1550-235X. doi: 10.1103/physrevb.88.245444.

[95] B. Eliasson and P. K. Shukla. Nonlinear quantum fluid equations for a finite temperature fermi plasma. *Physica Scripta*, 78(2):025503, jul 2008. doi: 10.1088/0031-8949/78/02/025503. URL https://doi.org/10.1088%2F0031-8949%2F78%2F02%2F025503.

[96] R. Bharuthram, H. Saleem, and P. K. Shukla. Two-stream instabilities in unmagnetized dusty plasmas. *Physica Scripta*, 45(5):512–514, may 1992. doi: 10.1088/0031-8949/45/5/017. URL https://doi.org/10.1088%2F0031-8949%2F45%2F5%2F017.

[97] L. E. Thode and R. N. Sudan. Two-stream instability heating of plasmas by relativistic electron beams. *Phys. Rev. Lett.*, 30:732–735, Apr 1973. doi: 10.1103/PhysRevLett.30.732. URL https://link.aps.org/doi/10.1103/PhysRevLett.30.732.

[98] B. B. Robinson and G. A. Swartz. Two-stream instability in semiconductor plasmas. *Journal of Applied Physics*, 38(6):2461–2465, 1967. doi: 10.1063/1.1709928. URL https://doi.org/10.1063/1.1709928.

[99] D. Pines and J. R. Schrieffer. Collective behavior in solid-state plasmas. *Phys. Rev.*, 124:1387–1400, Dec 1961. doi: 10.1103/PhysRev.124.1387. URL https://link.aps.org/doi/10.1103/PhysRev.124.1387.

[100] I. Zeba, M. Yahia, P. Shukla, and W. Moslem. Electron–hole two-stream instability in a quantum semiconductor plasma with exchange-correlation effects. *Physics Letters A*, 376(34):2309 – 2313, 2012. ISSN 0375-9601. doi: https://doi.org/10.1016/j.physleta.2012.05.049. URL http://www.sciencedirect.com/science/article/pii/S0375960112006743.

[101] C. M. Aryal, B. Y.-K. Hu, and A.-P. Jauho. Plasma wave instabilities in nonequilibrium graphene. *Phys. Rev. B*, 94:115401, Sep 2016. doi: 10.1103/PhysRevB.94.115401. URL https://link.aps.org/doi/10.1103/PhysRevB.94.115401.

[102] E. H. Hwang and S. Das Sarma. Plasmon modes of spatially separated double-layer graphene. *Phys. Rev. B*, 80:205405, Nov 2009. doi: 10.1103/PhysRevB.80.205405. URL https://link.aps.org/doi/10.1103/PhysRevB.80.205405.

[103] P. A. D. Gonçalves and N. M. R. Peres. An introduction to graphene plasmonics. Dec 2015. doi: 10.1142/9948. URL http://dx.doi.org/10.1142/9948.

[104] L. Lindsay, D. A. Broido, and N. Mingo. Flexural phonons and thermal transport in graphene. *Phys. Rev. B*, 82:115427, Sep 2010. doi: 10.1103/PhysRevB.82.115427. URL https://link.aps.org/doi/10.1103/PhysRevB.82.115427.

[105] E. Gorbar, V. Miransky, I. Shovkovy, and P. Sukhachov. Wigner function and kinetic phenomena for chiral plasma in a strong magnetic field. *Journal of High Energy Physics*, 2017, 07 2017. doi: 10.1007/JHEP08(2017)103.

Appendix A

A.1 Useful identities

For any phase-space variable $\boldsymbol{q}$, the volume element in d dimensions reads

$$d\boldsymbol{q} \doteq \prod_{i=1}^{d} dq_i \ . \tag{A.1}$$

We use the following definitions for the Fourier transform of d-dimensional phase-space variables

$$f(..., \boldsymbol{r}, ...) = \int d\boldsymbol{q}\ e^{i\boldsymbol{q}\cdot\boldsymbol{r}}\ f(..., \boldsymbol{q}, ...), \tag{A.2}$$

$$f(..., \boldsymbol{q}, ...) = \int \frac{d\boldsymbol{r}}{(2\pi)^d}\ e^{-i\boldsymbol{q}\cdot\boldsymbol{r}}\ f(..., \boldsymbol{r}, ...), \tag{A.3}$$

For the time-frequency domain,

$$f(..., t, ...) = \int d\omega\ e^{-i\omega t}\ f(..., \omega, ...), \tag{A.4}$$

$$f(..., \omega, ...) = \int \frac{dt}{2\pi}\ e^{i\omega t}\ f(..., t, ...). \tag{A.5}$$

The Dirac-delta $\delta(\boldsymbol{r})$ is given by

$$\delta(\boldsymbol{r}) = \int \frac{d\boldsymbol{y}}{(2\pi)^d}\ e^{i\boldsymbol{y}\cdot\boldsymbol{r}}, \tag{A.6}$$

and the Kronecker-delta δ_{ij} is

$$\delta_{ij} = \begin{cases} 1 & \text{for } i = j, \\ 0 & \text{for } i \neq j. \end{cases} \tag{A.7}$$

For a smooth function f, we can rewrite translations in the argument as

$$f(\boldsymbol{z} + \boldsymbol{s}) = e^{\boldsymbol{s}\cdot\boldsymbol{\nabla}_{\boldsymbol{z}}} f(\boldsymbol{z}) \tag{A.8}$$

where $e^{\boldsymbol{s}\cdot\boldsymbol{\nabla}_{\boldsymbol{z}}}$ is the translation operator[1].

[1] This result is easily proved using the Taylor series for the exponential $e^{\boldsymbol{s}\cdot\boldsymbol{\nabla}_{\boldsymbol{z}}} = \sum_n \frac{(\boldsymbol{s}\cdot\boldsymbol{\nabla}_{\boldsymbol{z}})^n}{n!}$.

Appendix B

B.1 Bohm-Pines dispersion relation

Let us start from

$$1 = \frac{e^2}{\varepsilon_0 q^2} \int d\boldsymbol{k}\, \frac{W_0(\boldsymbol{k}-\boldsymbol{q}/2) - W_0(\boldsymbol{k}+\boldsymbol{q}/2)}{\hbar(\omega - \hbar\boldsymbol{k}\cdot\boldsymbol{q}/m_e)}. \tag{B.1}$$

By separating the integral in its two terms, and performing a change of variables $\boldsymbol{k'} = \boldsymbol{k} - \boldsymbol{q}/2$ and $\boldsymbol{k'} = \boldsymbol{k} + \boldsymbol{q}/2$ for the first and second terms, respectively, we can recast (B.1) in a more useful form,

$$1 = \frac{\omega_p^2}{n_0} \int d\boldsymbol{k}\, \frac{W_0(\boldsymbol{k})}{(\omega - \hbar\boldsymbol{k}\cdot\boldsymbol{q}/m)^2 - \hbar^2 q^4/4m^2}, \tag{B.2}$$

where $\omega_p^2 = e^2 n_0/\varepsilon_0 m_e$ is the electron plasma frequency. We also changed the dummy variable $\boldsymbol{k'}$ back to $\boldsymbol{k}$, for convenience. Further manipulation leads to[1]

$$1 = \frac{\omega_p^2}{n_0\omega^2} \int d\boldsymbol{v}\, \frac{W_0(\boldsymbol{v})}{1 - 2\,\boldsymbol{v}\cdot\boldsymbol{q}/\omega + (\boldsymbol{v}\cdot\boldsymbol{q})^2/\omega^2 - \hbar^2 q^4/4m^2}. \tag{B.3}$$

where $\boldsymbol{v} = \hbar\boldsymbol{k}/m$. Let us define the following rescaled quantities

$$\Omega = \frac{\omega}{\omega_p}, \tag{B.4}$$

$$\Omega_p = \frac{\hbar^2 q^4}{4m^2\omega_p^2}, \tag{B.5}$$

$$\rho = \frac{qv}{\omega_p}. \tag{B.6}$$

Applying the expansion

$$\frac{1}{1-x} = 1 + x + x^2 + \mathcal{O}(x^3), \tag{B.7}$$

in the integrand, and keeping only the $\mathcal{O}\left(\Omega_p^2/\Omega^2, \overline{\rho^2}/\Omega^2\right)$ terms, we obtain

$$1 \simeq \frac{\omega_p^2}{n_0\omega^2}\left[n_0 + \frac{n_0}{\omega^2}\left(3\boldsymbol{q}^2\cdot\overline{\boldsymbol{v}^2}_0 + \frac{2\boldsymbol{q}\cdot\overline{\boldsymbol{v}}_0}{\omega} + \frac{\hbar^2 q^4}{4m^2}\right)\right], \tag{B.8}$$

[1] Recall the identity $d\boldsymbol{k}\; W_0(\boldsymbol{k}) = d\boldsymbol{v}\; W_0(\boldsymbol{v})$, which comes from the definition of a (*quasi-*)distribution function.

where $\overline{\boldsymbol{v}}_0$ and $\overline{\boldsymbol{v}^2}_0$ are calculated with the is the equilibrium Wigner function. Equation (B.9) is invariant under a global rotation in the $\boldsymbol{k}-\boldsymbol{q}$ space, given that it only shows a dependence on absolute values or intern products. So, we are free to align $\boldsymbol{q}$ with the $z-$direction (note that $\boldsymbol{q}$ is fixed), without loss of generality. It yields $\boldsymbol{q}\cdot\boldsymbol{v} = qv\cos\theta$, with θ being the polar angle of $\boldsymbol{v}$. Additionally, we can neglect the $\sim \boldsymbol{q}\cdot\overline{\boldsymbol{v}}_0$ term, which vanishes for a rotational invariant equilibrium configuration, *i.e.*, when $W_0(\boldsymbol{v})$ is only a function of the absolute value v. Under this (quite general) assumption, $\boldsymbol{q}\cdot\overline{\boldsymbol{v}}_0$ becomes proportional to $\int d\Omega\cos\theta$, which gives zero. Thus, (B.8) simplifies to

$$1 \simeq \frac{\omega_p^2}{n_0\omega^2}\left[n_0 + \frac{n_0}{\omega^2}\left(3q^2u_\parallel^2 + \frac{\hbar^2q^4}{4m^2}\right)\right], \tag{B.9}$$

where $u_\parallel^2$ is the average equilibrium parallel velocity,

$$u_\parallel^2 = \frac{1}{n_0}\int d\boldsymbol{v}\; W_0(\boldsymbol{v})\;(v\cos\theta)^2. \tag{B.10}$$

Solving the remaining quadratic equation in (B.9), with the same approximation as before, we finally arrive at (2.37).

B.2 Derivation of the quantum hydrodynamical equations for 3D parabolic plasmas

We intend to calculate

$$\frac{\partial n}{\partial t} = \int d\boldsymbol{k}\,\Big[-\frac{\hbar}{m}\boldsymbol{k}\cdot\boldsymbol{\nabla}W + \frac{i}{\hbar}\int d\boldsymbol{q}\; e^{i\boldsymbol{r}\cdot\boldsymbol{r}}\big(W_+ - W_-\big)V(\boldsymbol{q},t)\Big], \tag{B.11}$$

$$\frac{\partial(n\langle\boldsymbol{p}\rangle)}{\partial t} = \int d\boldsymbol{k}\;\hbar\boldsymbol{k}\,\Big[-\frac{\hbar}{m}\boldsymbol{k}\cdot\boldsymbol{\nabla}W + \frac{i}{\hbar}\int d\boldsymbol{q}\; e^{i\boldsymbol{r}\cdot\boldsymbol{r}}\big(W_+ - W_-\big)V(\boldsymbol{q},t)\Big], \tag{B.12}$$

where $W = W(\boldsymbol{r},\boldsymbol{k},t)$ and $W_\pm = W(\boldsymbol{r},\boldsymbol{k}\pm\boldsymbol{q}/2,t)$. The important thing to do, at this stage, is using identity (A.8) to rewrite $(W_+ - W_-)$ as

$$W(\boldsymbol{r},\boldsymbol{k}+\boldsymbol{q}/2,t) - W(\boldsymbol{r},\boldsymbol{k}-\boldsymbol{q}/2,t) = 2\sinh\Big(\frac{\boldsymbol{q}}{2}\cdot\boldsymbol{\nabla}_k\Big)\;W(\boldsymbol{r},\boldsymbol{k},t), \tag{B.13}$$

Furthermore, using the Taylor series for the hyperbolic-sine

$$\sinh\Big(\hat{A}\Big) = \sum_{n=0}^{+\infty}\frac{1}{(2n+1)!}\;\hat{A}^{2n+1}, \tag{B.14}$$

together with the Newton binomial theorem, allows us to write

$$\sinh\Big(\frac{\boldsymbol{q}}{2}\cdot\boldsymbol{\nabla}_k\Big)=\sum_{n=0}^{+\infty}\sum_{m=0}^{2n+1}\sum_{l=0}^{m}\theta_{nml}\Big(q_x\frac{\partial}{\partial k_x}\Big)^l\Big(q_y\frac{\partial}{\partial k_y}\Big)^{m-l}\Big(q_z\frac{\partial}{\partial k_z}\Big)^{2n+1-m},$$
$$=\frac{\boldsymbol{q}}{2}\cdot\boldsymbol{\nabla}_k+\mathcal{O}(\partial_{k_i}^3) \tag{B.15}$$

where $\mathcal{O}(\partial_{k_i}^3)$ are terms at least cubic on the derivatives with respect to $\boldsymbol{k}$, and θ_{nml} are non-zero expansion coefficients, given by

$$\theta_{nml}=\frac{1}{2^{2n+1}l!(m-l)!(2n+1-m)!}. \tag{B.16}$$

This differential operator applied to the Wigner function is part of the integrant function inside $\boldsymbol{k}$ integrations. By performing partial integration in $\boldsymbol{k}$, the summation of (B.15) will only retain terms up to the $\boldsymbol{k}$-order of the remaining integrand. The surface terms give no contribution because we assume the Wigner function to vanish as $k_i\to\pm\infty$, for all directions i. Therefore, introducing (B.13) and (B.15) into (B.11) yields no contribution for the second term in the l.h.s., given that the remaining integral is $\boldsymbol{k}-$independent. Furthermore, by writing $W(\boldsymbol{r},\boldsymbol{k},t)$ in terms of its Fourier transform $W(\boldsymbol{q},\boldsymbol{k},t)$, we get

$$\begin{aligned}\frac{\partial n}{\partial t}&=-\frac{i\hbar}{m}\int d\boldsymbol{k}\,d\boldsymbol{q}\,e^{i\boldsymbol{q}\cdot\boldsymbol{r}}\,\boldsymbol{k}\cdot\boldsymbol{q}\,W(\boldsymbol{q},\boldsymbol{k},t),\\&=-\frac{i\hbar}{m}\int\frac{d\boldsymbol{r'}}{(2\pi)^3}\,d\boldsymbol{k}\,d\boldsymbol{q}\,e^{i\boldsymbol{q}\cdot(\boldsymbol{r}-\boldsymbol{r'})}\,\boldsymbol{k}\cdot\boldsymbol{q}\,W(\boldsymbol{r'},\boldsymbol{k},t),\\&=-\frac{\hbar}{m}\boldsymbol{\nabla}\cdot\int\frac{d\boldsymbol{r'}}{(2\pi)^3}\,d\boldsymbol{k}\,d\boldsymbol{q}\,e^{i\boldsymbol{q}\cdot(\boldsymbol{r}-\boldsymbol{r'})}\,\boldsymbol{k}\,W(\boldsymbol{r'},\boldsymbol{k},t),\\&=-\frac{\hbar}{m}\boldsymbol{\nabla}\cdot\int d\boldsymbol{k}\,d\boldsymbol{r'}\,\delta(\boldsymbol{r}-\boldsymbol{r'})\,\boldsymbol{k}\,W(\boldsymbol{r'},\boldsymbol{k},t),\end{aligned} \tag{B.17}$$

where we used $i\boldsymbol{q}e^{i\boldsymbol{q}\cdot\boldsymbol{r}}=\boldsymbol{\nabla}e^{i\boldsymbol{q}\cdot\boldsymbol{r}}$. By performing the trivial integration over the delta function, and using (2.39), we finally obtain the quantum continuity equation

$$\frac{\partial n}{\partial t}+\frac{1}{m}\boldsymbol{\nabla}\cdot\big(n\langle\boldsymbol{p}\rangle\big)=0. \tag{B.18}$$

Next, using the same replacements as before, given by (B.13) and (B.15), (B.12) can be simplified

$$\frac{\partial(n\langle\boldsymbol{p}\rangle)}{\partial t}=-\frac{i\hbar^2}{m}\int d\boldsymbol{k}\,d\boldsymbol{q}\,e^{i\boldsymbol{q}\cdot\boldsymbol{r}}\,\boldsymbol{k}\,(\boldsymbol{k}\cdot\boldsymbol{q})\,W(\boldsymbol{q},\boldsymbol{k},t)+2i\int d\boldsymbol{k}\,d\boldsymbol{q}\,e^{i\boldsymbol{q}\cdot\boldsymbol{r}}\,\boldsymbol{k}$$
$$\times\Big(\frac{\boldsymbol{q}}{2}\cdot\boldsymbol{\nabla}_k\Big)\,W(\boldsymbol{r},\boldsymbol{k},t)\,V(\boldsymbol{q},t), \tag{B.19}$$

where, in the second term on the r.h.s., higher orders in the $\boldsymbol{k}-$derivatives were discarded, given that the remaining integrand is linear in $\boldsymbol{k}$, which implies that only derivatives up to first order will survive, after partial integration. Thus, performing partial differentiation in the second term, together with further

simplifications in the first term, yields

$$\begin{aligned}\frac{\partial(n\langle\boldsymbol{p}\rangle)}{\partial t} &= -\frac{\hbar^2}{m}\boldsymbol{\nabla}\cdot\int\frac{d\boldsymbol{r'}}{(2\pi)^3}\,d\boldsymbol{k}\,d\boldsymbol{q}\,e^{i\boldsymbol{q}\cdot(\boldsymbol{r}-\boldsymbol{r'})}\,\boldsymbol{k}\boldsymbol{k}\,W(\boldsymbol{r'},\boldsymbol{k},t) - \,i\int d\boldsymbol{k}\,d\boldsymbol{q}\,e^{i\boldsymbol{q}\cdot\boldsymbol{r}}\,\boldsymbol{q}\,W(\boldsymbol{r},\boldsymbol{k},t)\,V(\boldsymbol{q},t),\\ &= -\frac{\hbar^2}{m}\boldsymbol{\nabla}\cdot\int d\boldsymbol{k}\,\boldsymbol{k}\boldsymbol{k}\,W(\boldsymbol{r},\boldsymbol{k},t) - i\,n(\boldsymbol{r},t)\int d\boldsymbol{q}\,e^{i\boldsymbol{q}\cdot\boldsymbol{r}}\,\boldsymbol{q}\,V(\boldsymbol{q},t),\\ &= -\frac{1}{m}\boldsymbol{\nabla}\cdot\Big(n\langle\boldsymbol{p}\boldsymbol{p}\rangle\Big) - n(\boldsymbol{r},t)\boldsymbol{\nabla}V(\boldsymbol{r},t),\end{aligned} \tag{B.20}$$

where we defined

$$\langle\boldsymbol{p}\boldsymbol{p}\rangle = \frac{1}{n}\int d\boldsymbol{k}\,\boldsymbol{p}\boldsymbol{p}\,W(\boldsymbol{r},\boldsymbol{k},t), \tag{B.21}$$

and $\boldsymbol{p}\boldsymbol{p}$ denoting the dyadic product

$$\boldsymbol{p}\boldsymbol{p} = \begin{pmatrix} p_x^2 & p_xp_y & p_xp_z\\ p_xp_y & p_y^2 & p_yp_z\\ p_xp_z & p_yp_z & p_z^2\end{pmatrix}. \tag{B.22}$$

Now, we define the fluctuation $\delta g(\boldsymbol{p})$ of any given function of momentum $g(\boldsymbol{p})$ as

$$\delta g = g - \langle g\rangle, \tag{B.23}$$

which verifies $\langle\delta g\rangle = 0$. This definition enables us to rewrite $\langle\boldsymbol{p}\boldsymbol{p}\rangle$ as

$$\langle\boldsymbol{p}\boldsymbol{p}\rangle = \langle\boldsymbol{p}\rangle\langle\boldsymbol{p}\rangle + \langle\delta\boldsymbol{p}\delta\boldsymbol{p}\rangle. \tag{B.24}$$

Inserting this expression into (B.20) yields

$$n\frac{\partial\langle\boldsymbol{p}\rangle}{\partial t} + \cancel{\langle\boldsymbol{p}\rangle\frac{\partial n}{\partial t}} = -\frac{1}{m}\Big[\cancel{\langle\boldsymbol{p}\rangle\boldsymbol{\nabla}\cdot\big(n\langle\boldsymbol{p}\rangle\big)} + n\langle\boldsymbol{p}\rangle\cdot\boldsymbol{\nabla}\langle\boldsymbol{p}\rangle + \boldsymbol{\nabla}\langle\delta\boldsymbol{p}\delta\boldsymbol{p}\rangle\Big] - n\boldsymbol{\nabla}V. \tag{B.25}$$

Notice that, in the above equation, two of the terms cancel each other, which follows from (B.18). Therefore, collecting the remaining terms leads to

$$n\Big(\frac{\partial}{\partial t} + \frac{\langle\boldsymbol{p}\rangle}{m}\cdot\boldsymbol{\nabla}\Big)\langle\boldsymbol{p}\rangle = -\boldsymbol{\nabla}P - n\boldsymbol{\nabla}V, \tag{B.26}$$

where we identified P as the pressure-tensor, related with the averaged momentum fluctuations by

$$P_{ij}(\boldsymbol{r},t) = \frac{n}{m}\langle\delta p_i\delta p_j\rangle. \tag{B.27}$$

Expanding the r.h.s. of (B.27), with the help of (B.23), we get the familiar result

$$P_{ij}(\boldsymbol{r},t) = \frac{n}{m}\Big(\langle p_ip_j\rangle - \langle p_i\rangle\langle p_j\rangle\Big). \tag{B.28}$$

B.3 Macroscopic variables n, u and P in terms of ensemble wave-functions $\{\psi_\alpha\}$

The Wigner function is related to the ensemble wave-functions as

$$W(\boldsymbol{r},\boldsymbol{k},t) = \sum_\alpha \, c_\alpha \, \int \frac{d\boldsymbol{s}}{(2\pi)^d} \, e^{i\boldsymbol{s}\cdot\boldsymbol{k}} \, \psi^*_\alpha(\boldsymbol{r}+\boldsymbol{s}/2,t) \, \psi_\alpha(\boldsymbol{r}-\boldsymbol{s}/2,t). \tag{B.29}$$

where $d=3$ is the dimension of space. Using (2.38), the density is simply

$$\begin{aligned} n(\boldsymbol{r},t) &= \sum_\alpha \, c_\alpha \, \int d\boldsymbol{k} \, \frac{d\boldsymbol{s}}{(2\pi)^3} \, e^{i\boldsymbol{s}\cdot\boldsymbol{k}} \, \psi^*_\alpha(\boldsymbol{r}+\boldsymbol{s}/2,t) \, \psi_\alpha(\boldsymbol{r}-\boldsymbol{s}/2,t), \\ &= \sum_\alpha \, c_\alpha \, \int d\boldsymbol{s} \, \delta(\boldsymbol{s}) \, \psi^*_\alpha(\boldsymbol{r}+\boldsymbol{s}/2,t) \, \psi_\alpha(\boldsymbol{r}-\boldsymbol{s}/2,t), \\ &= \sum_\alpha \, c_\alpha |\psi_\alpha(\boldsymbol{r},t)|^2. \end{aligned} \tag{B.30}$$

Next, using (2.39) together with the relation $\boldsymbol{u} = \hbar\overline{\boldsymbol{k}}/m$, we can write

$$\begin{aligned} n(\boldsymbol{r},t)\boldsymbol{u}(\boldsymbol{r},t) &= \sum_\alpha \, c_\alpha \, \int d\boldsymbol{k} \, \frac{d\boldsymbol{s}}{(2\pi)^3} \, e^{i\boldsymbol{s}\cdot\boldsymbol{k}} \, \frac{\hbar\boldsymbol{k}}{m} \, \psi^*_\alpha(\boldsymbol{r}+\boldsymbol{s}/2,t) \, \psi_\alpha(\boldsymbol{r}-\boldsymbol{s}/2,t), \\ &= -\frac{i\hbar}{m} \sum_\alpha \, c_\alpha \, \int d\boldsymbol{s} \;\; \psi^*_\alpha(\boldsymbol{r}+\boldsymbol{s}/2,t) \, \psi_\alpha(\boldsymbol{r}-\boldsymbol{s}/2,t) \, \boldsymbol{\nabla}_{\boldsymbol{s}} \int \frac{d\boldsymbol{k}}{(2\pi)^3} \, e^{i\boldsymbol{s}\cdot\boldsymbol{k}}, \\ &= -\frac{i\hbar}{m} \sum_\alpha \, c_\alpha \, \int d\boldsymbol{s} \, \psi^*_\alpha(\boldsymbol{r}+\boldsymbol{s}/2,t) \, \psi_\alpha(\boldsymbol{r}-\boldsymbol{s}/2,t) \, \boldsymbol{\nabla}_{\boldsymbol{s}} \, \delta(\boldsymbol{s}), \end{aligned} \tag{B.31}$$

where we used $\boldsymbol{k} \, e^{i\boldsymbol{s}\cdot\boldsymbol{k}} = -i\boldsymbol{\nabla}_{\boldsymbol{s}} \, e^{i\boldsymbol{s}\cdot\boldsymbol{k}}$. By partial integrating the variable $\boldsymbol{s}$, and further assuming the wave-functions $\psi_\alpha(\boldsymbol{r},t)$ to vanish as $\boldsymbol{r} \to \pm\infty$, we get

$$n(\boldsymbol{r},t)\boldsymbol{u}(\boldsymbol{r},t) = \frac{i\hbar}{m} \sum_\alpha \, c_\alpha \, \int d\boldsymbol{s} \, \delta(\boldsymbol{s}) \boldsymbol{\nabla}_s \Big(\psi^*_\alpha(\boldsymbol{r}+\boldsymbol{s}/2,t) \, \psi_\alpha(\boldsymbol{r}-\boldsymbol{s}/2,t) \Big). \tag{B.32}$$

The identity

$$\boldsymbol{\nabla}_{\boldsymbol{s}} \, \psi(\boldsymbol{r} \pm \boldsymbol{s}/2) = \pm \frac{1}{2} \boldsymbol{\nabla} \, \psi(\boldsymbol{r} \pm \boldsymbol{s}/2), \tag{B.33}$$

enables us to perform the integration in $d\boldsymbol{s}$, which yields

$$n(\boldsymbol{r},t)\boldsymbol{u}(\boldsymbol{r},t) = \frac{i\hbar}{2m} \sum_\alpha c_\alpha \Big(\psi_\alpha \boldsymbol{\nabla} \psi^*_\alpha - \psi^*_\alpha \boldsymbol{\nabla} \psi_\alpha \Big). \tag{B.34}$$

To calculate (2.51), we recall the expression for the pressure

$$P_{ij}(\boldsymbol{r},t) = \frac{\hbar^2 n}{m} \, \overline{k_i k_j} - n m u_i u_j, \tag{B.35}$$

which can be calculated from the wave-functions ψ_α by

$$P_{ij}(\boldsymbol{r},t) = \frac{\hbar^2}{m} \sum_\alpha \, c_\alpha \, \int d\boldsymbol{k} \, \frac{d\boldsymbol{s}}{(2\pi)^3} \, e^{i\boldsymbol{s}\cdot\boldsymbol{k}} \, k_i k_j \, \psi^*_\alpha(\boldsymbol{r}+\boldsymbol{s}/2,t) \, \psi_\alpha(\boldsymbol{r}-\boldsymbol{s}/2,t) - n m u_i u_j. \tag{B.36}$$

A similar procedure to the one used before enables us to simplify last expression, and get

$$P_{ij}(\boldsymbol{r},t) = -\frac{\hbar^2}{m}\sum_{\alpha}\, c_\alpha \int d\boldsymbol{s}\; \delta(\boldsymbol{s})\; \frac{\partial^2}{\partial s_i \partial s_j}\Big(\psi^*_\alpha(\boldsymbol{r}+\boldsymbol{s}/2,t)\;\psi_\alpha(\boldsymbol{r}-\boldsymbol{s}/2,t)\Big) - nmu_iu_j. \tag{B.37}$$

Furthermore, introducing the identity (B.33) leads to

$$P_{ij}(\boldsymbol{r},t) = \frac{\hbar^2}{4m}\sum_{\alpha} c_\alpha\left(\left|\frac{\partial\psi^*_\alpha}{\partial r_i}\frac{\partial\psi_\alpha}{\partial r_j}\right|^2 - \psi_\alpha\frac{\partial^2\psi^*_\alpha}{\partial r_i\partial r_j} - \psi^*_\alpha\frac{\partial^2\psi_\alpha}{\partial r_i\partial r_j}\right) - nmu_iu_j. \tag{B.38}$$

Finally, introducing the $i-$th and $j-$th components of (B.34) into the r.h.s. of (B.38) gives

$$\begin{aligned} P_{ij}(\boldsymbol{r},t) = {}& \frac{\hbar^2}{4m}\sum_{\alpha} c_\alpha\left(\left|\frac{\partial\psi^*_\alpha}{\partial r_i}\frac{\partial\psi_\alpha}{\partial r_j}\right|^2 - \psi_\alpha\frac{\partial^2\psi^*_\alpha}{\partial r_i\partial r_j} - \psi^*_\alpha\frac{\partial^2\psi_\alpha}{\partial r_i\partial r_j}\right) \\ & + \frac{\hbar^2}{4mn}\sum_{\alpha,\beta} c_\alpha c_\beta\left(\psi_\alpha\frac{\partial\psi^*_\alpha}{\partial r_i} - \psi^*_\alpha\frac{\partial\psi_\alpha}{\partial r_i}\right)\left(\psi_\beta\frac{\partial\psi^*_\beta}{\partial r_j} - \psi^*_\beta\frac{\partial\psi_\beta}{\partial r_j}\right). \end{aligned} \tag{B.39}$$

B.4 Calculating the Bohm potential from the quantum pressure

We intend to show

$$\frac{1}{nm}\frac{\partial P^Q_{ij}}{\partial r_j} = -\frac{\hbar^2}{2m^2}\frac{\partial}{\partial r_i}\Big(\frac{\boldsymbol{\nabla}^2\sqrt{n}}{\sqrt{n}}\Big), \tag{B.40}$$

where

$$P^Q_{ij} = -\frac{\hbar^2 n}{4m}\frac{\partial^2 \ln n}{\partial r_i\partial r_j} \tag{B.41}$$

and the index j is implicitly summed over in (B.40). Expanding the l.h.s. of (B.40),

$$\begin{aligned} \frac{1}{nm}\frac{\partial P^Q_{ij}}{\partial x_j} &= -\frac{\hbar^2}{4nm^2}\frac{\partial}{\partial r_j}\Big(n\,\frac{\partial^2\ln n}{\partial r_i\partial r_j}\Big), \\ &= -\frac{\hbar^2}{4nm^2}\frac{\partial}{\partial r_j}\Big(\frac{\partial^2 n}{\partial r_i\partial r_j} - \frac{1}{n}\frac{\partial n}{\partial r_i}\frac{\partial n}{\partial r_j}\Big), \\ &= -\frac{\hbar^2}{4nm^2}\left(\frac{\partial^3 n}{\partial r_i\partial r_j\partial r_j} + \frac{1}{n^2}\frac{\partial n}{\partial r_i}\frac{\partial n}{\partial r_j}\frac{\partial n}{\partial r_j} - \frac{1}{n}\frac{\partial^2 n}{\partial r_i\partial r_j}\frac{\partial n}{\partial r_j} - \frac{1}{n}\frac{\partial^2 n}{\partial r_j\partial r_j}\frac{\partial n}{\partial r_i}\right). \end{aligned} \tag{B.42}$$

Doing the same for the r.h.s.[2]

$$\begin{aligned} -\frac{\hbar^2}{2m^2}\frac{\partial}{\partial r_i}\Big(\frac{\boldsymbol{\nabla}^2\sqrt{n}}{\sqrt{n}}\Big) &= -\frac{\hbar^2}{2m^2}\frac{\partial}{\partial r_i}\left[\frac{1}{\sqrt{n}}\frac{\partial}{\partial r_j}\Big(\frac{1}{2\sqrt{n}}\frac{\partial n}{\partial r_j}\Big)\right], \\ &= -\frac{\hbar^2}{4m^2}\frac{\partial}{\partial r_i}\left(\frac{1}{n}\frac{\partial^2 n}{\partial r_j\partial r_j} - \frac{1}{2n^2}\frac{\partial n}{\partial r_j}\frac{\partial n}{\partial r_j}\right), \\ &= -\frac{\hbar^2}{4nm^2}\left(\frac{\partial^3 n}{\partial r_i\partial r_j\partial r_j} + \frac{1}{n^2}\frac{\partial n}{\partial r_i}\frac{\partial n}{\partial r_j}\frac{\partial n}{\partial r_j} - \frac{1}{n}\frac{\partial^2 n}{\partial r_i\partial r_j}\frac{\partial n}{\partial r_j} - \frac{1}{n}\frac{\partial^2 n}{\partial r_j\partial r_j}\frac{\partial n}{\partial r_i}\right), \end{aligned} \tag{B.43}$$

which is the same as (B.42), as we intended to show.

[2]Using Einstein's convention for repeated indices, we may write $\boldsymbol{\nabla^2} = \frac{\partial^2}{\partial r_j\partial r_j}$.

Appendix C

C.1 Transport equation for electrons and holes

Let us start with (3.11) written for the conduction and valence band operators in (3.51)−(3.54). Using $\Delta \simeq -\hbar v_F(q_x - iq_y)$, valid close to the Dirac point $\boldsymbol{K}$, we obtain

$$\hat{H} = \sum_{\boldsymbol{q}\in BZ} \xi(\boldsymbol{q})\big(\hat{c}^\dagger_{\boldsymbol{q}}\hat{c}_{\boldsymbol{q}} - \hat{v}^\dagger_{\boldsymbol{q}}\hat{v}_{\boldsymbol{q}}\big), \tag{C.1}$$

where $\xi(\boldsymbol{q}) = \hbar v_F|\boldsymbol{q}|$, and the summation in $\boldsymbol{q}$ is performed within the first Brillouin zone (BZ). Thus, the kinetic energy of conduction electrons is positive, whereas that of the valence electrons is negative. To circumvent this problem, we call forth the ground-state of our case of interest. As mentioned before, the ground-state of neutral graphene comprises a completely filled valence band and an empty conduction band. Such an electronic configuration is known as Fermi Sea, which we denote by $|\Omega_{\rm FS}\rangle$. It is written as

$$|\Omega_{\rm FS}\rangle = \prod_{\boldsymbol{q}\in BZ} \hat{v}^\dagger_{\boldsymbol{q}}\,|0\rangle\,, \tag{C.2}$$

and $|0\rangle$ is the vacuum state (zero particles). Recall that a general state in Fock space is written in the occupation-number basis, i.e., it is an eigenstate of $\hat{n}_{c,\boldsymbol{q}} = \hat{c}^\dagger_{\boldsymbol{q}}\hat{c}_{\boldsymbol{q}}$ and $\hat{n}_{v,\boldsymbol{q}} = \hat{v}^\dagger_{\boldsymbol{q}}\hat{v}_{\boldsymbol{q}}$, for all $\boldsymbol{q}$. Therefore, each state $|\mathfrak{n}\rangle$ can be identified with a set of numbers $\mathfrak{n} = \{\mathfrak{n}^i_c, \mathfrak{n}^i_v\}^N_{i=1}$, where each superscript i indicates the order of the corresponding discretised mode in the set $\boldsymbol{q} = \{\boldsymbol{q}_i\}^N_{i=1}$ associated with the occupation number $\mathfrak{n}^i_a$. The creation and annihilation operators acting on Fock states give

$$\hat{a}_{\boldsymbol{q}_i}\,|\mathfrak{n}\rangle = (-1)^{\ell_i}\sqrt{\mathfrak{n}^i_a}\;\big|\{\mathfrak{n}^1_c, \mathfrak{n}^1_v, \dots, \mathfrak{n}^i_a - 1, \dots, \mathfrak{n}^N_c, \mathfrak{n}^N_v\}\big\rangle\,, \tag{C.3}$$

$$\hat{a}^\dagger_{\boldsymbol{q}_i}\,|\mathfrak{n}\rangle = (-1)^{\ell_i}\sqrt{\mathfrak{n}^i_a + 1}\;\big|\{\mathfrak{n}^1_c, \mathfrak{n}^1_v, \dots, \mathfrak{n}^i_a + 1, \dots, \mathfrak{n}^N_c, \mathfrak{n}^N_v\}\big\rangle\,, \tag{C.4}$$

where $a \in \{c, v\}$ and ℓ_i is the total number of occupied states that are ordered to the left of the state corresponding to $\boldsymbol{q}_i$. This leads to

$$|\mathfrak{n}\rangle = \left(\prod_{i\in BZ} \frac{(\hat{c}^\dagger_{\boldsymbol{q}_i})^{\mathfrak{n}^i_v}}{\sqrt{\mathfrak{n}^i_c!}}\right)\left(\prod_{j\in BZ} \frac{(\hat{v}^\dagger_{\boldsymbol{q}_j})^{\mathfrak{n}^j_v}}{\sqrt{\mathfrak{n}^j_v!}}\right)|0\rangle\,, \tag{C.5}$$

$$\hat{n}_{a,\boldsymbol{q}_i}\,|\mathfrak{n}\rangle = \mathfrak{n}^i_a\,|\mathfrak{n}\rangle\,, \tag{C.6}$$

The set $\mathfrak{n}$ is composed by the eigenvalues of the number operators, which form a complete basis once the relation $[\hat{n}_{a,\boldsymbol{q}}, \hat{n}_{a',\boldsymbol{q'}}] = \delta_{aa'}\delta_{\boldsymbol{q},\boldsymbol{q'}}$ holds; that is to say, all number operators commute for different $\boldsymbol{q}$. The last relation follows straightforwardly from the anti-commutation relations for fermionic fields $\{\hat{c}_{\boldsymbol{q}}, \hat{c}^{\dagger}_{\boldsymbol{q'}}\} = \delta_{\boldsymbol{q}\boldsymbol{q'}}$, $\{\hat{v}_{\boldsymbol{q}}, \hat{v}^{\dagger}_{\boldsymbol{q'}}\} = \delta_{\boldsymbol{q}\boldsymbol{q'}}$, $\{\hat{c}_{\boldsymbol{q}}, \hat{v}^{\dagger}_{\boldsymbol{q'}}\} = 0$, which restrict the values of $\mathfrak{n}^i_a$ to the set $\{0, 1\}$. With this in mind, it is easy to calculate the energy of $|\Omega_{FS}\rangle$, which gives

$$\hat{H}\,|\Omega_{\mathrm{FS}}\rangle = E_{\mathrm{FS}}\,|\Omega_{\mathrm{FS}}\rangle\,, \tag{C.7}$$

$$E_{\mathrm{FS}} = \sum_{\boldsymbol{q}\in BZ} -\xi(\boldsymbol{q}). \tag{C.8}$$

Given that $E_{\mathrm{FS}} < 0$, acting on Ω_{FS} with any $\hat{v}_{\boldsymbol{q}}$ leads to a new state $|\Omega'\rangle$ such that $E_{\Omega'} > E_{FS}$. Hence, destroying a valence electron creates a positive energy excitations to the ground-state, which suggests that the absence of a valence electron (or the presence of a hole in the almost filled Fermi sea) behaves as a positive-energy particle. Therefore, we define two new fermionic creation and annihilation operators $\hat{h}^{\dagger}_{\boldsymbol{q}}$ and $\hat{h}_{\boldsymbol{q}}$ as

$$\hat{h}^{\dagger}_{\boldsymbol{q}} = \hat{v}_{-\boldsymbol{q}}, \tag{C.9}$$

$$\hat{h}_{\boldsymbol{q}} = \hat{v}^{\dagger}_{-\boldsymbol{q}}, \tag{C.10}$$

which obey, *mutatis mutandis*, the exact same fermionic anti-commutation relations. Physically, $\hat{h}^{\dagger}_{\boldsymbol{q}}$ creates a hole with momentum $\boldsymbol{q}$ and $\hat{h}_{\boldsymbol{q}}$ destroys a hole with momentum $\boldsymbol{q}$. The reason for writing $-\boldsymbol{q}$ instead of $\boldsymbol{q}$ in (C.10) and (C.9) is that, when we act on any Fock state with $\hat{v}_{\boldsymbol{q}}$, the net momentum of the system changes by $-\boldsymbol{q}$. However, when we create a hole with momentum $\boldsymbol{q}$, we must require the net value to increase by $\boldsymbol{q}$, and not the contrary, which leads to (C.10) and (C.9) as they are. Physically, this means a hole corresponds to an electron flowing in the opposite direction, which also guarantees that a current of holes entering a volume V increases the net charge of V, because in reality valence electrons are going out. Using this change of basis, together with the anti-commutation relations, the Hamiltonian of (C.1) goes to

$$\hat{H} = E_{FS} + \sum_{\boldsymbol{q}\in BZ} \xi(\boldsymbol{q})\big(\hat{c}^{\dagger}_{\boldsymbol{q}}\hat{c}_{\boldsymbol{q}} + \hat{h}^{\dagger}_{\boldsymbol{q}}\hat{h}_{\boldsymbol{q}}\big), \tag{C.11}$$

which represents a free Hamiltonian for two different species with positive energy, as desired. The constant E_{FS} can be absorbed into $\hat{H}$, and will then be discarded. The Wigner transport equation can be obtained, following the same procedure as in chapter 3.3. Let us define $\boldsymbol{\Psi}^T(\boldsymbol{q}, t) = (\hat{c}_{\boldsymbol{q}}, \hat{h}_{\boldsymbol{q}})$ and write the one particle Shcrödinger equation as[1]

$$i\hbar\frac{\partial}{\partial t}\Psi^{\alpha}(\boldsymbol{q}, t) = \xi(\boldsymbol{q})\Psi^{\alpha}(\boldsymbol{q}, t) + \int d\boldsymbol{q'}\; V^{\alpha}(\boldsymbol{q'}, t)\Psi^{\alpha}(\boldsymbol{q} - \boldsymbol{q'}, t), \tag{C.12}$$

where $V^{\alpha}(\boldsymbol{q}, t)$ is the Fourier transform of the mean-field potential. The form of $V^{\alpha}(\boldsymbol{r}, t)$ is slightly modified in the electron-hole case, due to the charge of holes being symmetric to that of electrons.

[1] This is equivalent to establish the corresponding Heisenberg equation of motion for the expectation value of the creation and annihilation operators, in the mean-field approximation.

In fact, the charge operator $\hat{Q}$ renders $\hat{Q}\ \hat{h}^{\dagger}_{\boldsymbol{q}}|\Omega_{FS}\rangle = (+e)\ \hat{h}^{\dagger}_{\boldsymbol{q}}|\Omega_{FS}\rangle$, *i.e*, holes have positive charge against the almost filled Fermi sea. Such a modification is accomplished with the new dependence of the potential $V^{\alpha}(\boldsymbol{q},t)$ on the band index α. Therefore, the Poisson equation must be rewritten as

$$\boldsymbol{\nabla}^2\phi(\boldsymbol{r},t) = -\frac{e}{\varepsilon}\big[n^2(\boldsymbol{r},t) - n^1(\boldsymbol{r},t)\big], \tag{C.13}$$

where n_1 and n_2 denotes the electron and hole density, respectively, and $\phi(\boldsymbol{r},t)$ is the electrostatic potential. This last is related to the potential via

$$V^{\alpha}(\boldsymbol{r},t) = s^{\alpha}e\phi(\boldsymbol{r},t), \tag{C.14}$$

where $s^{\alpha} = 2\alpha - 3$ is the sign of the electric charge. The real space densities are calculated through the diagonal components of the Wigner matrix as

$$n^1(\boldsymbol{r},t) = \int d\boldsymbol{k}\ W^{11}(\boldsymbol{r},\boldsymbol{k},t), \tag{C.15}$$

$$n^2(\boldsymbol{r},t) = \int d\boldsymbol{k}\ W^{22}(\boldsymbol{r},\boldsymbol{k},t). \tag{C.16}$$

For the solution of (C.13), we get

$$\phi(\boldsymbol{r},t) = \frac{e}{4\pi\varepsilon}\int d\boldsymbol{r'}\ \frac{n^2(\boldsymbol{r'},t) - n1(\boldsymbol{r'},t)}{|\boldsymbol{r}-\boldsymbol{r'}|}. \tag{C.17}$$

Further manipulation of (C.12) leads to

$$\begin{aligned} i\hbar\,\frac{\partial}{\partial t}W^{\alpha\gamma}(\boldsymbol{q},\boldsymbol{k},t) = &\Big[\xi(\mathbf{k}+\mathbf{q}/2) - \xi(\mathbf{k}-\mathbf{q}/2)\Big]\ W^{\alpha\gamma}(\boldsymbol{q},\boldsymbol{k},t) \\ &+ e\int d\boldsymbol{q}'\ \phi(\mathbf{q}',t)\ \Delta W^{\alpha\gamma}(\mathbf{q},\mathbf{k},\mathbf{q}',t), \end{aligned} \tag{C.18}$$

where $\phi(\boldsymbol{q},t)$ is the Fourier transform of the electrostatic potential, and the following definitions were employed:

$$W^{\alpha\gamma}(\boldsymbol{q},\boldsymbol{k},t) = \Psi^{*\alpha}(\boldsymbol{k}-\boldsymbol{q}/2,t)\ \Psi^{\gamma}(\boldsymbol{k}+\boldsymbol{q}/2,t), \tag{C.19}$$

$$\Delta W^{\alpha\gamma}(\boldsymbol{q},\boldsymbol{k},\boldsymbol{q'},t) = s^{\alpha}W^{\alpha\gamma}(\boldsymbol{q}-\boldsymbol{q'},\boldsymbol{k}-\boldsymbol{q'}/2,t) - s^{\gamma}W^{\alpha\gamma}(\boldsymbol{q}-\boldsymbol{q'},\boldsymbol{k}+\boldsymbol{q'}/2,t). \tag{C.20}$$

As before, the equation for W^{11} describes the evolution of the (conducting) electronic system, whilst in its turn, W^{22} fully represents the hole system, such that valence electrons no longer show up, henceforth.

Appendix D

D.1 Coulomb potential in Fourier space

Let $\mathcal{C}\{u,v\}(\boldsymbol{r})$ denote the convolution between $u(\boldsymbol{r})$ and $v(\boldsymbol{r})$, that is defined by

$$\mathcal{C}\{u,v\}(\boldsymbol{r}) = \int d\boldsymbol{r'}\; u(\boldsymbol{r'})\; v(\boldsymbol{r'}-\boldsymbol{r}). \tag{D.1}$$

The Fourier transform of a convolution yields a simple result involving the Fourier transform of each of the functions subjected to the operation, namely

$$\begin{aligned}\mathcal{C}\{u,v\}(\boldsymbol{q}) &= \int \frac{d\boldsymbol{r}}{(2\pi)^d}\; e^{-i\boldsymbol{q}\cdot\boldsymbol{r}}\; \mathcal{C}\{u,v\}(\boldsymbol{r}),\\ &= (2\pi)^d\; u(\boldsymbol{q})\; v(\boldsymbol{q}),\end{aligned} \tag{D.2}$$

where $u(\boldsymbol{q})$ and $v(\boldsymbol{q})$ are the Fourier transforms of the initial functions, and d is the dimensionality of the variables involved in the transformation. This is known as the convolution theorem and follows straightforwardly after a simple manipulation. In the mean-field approximation, the potential is found to be given by a convolution between the density and the time independent Coulomb potential, $\mathcal{V}(\mathbf{r})$

$$\mathcal{V}(\mathbf{r}) = \frac{e^2}{4\pi\varepsilon_r\varepsilon_0|\boldsymbol{r}|}. \tag{D.3}$$

Hence, we are interested in calculating the Fourier transform of

$$V(\boldsymbol{r},t) = \mathcal{C}\{\mathcal{V}(\mathbf{r}), n(\boldsymbol{r},t)\}, \tag{D.4}$$

which gives

$$V(\boldsymbol{q},t) = (2\pi)^d\; \mathcal{V}(\boldsymbol{q})\; n(\boldsymbol{q},t). \tag{D.5}$$

Next, we calculate $\mathcal{V}(\boldsymbol{q})$ for three distinct cases of interest.

D.1.1 3-dimensional case

In the three dimensional case, $\mathcal{V}(\boldsymbol{q})$ reads

$$\mathcal{V}(\boldsymbol{q}) = \frac{e^2}{4\pi\varepsilon_r\varepsilon_0}\int \frac{d\boldsymbol{r}}{(2\pi)^3}\,\frac{e^{-i\boldsymbol{q}\cdot\boldsymbol{r}}}{|\boldsymbol{r}|}, \qquad \boldsymbol{r}\in\mathbb{R}^3. \tag{D.6}$$

We emphasise again that the above integral is invariant under a $\boldsymbol{q}$ rotation, which means that if we let $\boldsymbol{q}\to\Lambda\boldsymbol{q}$, with Λ being the unitary transformation corresponding to the rotation, then $\mathcal{V}(\boldsymbol{q})$ remains unchanged, *i.e.*, $\mathcal{V}(\boldsymbol{q}) = \mathcal{V}(q)$. We then choose to align $\boldsymbol{q}$ with the $z-$axis, for which $\boldsymbol{q}\cdot\boldsymbol{r} = qr\cos\theta$ holds, where θ is the polar angle of $\boldsymbol{r}$ and q,r denote the absolute value of the respective variable. In spherical coordinates, we obtain

$$\begin{aligned}\mathcal{V}(q) &= \frac{e^2}{4\pi\varepsilon_r\varepsilon_0}\int_0^{2\pi} d\phi\int_0^{\pi} d\theta\,\sin\theta\int_0^{+\infty}\frac{dr}{(2\pi)^3}\,r\,e^{-iqr\cos\theta},\\ &= \frac{e^2}{2\varepsilon_r\varepsilon_0}\int_0^{+\infty}\frac{dr}{(2\pi)^3}\,\frac{1}{iq}\Big(e^{iqr}-e^{-iqr}\Big).\end{aligned} \tag{D.7}$$

To perform the last integration, we add a convergence factor δ and evaluate the integral in the limit $\delta\to 0$, *i.e.*,

$$\begin{aligned}\mathcal{V}(q) &= \lim_{\delta\to 0}\,\frac{e^2}{2\varepsilon_r\varepsilon_0}\int_0^{+\infty}\frac{dr}{(2\pi)^3}\,\frac{1}{iq}\Big(e^{ir(q+i\delta)}-e^{-ir(q-i\delta)}\Big),\\ &= \frac{e^2}{2\varepsilon_r\varepsilon_0}\,\frac{1}{iq(2\pi)^3}\,\lim_{\delta\to 0}\,\frac{2iq}{q^2+\delta^2},\\ &= \frac{1}{(2\pi)^3}\,\frac{e^2}{\varepsilon_r\varepsilon_0 q^2}.\end{aligned} \tag{D.8}$$

The mean-field potential is, thus

$$V_{3\mathrm{D}}(\boldsymbol{q},t) = \frac{n(\boldsymbol{q},t)e^2}{\varepsilon_r\varepsilon_0 q^2}. \tag{D.9}$$

D.1.2 2-dimensional case

For the two dimensional case, we have

$$\mathcal{V}(\boldsymbol{q}) = \frac{e^2}{4\pi\varepsilon_r\varepsilon_0}\int \frac{d\boldsymbol{r}}{(2\pi)^2}\,\frac{e^{-i\boldsymbol{q}\cdot\boldsymbol{r}}}{|\boldsymbol{r}|}, \qquad \boldsymbol{r}\in\mathbb{R}^2. \tag{D.10}$$

As in the previous case, $\mathcal{V}(\boldsymbol{q})$ is only a function of q, which allows us to align $\boldsymbol{q}$ with the $x-$direction, such that

$$\mathcal{V}(q) = \frac{e^2}{4\pi\varepsilon_r\varepsilon_0}\int_0^{+\infty}\frac{dr}{(2\pi)^2}\int_0^{2\pi} d\theta\,e^{-iqr\cos\theta}, \tag{D.11}$$

where we maintained the same definitions as before. Using the identity

$$e^{-ix\cos\theta} = J_0(x) + 2\sum_{n=1}^{+\infty}(-i)^n J_n(x)\cos(n\theta), \tag{D.12}$$

with $J_n(x)$ denoting the $n-$order Bessel function of the first kind ($n \in \mathbb{N}$), the above expression reduces to

$$\mathcal{V}(q) = \frac{1}{(2\pi)^2}\,\frac{e^2}{4\pi\varepsilon_r\varepsilon_0 q}\int_0^{+\infty} dx\; 2\pi J_0(x), \tag{D.13}$$

where we changed the variable of integration using $x = qr$, and used the property $\int_0^{+\infty} d\theta\cos(n\theta) = 0$. Given that $J_n(x)$ obeys the normalization condition $\int_0^{+\infty} J_n(x) = 1$, then

$$\mathcal{V}(q) = \frac{1}{(2\pi)^2}\,\frac{e^2}{2\varepsilon_r\varepsilon_0 q}. \tag{D.14}$$

Hence, the mean-field potential in 2 dimensions is

$$V_{2\mathrm{D}}(\boldsymbol{q}, t) = \frac{n(\boldsymbol{q}, t)e^2}{2\varepsilon_r\varepsilon_0 q}. \tag{D.15}$$

D.1.3 Two parallel planes configuration

For this particular configuration, we need to compute

$$\mathcal{V}(\boldsymbol{q}) = \frac{e^2}{4\pi\varepsilon_r\varepsilon_0}\int \frac{d\boldsymbol{r}}{(2\pi)^2}\,\frac{e^{-i\boldsymbol{q}\cdot\boldsymbol{r}}}{|\boldsymbol{r} + d\hat{\boldsymbol{z}}|}, \qquad \boldsymbol{r} \in \mathbb{R}^2, \tag{D.16}$$

where $d > 0$ is the distance between the planes and $\hat{\boldsymbol{z}}$ is the unit vector pointing in the $z-$direction. As before, this is equivalent to

$$\begin{aligned}
\mathcal{V}(q) &= \frac{e^2}{4\pi\varepsilon_r\varepsilon_0}\int_0^{+\infty}\frac{dr}{(2\pi)^2}\int_0^{2\pi} d\theta\,\frac{re^{-iqr\cos\theta}}{\sqrt{r^2+d^2}},\\
&= \frac{e^2}{4\pi\varepsilon_r\varepsilon_0 q}\int_0^{+\infty}\frac{dx}{(2\pi)^2}\int_0^{2\pi} d\theta\,\frac{xe^{-ix\cos\theta}}{\sqrt{x^2+(qd)^2}},\\
&= \frac{e^2}{2\varepsilon_r\varepsilon_0 q}\int_0^{+\infty}\frac{dx}{(2\pi)^2}\,\frac{xJ_0(x)}{\sqrt{x^2+(qd)^2}}.
\end{aligned} \tag{D.17}$$

Using the property $\int_0^{+\infty} dx\frac{xJ_0(x)}{\sqrt{x^2+a^2}} = e^{-|a|}$, we finally get

$$V_{2\mathrm{D}}^{\parallel}(\boldsymbol{q}, t) = \frac{n(\boldsymbol{q}, t)e^2}{2\varepsilon_r\varepsilon_0 q}e^{-qd}. \tag{D.18}$$